ATOMIC FORCE MICROSCOPY AND IMAGE ANALYSIS OF EPITAXIAL 2D WS_2 CRYSTALS GROWN VIA METAL-ORGANIC CHEMICAL VAPOR DEPOSITION

FRANÇOIS DROUIN

Thesis submitted to the University of Ottawa
in partial Fulfillment of the requirements for the
Master's degree in physics

Department of Physics
Faculty of Science
University of Ottawa

© François Drouin, Ottawa, Canada, 2025

Examining Committee

The following served on the Examining Committee for this thesis:

External Member: Louis Gaudreau
Research Officer
National Research Council Canada

Internal Member: Pawel Hawrylak
Professor, Department of Physics
University of Ottawa

Supervisors: Hang Chi
Professor, Department of Physics
University of Ottawa

James Gupta
Professor, Department of Physics
University of Ottawa

Abstract

The controlled synthesis of monolayer tungsten disulfide (WS_2) is essential for its application in next-generation electronic and optoelectronic devices. Metal-organic chemical vapor deposition (MOCVD) has emerged as a scalable and reliable method for growing high-quality WS_2 monolayers. However, optimizing the growth parameters remains challenging for achieving uniform coverage and well-defined domain structures. This study focuses on characterizing WS_2 monolayers grown on c-plane sapphire substrates under varying annealing and growth temperatures and times. Atomic force microscopy (AFM) and ImageJ analysis have been employed to quantify monolayer coverage, nucleation density, and domain size.

Our findings reveal that WS_2 monolayer coverage increases proportionally with the nucleation growth time, indicating a direct correlation between deposition duration and surface coverage. Additionally, we observe that the nucleation density decreases as the nucleation temperature increases, while the domain size grows larger at higher temperatures. Notably, the step edges on sapphire wafers strongly influence the WS_2 growth process, facilitating domain alignment along these steps and suggesting a potential method for improving film uniformity.

These results contribute to a deeper understanding of the WS_2 monolayer growth mechanisms and provide insights into optimizing the synthesis conditions. Future research will focus on refining growth parameters to achieve continuous monolayer coverage, investigating the role of step-edge depth in influencing nucleation density and domain size, and analyzing domain orientation at different nucleation temperatures. These findings could guide the development of scalable WS_2 synthesis techniques and other transition metal dichalcogenides (TMDs) for electronic and optoelectronic applications.

Acknowledgement

First and foremost, I would like to express my deepest gratitude to my supervisor, Dr. Hang Chi, for his continuous support, guidance, and encouragement throughout my graduate studies. His expertise, mentorship, and patience have shaped my research skills and pushed me to grow as a scientist. I am sincerely thankful for the opportunities he provided me—both in the lab and in professional development—which have greatly enriched my academic experience.

I would also like to extend my sincere thanks to Dr. Hawrylak and Dr. Gaudreau, who agreed to serve on my thesis examination committee. Your time and input are greatly appreciated, and I value your expertise in evaluating this work.

I am especially grateful to all members of the Chi Research Group and James Gupta Research Group for their support, insight, and camaraderie over the past two years. I truly appreciated the stimulating discussions, shared troubleshooting sessions, and moments of laughter that helped make long days in the lab more enjoyable.

A heartfelt thank you to the staff and technicians at the University of Ottawa Nanofabrication Facility for their training, assistance, and help with various aspects of the experimental work, especially in the cleanroom and thin-film deposition processes. Your expertise and attention to detail were crucial to the success of this research.

I would also like to acknowledge the Department of Physics at the University of Ottawa for the academic and financial support provided throughout my studies. Special thanks to the

faculty and administrative staff who contributed to a supportive learning environment, and to the undergraduate students I had the pleasure of teaching as a TA—your curiosity reminded me of the joy in learning and teaching physics.

On a personal note, I want to thank my family for their unwavering support and encouragement throughout this journey. To my parents—thank you for believing in me, even during moments when I doubted myself. Your constant motivation and love gave me strength to persist.

Finally, to my friends, both within and outside of academia, thank you for grounding me, keeping me sane, and offering a much-needed balance to my life outside of research. Your support, humor, and perspective meant more than I can express.

This thesis is the result of many hands, minds, and hearts coming together—thank you all for being a part of it.

List of Abbreviations

Abbreviation	Definition	Page
2D	Two Dimensional	12
AFM	Atomic Force Microscopy	18
BL	Bilayer	27
CCS	Closed-Coupled Showerhead	57
CMOS	Complementary Metal-Oxide-Semiconductor	17
COF	Covalent Organic Framework	36
CVD	Chemical Vapor Deposition	16
DI	Deionized	63
DTBS	Di-tert-butyl sulfide	43
EDS	Energy-Dispersive X-ray Spectroscopy	19
FET	Field-Effect Transistor	29
GE-MOCVD	Growth-Etch Metal-Organic Chemical Vapor Deposition	54
h-BN	Hexagonal Boron Nitride	23
IDB	Inverse Domain Boundaries	17
IPA	Isopropanol	63
LED	Light-Emitting Device	13
MBE	Molecular Beam Epitaxy	35
MFC	Mass Flow Controllers	45
MOCVD	Metal-Organic Chemical Vapor Deposition	15
MOF	Metal-Organic Framework	36
PE-ALD	Plasma-Enhanced Atomic Layer Deposition	47
PL	Photoluminescence	12
SAED	Selected-Area Electron Diffraction	19
SEM	Scanning Electron Microscopy	18
SHG	Second-Harmonic Generation	40
TEM	Transmission Electron Microscopy	19
TMDs	Transition metal dichalcogenides	12
UV	Ultraviolet	36
XPS	X-ray Photoelectron Spectroscopy	19

Table of Contents

List of Figures

Chapter 1 - Introduction

1.1 - Context & Motivation

Two-dimensional (2D) materials have emerged as a significant focus in modern materials research due to their unique properties at atomic thickness. The discovery of graphene in 2004 sparked the field, which demonstrated exceptional electrical and mechanical properties but lacked an intrinsic bandgap [1]. This limitation has generated attention in semiconducting 2D materials, particularly transition metal dichalcogenides (TMDs), which offer suitable bandgaps and strong light–matter interactions. Tungsten disulfide (WS_2) is one of the most intriguing TMDs, distinguished by several superior properties compared to its peers. Monolayer WS_2 possesses a direct bandgap (~2.0 eV) in the visible range and exhibits relatively high carrier mobility, large exciton binding energy, strong spin–orbit coupling, and intense photoluminescence (PL) [1]. These attributes make WS_2 an ideal candidate for next-generation electronic and optoelectronic devices [1]. In short, WS_2 combines the advantages of 2D materials (atomic thickness, flexibility) with excellent semiconducting behavior, motivating the exploration of this material in fundamental studies and practical applications.

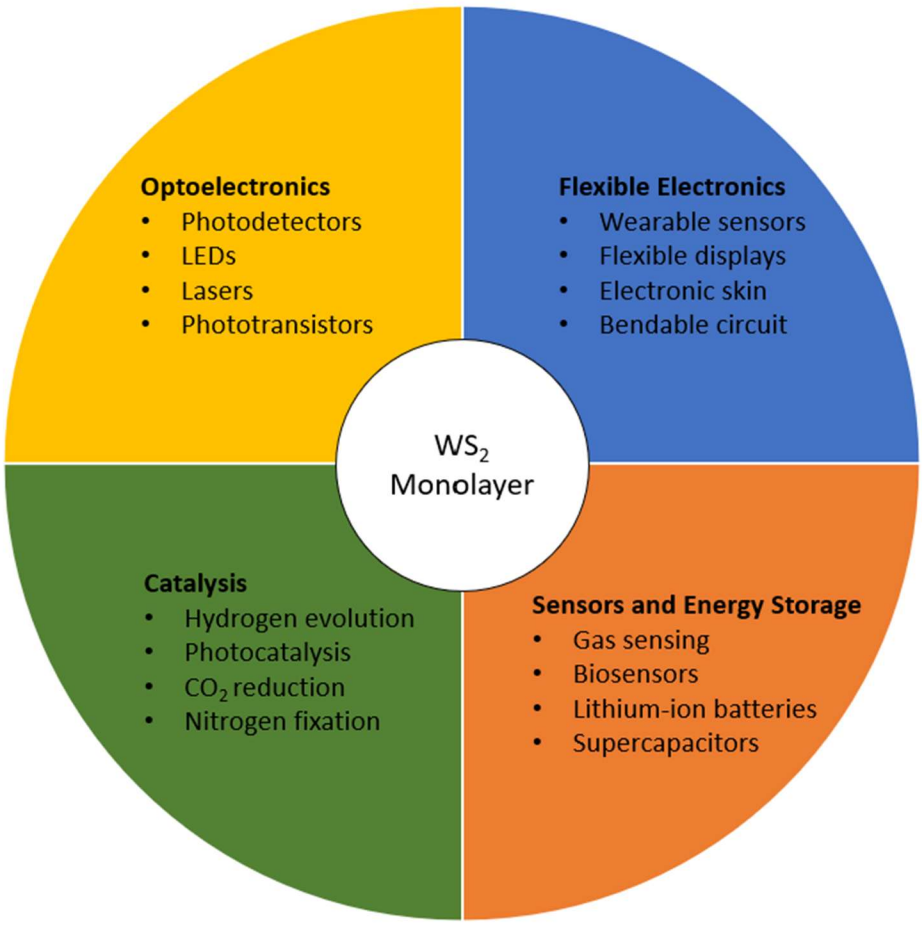

Figure 1.1: Overview of significant technological applications of WS_2 monolayers, highlighting its versatility in optoelectronics, flexible electronics, catalysis, sensors, and energy storage systems.

WS_2's unique properties translate into a broad range of applications in modern technology. In optoelectronics, WS_2's direct bandgap and strong PL enable high-performance photodetectors, light-emitting devices (LEDs), and lasers at the nanoscale [1]. Monolayer WS_2 can efficiently absorb and emit light, leading to photodetectors with fast response and LEDs in the visible spectrum. Its high photoresponsivity and tunable optical properties have

been leveraged in phototransistors and even quantum optoelectronic devices (e.g. single-photon emitters) [1].

The realm of flexible electronics also greatly benefits from WS_2. As an atomically thin material, WS_2 can be transferred onto plastic substrates or integrated into bendable circuits without losing functionality. WS_2 monolayers remain operational under strain, making them suitable for flexible transistors and wearable sensors. Notably, WS_2 can be synthesized at relatively low temperatures (~250 °C) without degrading its quality, which is compatible with polymer substrates and back-end-of-line processes [1]. This means WS_2 devices can be built on flexible or existing electronic platforms, an essential advantage for future flexible displays and integrated circuits.

WS_2 has attracted significant interest as a catalyst in chemical reactions, especially in energy applications. WS_2 and its sister compound MoS_2 are promising catalysts for the hydrogen evolution reaction (HER) due to their platinum-like d-band electronic structure, low cost, and good chemical stability [2]. The edge sites of WS_2 provide active centers for electrocatalysis, enabling efficient hydrogen generation in water-splitting reactions. WS_2's high surface-to-volume area and tunable chemistry are also useful in photocatalysis and other reactions, facilitating processes like CO_2 reduction and nitrogen fixation.

Beyond electronics and catalysis, WS_2's versatility extends to sensors, energy storage, and biomedical applications. For example, WS_2 has shown potential in gas sensing and photothermal therapy, and its inherent biocompatibility makes it attractive for biosensors and drug delivery systems [3]. Due to their layered structure and conductivity, WS_2-based

nanocomposites have been explored in lithium-ion batteries and supercapacitors as electrode materials. This broad application spectrum underscores the significance of WS_2 in scientific research and technological innovation.

Given these diverse and high-impact applications, WS_2 stands out among 2D materials as a platform of particular interest. Researchers are mainly motivated by recent breakthroughs that highlight WS_2's potential. For instance, advances in large-area synthesis now allow the growth of wafer-scale WS_2 monolayers with electronic qualities approaching those of exfoliated crystals [4]. High-quality WS_2 films have enabled transistors with room-temperature mobilities on the order of 100–200 $cm^2/V{\cdot}s$, comparable to mechanically cleaved flakes [5]. Such progress in synthesis has led to record performances in WS_2-based devices, including ultrafast photodetectors and light-emitting tunneling devices. Moreover, novel synthesis approaches (e.g. mediator-assisted growth and hydroxide vapor phase deposition) have drastically reduced defect densities in WS_2, yielding defect-free monolayers with superior optoelectronic properties [5]. These breakthroughs validate the importance of WS_2 in current research and provide the impetus to investigate further and optimize WS_2 material quality for next-generation applications.

1.2 - Problem Statement

Despite the promise of WS_2, growing high-quality monolayer WS_2 at scale remains challenging. In particular, metal–organic chemical vapor deposition (MOCVD) – a scalable technique for synthesizing 2D materials – faces several difficulties that must be addressed to fully exploit WS_2's potential. One major challenge is nucleation control. Achieving uniform

WS_2 monolayers requires careful control over the nucleation of WS_2 islands on the substrate. If too few nuclei form, the film will be discontinuous; if too many form, the domains remain small and can overlap into multilayers. Controlling the density and placement of nucleation sites is notoriously difficult. Studies have shown that growth parameters can be tuned to manipulate flake density and size. but finding the optimal balance for uniform monolayer coverage is non-trivial. Uncontrolled nucleation also leads to variability in domain orientations and edge structures, which can impact the electrical continuity of the film.

Another significant issue is growth uniformity and continuity. Even after nucleation, growing a continuous, wafer-scale WS_2 monolayer is difficult. Domains must expand and coalesce without leaving gaps or forming multilayer patches. A persistent problem is that when randomly oriented WS_2 domains merge, they can form grain or inversion domain boundaries that disrupt the film's uniformity [4]. Achieving a single-crystalline monolayer often requires epitaxial alignment of all domains. For example, on c-plane sapphire (an oriented crystalline substrate), WS_2 domains can be aligned in the same crystallographic orientation, preventing the formation of mirror-twin grain boundaries [4]. However, on amorphous substrates like SiO_2, domains nucleate with arbitrary orientation, leading to a polycrystalline film. The challenge is to develop growth processes (e.g. multi-step MOCVD processes or introduction of seed promoters) that yield large-area, continuous WS_2 monolayers with minimal thickness variation.

Mitigating defects also poses considerable difficulty. WS_2 films grown by MOCVD often suffer from defects, including point defects (such as sulfur vacancies), grain boundaries between domains, and impurities from precursors. Chemical vapor deposition (CVD)

methods are known for their high defect densities in TMD monolayers [5], which can quench PL and degrade electronic performance. Of particular concern are inversion domain boundaries (IDBs), which occur when two oppositely oriented WS_2 domains meet; these boundaries exhibit metallic character that creates leakage paths in an otherwise semiconducting layer [4]. Eliminating such defects is critical, as they limit carrier mobility and device functionality. To overcome these challenges, the present research focuses on optimizing MOCVD growth conditions and performing comprehensive morphological characterization of WS_2 monolayers, as outlined in the following research objectives. Carbon-based residues from metal–organic precursors or incomplete sulfurization can also introduce contamination. Mitigating defects requires optimizing growth chemistry (for example, using more reactive precursors or adding agents to improve sulfur incorporation) and possibly post-growth treatments to heal or passivate defects. Recent approaches like hydroxide vapor phase deposition have demonstrated that alternative precursor chemistry can reduce defect densities by an order of magnitude [5], indicating a clear need to address defects in WS_2 growth.

Finally, substrate compatibility represents another critical challenge. WS_2 must be grown on substrates suitable for its intended application (e.g. sapphire for optoelectronic devices, silicon wafers for integration with CMOS, or flexible polymers for wearable electronics). Each substrate presents its own challenges. Crystalline substrates (e.g., sapphire, hexagonal BN) can support epitaxial growth, typically at elevated temperatures with pristine surface conditions. However, while lower growth temperatures are also possible on crystalline substrates, these conditions usually compromise epitaxial alignment. Amorphous or flexible

substrates can readily accommodate lower temperature growth, though they often lead to random nucleation and stress-induced defects. There is also the issue of thermal expansion mismatch – WS_2 grown on mismatched substrates can crack or wrinkle upon cooling. In the context of MOCVD, ensuring the process is adaptable to different substrate materials and sizes is part of the challenge. Developing a process that yields high-quality WS_2 on diverse substrates (from rigid wafers to flexible foils) is essential for broad applicability. However, tuning the growth conditions for each case remains a complex problem.

To tackle these synthesis challenges, various characterization techniques are employed to analyze WS_2 monolayers and guide process improvements. Optical microscopy and scanning electron microscopy (SEM) are employed to first examine the WS_2 coverage, domain size, and film continuity across the substrate. Atomic force microscopy (AFM) is used to verify layer thickness (a ~ 0.616 nm step height confirms a monolayer) and to inspect surface morphology for pits or bumps. PL spectroscopy is extremely sensitive to WS_2's optical quality – a high-quality monolayer shows a strong PL peak near 1.95–2.0 eV (around 620-636 nm), whereas PL quenching often signifies nonradiative recombination due to defects or grain boundaries.

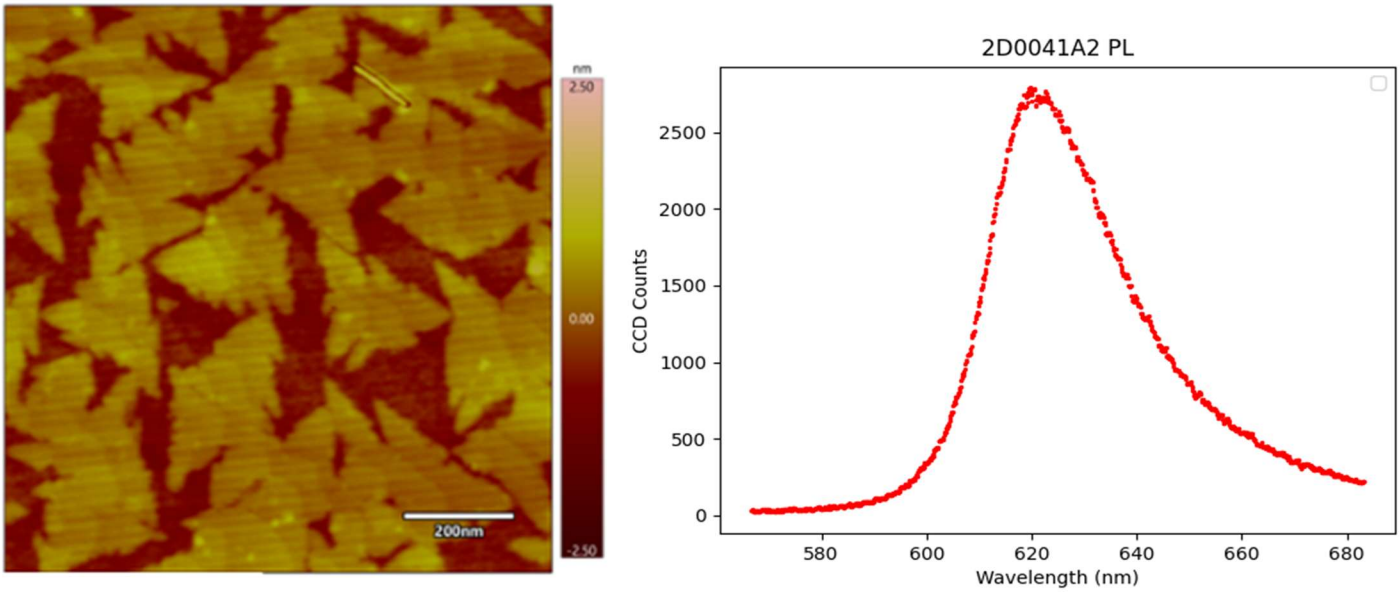

Figure 1.2: Representative photoluminescence (PL) spectrum of monolayer WS_2 exhibiting a sharp excitonic peak near 620 nm (~2.0 eV). The sample was grown on a sapphire substrate with 0.15° miscut towards the m-plane, annealed at 1200 °C for 10 minutes, and nucleated at 700 °C for 75 minutes.

X-ray photoelectron spectroscopy (XPS) and energy-dispersive X-ray spectroscopy (EDS) can help verify the chemical composition (confirming the correct W:S ratio and checking for contaminants). For atomic-level insight, transmission electron microscopy (TEM) can directly image the WS_2 lattice, revealing the presence or absence of dislocations and grain boundaries; selected-area electron diffraction (SAED) in TEM can confirm if domains are epitaxially aligned or randomly oriented. Each of these techniques has its strengths: for example, Raman and PL mapping can non-destructively survey large areas to statistically evaluate uniformity and defect density, while high-resolution TEM can pinpoint atomic defects albeit on a small sampled region. Researchers can comprehensively assess the

quality of WS_2 monolayers by combining multiple characterization methods. This multifaceted analysis is crucial for diagnosing problems in MOCVD-grown WS_2 and iterating toward better synthesis conditions.

1.3 - Research Objectives

To address the nucleation control and film continuity challenges identified in Section 1.2, this study defines several key objectives aimed at characterizing and optimizing the MOCVD growth of monolayer WS_2 on c-plane sapphire. A primary goal is to systematically investigate how varying growth conditions affect the morphology of WS_2 domains, using AFM as the principal characterization tool. We examine the influence of substrate annealing conditions, including pre-growth high temperature annealing and a slight substrate miscut, on domain nucleation and alignment. Annealing the sapphire can introduce well-defined atomic step terraces that serve as preferential nucleation sites; thus, this study observes how substrate preparation impacts domain alignment along these steps and the epitaxial alignment of WS_2 islands on the wafer. Additionally, this study examines how nucleation-stage parameters, such as the nucleation temperature and ambient conditions during the initial MOCVD reaction, affect the density of WS_2 nuclei. By controlling the nucleation density, we directly influence the domain size, as a lower density of nuclei allows each domain to grow larger before impinging on its neighbours.

Another objective is to understand how lateral growth conditions – including the growth temperature ramp (implemented here as a two-step MOCVD process with a higher-temperature stage following the initial nucleation step), the precursor flow rates, and the

overall growth duration – govern the expansion and coalescence of WS_2 domains. These conditions determine the extent of lateral domain growth and, ultimately, the monolayer coverage – the fraction of the substrate surface that becomes covered by the WS_2 monolayer film. By optimizing growth parameters for maximal coalescence, we aim to achieve nearly continuous WS_2 monolayer coverage across the substrate while minimizing the formation of multilayer islands or voids.

To quantitatively evaluate these objectives, AFM is employed throughout this work to measure key morphological outcomes under each set of conditions quantitatively: the monolayer coverage, the nucleation density (domains per unit area), the lateral size distribution of domains, the alignment of domains along build-in steps, and the in-plane crystallographic orientation of domains relative to the substrate. Correlating these measurable properties with specific process conditions will elucidate the growth dynamics of WS_2 – for instance, revealing how higher nucleation temperatures might reduce nucleation density and yield larger domains, or how substrate miscut and annealing can induce aligned growth along step edges. Each of these parameters is chosen for its significance: monolayer coverage indicates how close we get to a wafer-scale continuous film, domain size and nucleation density together reflect the trade-off between having many small domains versus fewer large domains, and domain orientation uniformity is linked to the presence of grain boundaries (misoriented domains merging can form mirror-twin boundaries that act as electrical defects [1]). By meeting these objectives, the study will build a comprehensive understanding of how annealing, nucleation, growth, and coalescence conditions can be tuned to control WS_2 monolayer morphology on sapphire.

In addition to purely morphological investigations, a further objective is to highlight the potential practical benefits of achieving optimized WS_2 monolayers. These objectives collectively align with the broader efforts in the 2D materials community to produce wafer-scale, high-quality semiconductor films for advanced applications. While direct device fabrication or performance testing is beyond the scope of this thesis, the improvements in WS_2 monolayer coverage and alignment achieved here are discussed in terms of their implications for future device integration and performance. There is concerted interests in growing TMD monolayers over large areas with minimal defects, to enable integrating 2D materials into state-of-the-art electronic manufacturing [5]. By focusing on MOCVD process optimization, our work addresses a key aspect in TMD materials research and development – MOCVD is among the most viable methods for scalable production, so insights gained here contribute to the general roadmap for scaling up 2D semiconductors. Moreover, emphasizing the control of nucleation and the elimination of deleterious grain boundaries resonates with recent studies showing that high-performance devices (for instance, transistors with record carrier mobilities) are only attainable when the monolayer crystals have nearly perfect continuity and orientation uniformity [4,5].

1.4 - Thesis Structure

This thesis is organized into chapters forming a cohesive exploration of WS_2 monolayer growth and characterization. Below is a roadmap of the thesis structure, along with the contribution of each chapter to the overall study:

Chapter 1 – Introduction: This initial chapter establishes the importance and relevance of tungsten disulfide (WS_2) research within the rapidly evolving field of 2D materials. It highlights the technological and scientific motivations driving the study, outlines key research objectives, and delineates the specific scope of the investigation. Furthermore, it briefly discusses the anticipated contributions of this research towards enabling advanced electronic and optoelectronic applications.

Chapter 2 – 2D Materials: Here, the discussion broadens to encompass the extensive family of 2D materials beyond WS_2. The chapter details the discovery and fundamental properties of various prominent 2D materials, including graphene, phosphorene, hexagonal boron nitride (h-BN), TMDs, and MXenes. Special attention is given to these materials' unique electronic, optical, mechanical, and chemical properties, providing a comparative perspective that contextualizes the advantages and limitations of WS_2 relative to other well-known materials.

Chapter 3 – Background: This chapter discusses the intrinsic properties and specific characteristics of WS_2. It covers aspects such as the crystal structure, electronic band structure, bandgap engineering, excitonic effects, and mechanical robustness of WS_2 monolayers. Additionally, it reviews the primary growth methods for synthesizing WS_2, highlighting CVD, MOCVD, and mechanical exfoliation, while also addressing the associated synthesis challenges, including defects and substrate interactions.

Chapter 4 – Literature Review of WS_2 Monolayer Synthesis, Characterization, and Applications: This comprehensive review chapter situates the current research within

existing literature, critically analyzing prior studies on WS_2 monolayer synthesis methods, characterization approaches, and various technological applications. It emphasizes recent advancements, state-of-the-art experimental techniques, and cutting-edge applications such as electronics, optoelectronics, valleytronics, flexible electronics, and catalysis. This chapter identifies knowledge gaps and underscores the contribution of the current research towards addressing these gaps.**Chapter 5 – Methodology:** Focused on the experimental procedures undertaken in this research, this chapter describes the methodology employed. Detailed descriptions of the MOCVD system, growth conditions, precursor chemistry, and substrate preparation techniques are provided. Additionally, this chapter covers the characterization methodologies, primarily focusing on AFM imaging techniques used for topographical analysis and the ImageJ image analysis approach, which is utilized to quantitatively assess monolayer coverage, nucleation density, and domain size distributions.

Chapter 6 – Experimental Results: As the core of the thesis, this chapter details experimental findings obtained from systematic MOCVD growth experiments. It presents comprehensive data on the influence of varying growth parameters, including annealing temperature, nucleation temperature, nucleation duration, and lateral growth duration. Key results discussed include the achieved WS_2 monolayer coverage percentages, nucleation density trends, domain size distributions, domain orientation relative to substrate miscut directions, and step-edge impacts. In-depth analyses and visual representations (AFM images and quantitative graphs) support clear interpretation and discussion of the results,

providing valuable insights into the optimized conditions necessary for large-area WS_2 growth.

Chapter 7 – Discussion and Conclusion: The final chapter synthesizes the key experimental insights and discusses their broader scientific and technological implications. It critically evaluates how the achieved results align or diverge from existing literature, highlighting significant advancements in WS_2 growth techniques and identifying limitations and areas for future improvement. Concluding the thesis, this chapter suggests directions for further optimization of growth conditions, exploration of alternative substrates, potential application-specific optimizations, and advanced characterization methods, reinforcing the importance of continued research efforts toward realizing large-scale, high-quality WS_2 monolayers suitable for next-generation technological applications.

Chapter 2 - 2D Materials

2.1 - Introduction

The discovery of graphene in 2004 ushered in a new era of 2D materials research [6]. Since then, over a hundred distinct 2D materials have been identified, spanning metallic, semiconducting, and insulating types [7], and high-throughput computations suggest more than 1800 layered compounds could potentially be exfoliated into atomically-thin sheets [8]. These materials exhibit diverse electronic, optical, and mechanical properties, often unattainable in bulk form [9]. In the following, we survey the major families of 2D materials, including elemental monolayers, TMDs, h-BN, MXenes, and other emerging materials, discussing their unique properties, applications, and synthesis challenges. We then focus on recent advances in the growth of one notable 2D material (WS_2) by MOCVD, highlighting key experimental and theoretical developments.

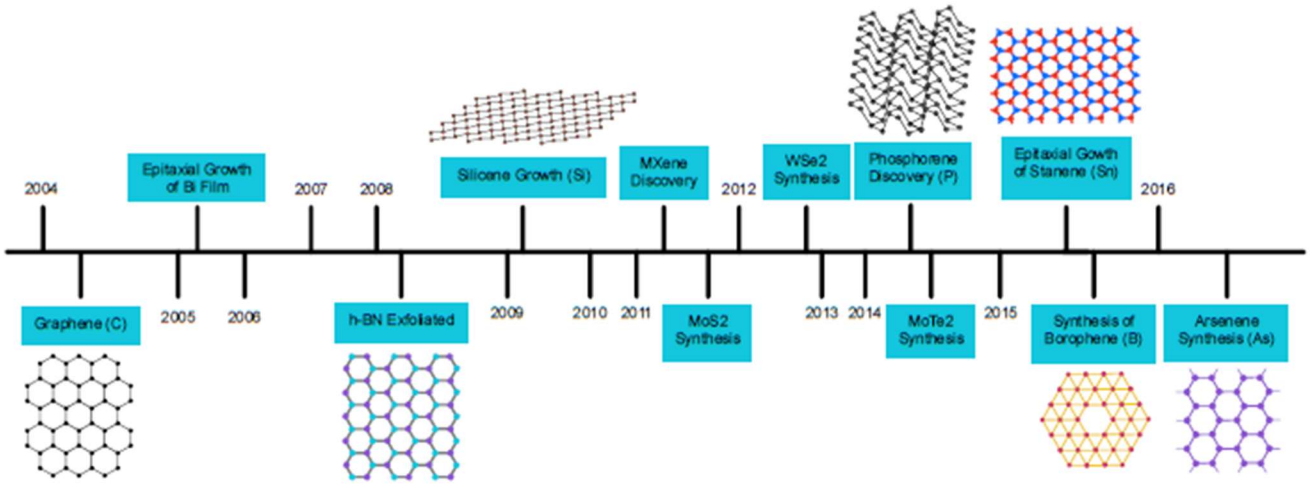

Figure 2.1: Timeline of major 2D materials discovered or synthesized following the isolation of graphene in 2004.

2.2 - Graphene

Graphene is a single layer of sp^2-bonded carbon atoms arranged in a honeycomb lattice, and it was the first 2D material isolated from graphite [6]. It possesses extraordinary properties: a high specific surface area (~2600 m^2/g), ultrahigh carrier mobility (~200,000 $cm^2/V{\cdot}s$), excellent thermal conductivity (3000–5000 W/m·K), optical transparency (~97%), and exceptional mechanical strength (Young's modulus ~1 TPa) [10]. These attributes make graphene promising for high-speed electronics, transparent conductors, composites, and sensor applications [10]. However, graphene is a zero-bandgap semimetal – its conduction and valence bands meet at the Dirac points, resulting in no intrinsic bandgap [10]. This absence of a bandgap poses a challenge for digital electronics requiring an off-state, prompting extensive research into bandgap engineering (e.g. bilayer (BL) graphene with an applied field, graphene nanoribbons) [10]. Despite this, graphene's combination of

conductivity and strength has already led to applications in RF electronics, flexible displays, and composite materials [10].

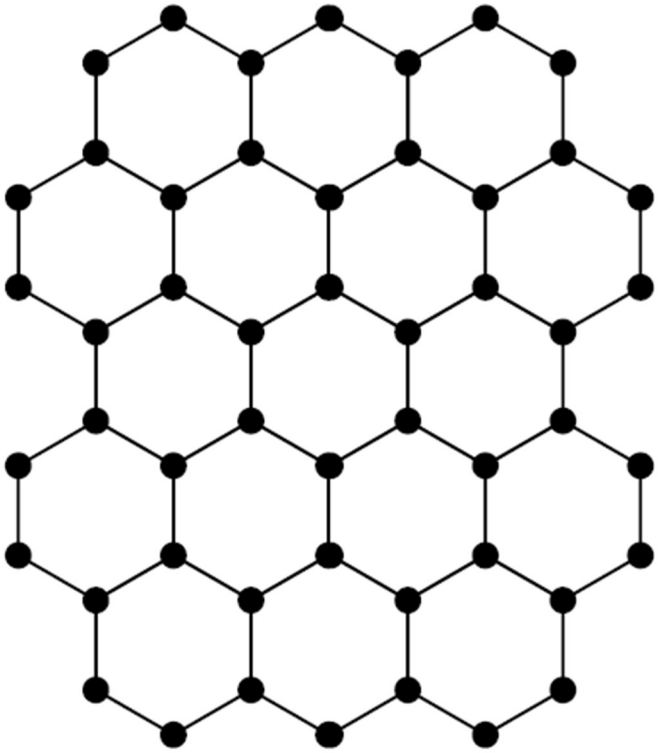

Figure 2.2: Atomic Structure Representation of Graphene.

2.3 - Phosphorene

Phosphorene, a monolayer of black phosphorus first isolated in 2014, is another elemental 2D material with distinct characteristics. Unlike graphene, phosphorene is a semiconductor with a direct bandgap (~1.5–2.0 eV in monolayer, ~0.3 eV in bulk) that enables efficient PL and transistor switching. Its crystal structure is puckered, yielding highly anisotropic properties – charge transport, optical response, and mechanical strength differ along the armchair vs. zigzag in-plane directions [11].

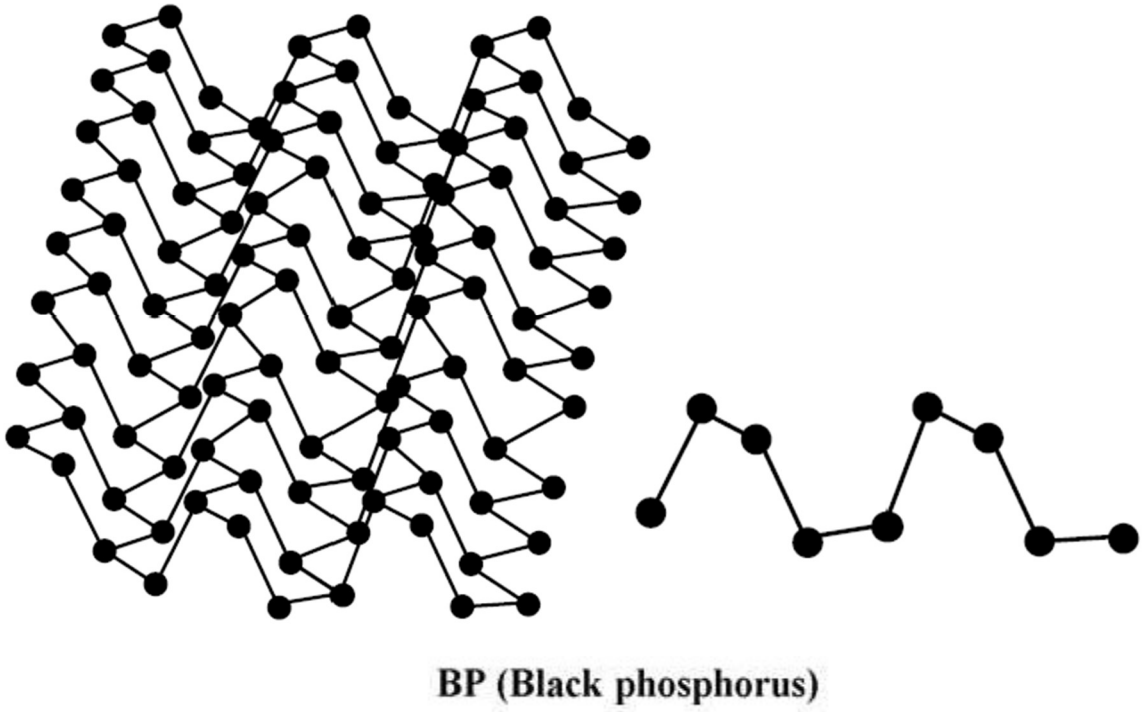

Figure 2.3: Atomic Structure Representation of Black Phosphorus (Phosphorene).

This intrinsic anisotropy, absent in the symmetric honeycomb lattice of graphene or the hexagonal lattice of many TMDs, can be exploited in polarized photodetectors and direction-dependent devices [11]. Phosphorene also exhibits reasonably high carrier mobilities (up to a few hundred $cm^2/V{\cdot}s$ in few-layer form) and has garnered interest for field-effect transistors (FETs), sensors, and photovoltaics. A significant challenge, however, is its environmental instability – thin black phosphorus layers degrade in ambient conditions by reacting with oxygen, moisture, and light. This degradation leads to oxidized byproducts and mobility loss, limiting practical use unless protective encapsulation (e.g. in h-BN) or passivation strategies are employed. Current research on phosphorene includes theoretical studies on strain-

tuning (where its bandgap is modulated) and experimental efforts to improve stability (for example, coating with Al_2O_3 or storing in inert atmospheres).

2.4 - Transition Metal Dichalcogenides

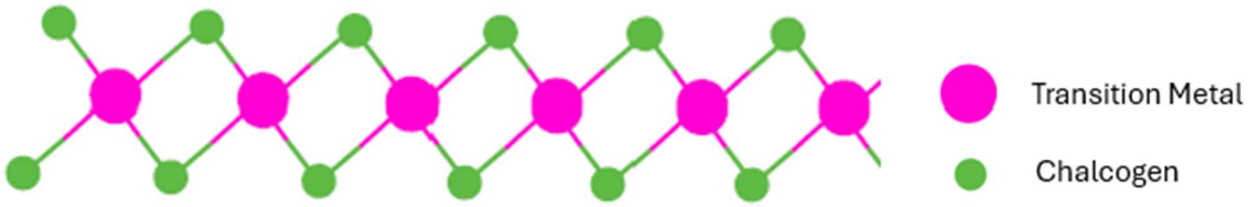

Figure 2.4: Atomic structure representation of Transition Metal Dichalcogenides (sideview), where the middle plane is the transition metal and the top-bottom planes are chalcogens.

TMDs are a broad class of 2D compounds with the formula MX_2, where M is a transition metal (Mo, W, etc.) and X is a chalcogen (S, Se, Te). Each monolayer consists of a plane of metal atoms sandwiched between two planes of chalcogen atoms. Unlike graphene's zero-gap semimetallicity, TMD monolayers have finite bandgaps, typically in the visible or near-IR range [6]. For example, MoS_2 and WS_2 monolayers have direct bandgaps (~1.8–2.0 eV), making them well-suited for transistor channels and optoelectronic devices [6]. A remarkable feature of many TMDs is that their bandgap is thickness-dependent – a bulk TMD (indirect-gap semiconductor) often becomes direct-gap when thinned to a single layer, enabling layer-tunable optical and electronic properties [6].

Monolayer TMDs exhibit strong light–matter interactions and robust excitonic effects (binding energies hundreds of meV), leading to bright PL and efficient photodetection. They also possess moderately high carrier mobilities (tens to hundreds of $cm^2/V{\cdot}s$) – while lower

than graphene's, these are sufficient for many electronic applications and come with the advantage of an intrinsic bandgap. TMDs like MoS_2 have been made into ultrathin FETs that can achieve high on/off ratios ~10^8, proving their viability for low-power electronics. Their mechanical flexibility and strength make TMDs attractive for flexible and transparent electronics. Additionally, certain TMDs harbor unique spin–valley coupled physics arising from strong spin–orbit coupling in non-centrosymmetric lattices (notably in WSe_2, WS_2), which enables valleytronic applications where information is encoded in the valley index of electrons [9]. Beyond semiconductors, some TMDs can exhibit superconductivity (e.g. $NbSe_2$ monolayers are Ising superconductors) or charge density waves, especially in metallic or 1T polymorphs. These phenomena highlight the richness of TMD physics.

Experimentally, many TMDs can be exfoliated from layered bulk crystals (e.g. MoS_2, $MoSe_2$, WS_2, WSe_2 are found in nature as molybdenite, etc.), and large-area synthesis has been achieved via CVD and MOCVD. Synthesis challenges include controlling the layer number, grain size, and phase purity. TMD monolayers synthesized via common methods like CVD and MOCVD often form polycrystalline films due to the nucleation and growth kinetics involved in deposition processes, unless specific measures such as epitaxial growth on oriented substrates or controlled nucleation density are employed. Point defects (sulfur vacancies, etc.) are common in CVD-grown TMDs and can quench optical emission or degrade device performance. Ongoing research addresses these issues with advanced growth techniques (see the WS_2 MOCVD section below) and passivation methods. Despite the challenges, steady progress in TMD growth has enabled wafer-scale electronics and

heterostructures; for instance, heterogeneous integration of monolayer MoS_2 transistors on Si circuits has been demonstrated for ultra-scaled devices.

2.5 - Hexagonal Boron Nitride (h-BN)

Often nicknamed “white graphene”, h-BN is a 2D material consisting of alternating boron and nitrogen atoms in a planar hexagonal lattice [12]. Structurally, it resembles graphene, but in contrast it is an electrical insulator with a wide bandgap of ~5.9 eV [6]. This large bandgap and its excellent thermal and chemical stability distinguish h-BN as an ideal supporting material and dielectric in 2D electronics. Indeed, h-BN is noted for its mechanical robustness, high thermal conductivity, and chemical inertness. It remains stable even at high temperatures or in harsh environments where other 2D materials might oxidize or decompose.

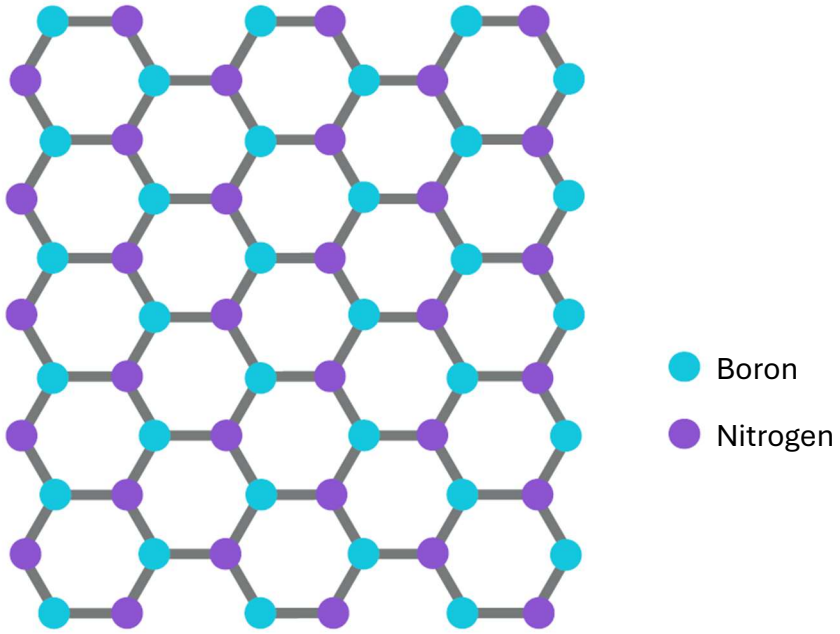

Figure 2.5: Atomic Structure Representation of Hexagonal Boron Nitride.

Key applications of monolayer or few-layer h-BN include serving as an ultra-flat substrate and encapsulating layer for other 2D materials. Because h-BN has no dangling bonds on its surface and is atomically smooth, graphene or TMD monolayers placed on h-BN show enhanced mobility and reduced charge inhomogeneity (h-BN screens charged impurities) [6,7]. In addition, h-BN's high breakdown field and low leakage currents make it an excellent nano-dielectric – for example, it has been used as the gate insulator in graphene transistors and as tunneling barriers in nano-devices [6]. Recent research also exploits defects in h-BN as single-photon emitters for quantum optics, since point defects (like carbon or vacancies) in h-BN can act as quantum light sources even at room temperature.

From a synthesis perspective, 2D h-BN can be exfoliated from bulk h-BN crystals or grown by CVD on metal foils (similar to graphene growth). Achieving large single-crystalline h-BN domains is an active area of work; advances have been made (e.g. epitaxial growth on molten gold, or using BN seeding techniques) but typically h-BN domains are smaller than graphene domains under similar growth conditions. Nonetheless, multi-inch wafer-scale h-BN has been demonstrated via CVD, which is crucial for integrating h-BN in semiconductor manufacturing processes. Overall, h-BN's role as the insulating counterpart in the 2D material family is well established – it is often the indispensable "supporting actor" that enables the stellar performance of other 2D materials in heterostructures [6].

2.6 - MXenes

MXenes are a rapidly growing family of 2D materials discovered in 2011 [13], distinguished by their transition metal carbides, nitrides, or carbonitrides composition. MXenes are

typically produced by etching out the “A” element from layered MAX phase precursors (M: early transition metal, A: group 13 or 14 element, X: C and/or N) [6]. For example, $Ti_3C_2T_x$ – the most studied MXene – is derived from Ti_3AlC_2 by selectively etching aluminum atoms and delaminating the layers. The resulting monolayers of MXene have the formula $M_nX_{n-1}T_x$, where T_x represents surface termination groups (O, OH, F, etc.) from the etching process.

MXenes combine metallic electrical conductivity (in many cases) with hydrophilicity, owing to their hydroxyl or oxygen terminated surfaces [6]. This rare mix of traits makes them attractive for electrochemical applications – unlike graphene (which is conductive but not intrinsically hydrophilic), MXenes can disperse in water and interact with ions readily, while still offering high conductivity. Their chemistry is highly tunable; a wide range of transition metals (Ti, V, Nb, Mo, etc.) and variable surface terminations allow the properties of MXenes to be adjusted. MXenes generally exhibit outstanding electronic, optical, and mechanical properties, and their surface chemistries can be engineered for specific functions [14]. They are also mechanically robust and stable in ambient conditions, with many MXenes showing stability in colloidal form or as films [14].

A challenge for MXenes is that the wet chemical etching often yields small flakes and can introduce defects or non-uniform terminations. Achieving large-area, single-crystalline MXene sheets is not straightforward via current synthesis routes. There are efforts to improve MXene quality by mild etchants or alternative approaches (e.g. bottom-up deposition of carbide films then etching). Another practical challenge is preventing MXene oxidation; many MXenes (especially those with Ti) will slowly oxidize in water or air to form oxides, which can diminish their performance. Storing MXenes in inert environments or with

antioxidant additives is an active area of research. Despite these challenges, MXenes' rapid emergence and impressive performance in multiple domains have solidified their status as a leading 2D material family [14].

2.7 - Emerging 2D Materials

Beyond the well-established families above, there is a growing list of emerging 2D materials with novel compositions and properties. In addition to graphene and phosphorene, researchers have synthesized or theoretically predicted monolayers of silicon (silicene), germanium (germanene), tin (stanene), and others. These 2D allotropes typically require specific growth conditions (e.g., silicene epitaxially grown on Ag(111) surfaces under ultrahigh vacuum conditions [15]) and tend to exhibit lower stability compared to graphene. Stanene and germanene have been predicted to exhibit topological insulating behavior at low temperatures [16], and silicene-based field-effect transistors have been experimentally demonstrated, although stability under ambient conditions remains challenging. Likewise, monolayers of arsenic (arsenene) and antimony (antimonene) have been successfully grown using molecular beam epitaxy (MBE), exhibiting semiconducting properties and potential applications in electronics and thermoelectrics [17]. Although exfoliation from bulk crystals of these materials has been reported (e.g., exfoliation of antimonene nanosheets from bulk antimony crystals [18]), it remains less common due to challenges related to stability and layer uniformity. Consequently, many of these "Xenes" remain in the early stages of research and development.

Apart from h-BN, borophene is an exciting material–a boron atom monolayer. Borophene does not occur naturally and was first synthesized on silver surfaces in 2015 [19]. It has a metallic character and exhibits diverse polymorphs (due to boron's electron deficiency, it can form various arrangements). Borophene is lightweight, conductive, and has shown superconductivity at low temperatures, but it is also chemically reactive and can only be made on substrates under vacuum. If methods to stabilize free-standing borophene are identified, its high theoretical capacity for Li storage and anisotropic conductivity could be exploited.

Certain layered oxides can be exfoliated into monolayers, though many are non-layered (making 2D fabrication challenging). Examples include monolayer V_2O_5 (a layered oxide useful for batteries) and bismuth oxyhalides like BiOCl, BiOBr, which have a natural structure and can form 2D nanosheets [20]. These tend to be wide-bandgap semiconductors with applications in photocatalysis (e.g. BiOCl is active under UV for pollutant degradation). Additionally, layered double hydroxides (LDHs) can be delaminated into positively charged 2D sheets and used in catalysis and as anion exchangers [20].

An emerging frontier is purely organic 2D materials such as 2D polymers and covalent organic frameworks (COFs), as well as metal–organic frameworks (MOFs) in layered form. These can in principle yield single-layer sheets held together by strong in-plane covalent bonds or coordination bonds. For instance, 2D MOFs have been synthesized where metal nodes and organic linkers form a sheet; these can have designer pores and functionalities for membranes or sensing. Graphene analogues like graphitic carbon nitride (g-C_3N_4), which

is a 2D network of carbon and nitrogen, have attracted interest in photocatalysis and CO_2 reduction due to their semiconducting nature and chemical stability [20].

Recent breakthroughs have expanded 2D materials into magnetic and topologically non-trivial realms. In 2017, the first intrinsic 2D magnet was discovered: monolayer CrI_3 was found to be a ferromagnet with $T_C \approx 45$ K [9], demonstrating that magnetic order can exist in a single layer (via magnetic anisotropy overcoming the Mermin–Wagner theorem [9]). Concurrent studies also demonstrated intrinsic magnetism in other 2D materials such as $Cr_2Ge_2Te_6$ (CGT) [21] and Fe_3GeTe_2 (FGT) [22], which hold promise for ultrathin spintronic devices. Likewise, 2D materials with non-trivial band topology have been identified – for example, monolayer WTe_2 was experimentally confirmed as a quantum spin Hall insulator, exhibiting robust edge states. Additionally, monolayer bismuthene on SiC substrates was engineered to be a large-gap 2D topological insulator. Furthermore, some layered superconductors like $NbSe_2$ retain superconductivity down to monolayer thickness, exhibiting Ising pairing protected by spin–orbit fields [23]. These examples illustrate that 2D materials now encompass virtually every major materials category: metals, semiconductors, insulators, magnets, superconductors, and topological matter. Comprehensive review articles summarizing recent advances and perspectives on these emerging 2D phenomena are available in the literature [24]. Heterostructures of different 2D layers (assembled like “atomic Lego”) further enable new properties, such as proximitized superconductivity or moiré physics, which are at the cutting edge of condensed matter research.

Chapter 3 – Background and Literature Review

3.1 - Fundamental Properties of WS_2

WS_2 is a layered transition metal dichalcogenide (TMD) composed of sheets of W atoms sandwiched between S atoms in an S–W–S arrangement. The most stable configuration is the 2H phase (hexagonal, also noted as 1H for a single layer), where W atoms occupy trigonal prismatic coordination sites, yielding a semiconducting structure [25]. In contrast, WS_2 can also exist in a metastable 1T phase (octahedral coordination) and a distorted 1T' phase; these phases are metallic or semi-metallic in character [25]. Phase transitions between 2H and 1T can be induced by external treatments (e.g. chemical intercalation or strain), but at ambient conditions the 2H phase is dominant due to its lower energy. The ability to form different allotropes means WS_2 can exhibit dramatically different electrical behavior (semiconducting vs. metallic) depending on its phase, a feature it shares with other group-6 TMDs like MoS_2 [25].

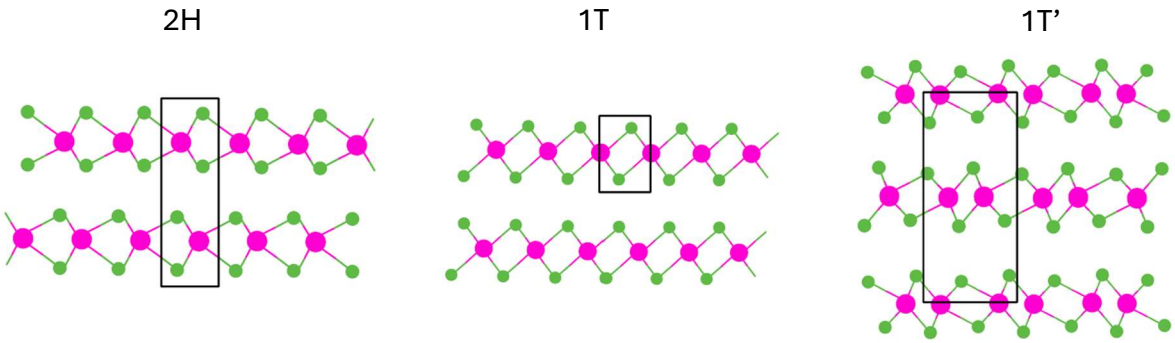

Figure 3.1 : Common polymorphs of TMDs: 2H (semiconducting), 1T (metallic), and 1T' (semi-metallic)

Monolayer WS_2 is a direct bandgap semiconductor with an optical gap of about 2.0 eV [26]. When thinning down to a monolayer, this transition from indirect to direct gap leads to a pronounced PL in monolayer WS_2. In fact, monolayer WS_2 exhibits a PL quantum yield roughly three orders of magnitude higher than its bulk form. Notably, WS_2's PL intensity is observed to be much stronger than that of MoS_2 under similar conditions – WS_2 can have ~20× higher PL yield than MoS_2, making it particularly attractive for optoelectronic devices that require efficient light emission [27]. The band structure of WS_2 (and related TMDs) features band extrema at the Brillouin zone K-points for monolayers, giving a direct gap, while the bulk's valence band maximum shifts to the Γ-point, causing the indirect gap. WS_2 also exhibits significant spin–orbit coupling due to the heavy W atom, leading to a large splitting between its spin-up and spin-down valence subbands. This splitting (hundreds of meV) is larger than in MoS_2, and is comparable to WSe_2, and results in two prominent excitonic transitions (labeled A and B excitons). Overall, compared to other TMDs, WS_2 has a relatively larger bandgap (e.g. MoS_2 monolayer ~1.8–1.9 eV, WSe_2 ~1.65 eV) and strong spin–orbit effects, which can influence its electronic and optical behavior. Monolayer WS_2 displays strong optical absorption and emission in the visible range owing to its direct gap and robust excitonic effects. The reduced dimensionality and dielectric screening lead to tightly bound excitons with large binding energies on the order of 0.3–0.7 eV in WS_2 and similar TMDs, meaning the excitonic peaks dominate the optical spectra even at room temperature. WS_2's exciton (often called the A exciton at ~625 nm wavelength for monolayers) and a higher-energy B exciton (due to the split valence band) give distinct absorption/PL peaks. The direct bandgap and non-centrosymmetric crystal structure of monolayer WS_2 also enable strong

second-harmonic generation (SHG) and unique valley-selective optical selection rules. Like MoS_2 and WSe_2, monolayer WS_2 can exhibit valley polarization – carriers in K and K' valleys can be addressed by circularly polarized light, a helpful feature for valleytronic applications. The combination of a high radiative recombination rate and large exciton binding energy makes WS_2 one of the brightest TMD monolayers in PL, advantageous for photonic and excitonic devices.

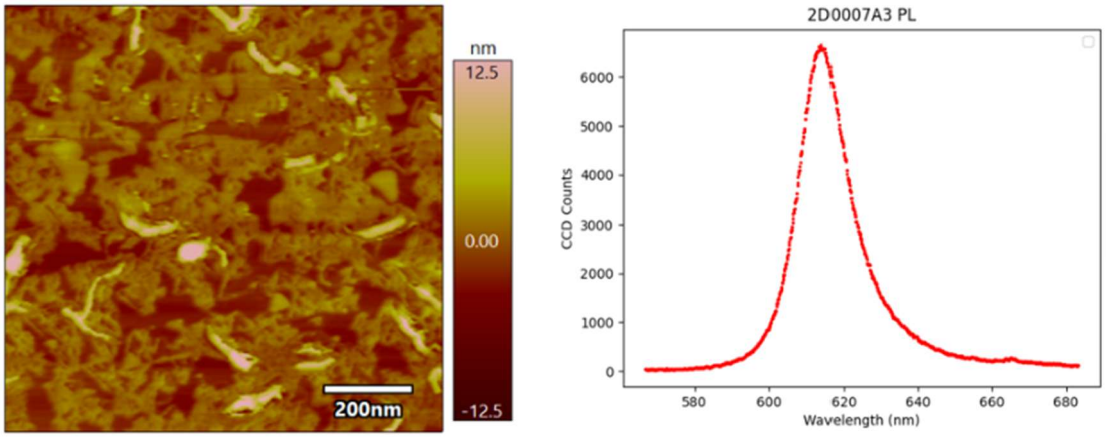

Figure 3.2: Representative photoluminescence (PL) spectrum of monolayer WS_2 exhibiting a sharp excitonic peak near 620 nm (~2.0 eV). The sample was grown on a sapphire substrate, where it was annealed at 1050 °C for 30 minutes, nucleated at 700 °C for 15 minutes, and had lateral growth at 820 °C for 100 minutes. Here, the peak has a CCD count of around 6200 compared to 2600 in Figure 1.2

Despite being only three atoms thick, WS_2 is mechanically robust and flexible. It is among the strongest TMDs, with a single-layer Young's modulus exceeding 300 GPa [28], comparable to or higher than monolayer MoS_2. This high stiffness and inherent flexibility allow WS_2 films to tolerate substantial strain before failure, making them suitable for flexible

electronics. WS_2 monolayers can be bent or stretched while largely maintaining structural integrity, and they can conform to substrates or bend in flexible devices. Applying strain is a powerful tool to engineer WS_2's properties: theoretical and experimental studies show that tensile strain can significantly modulate the bandgap, even potentially turning the semiconducting 2H phase into a metallic phase at large strain values [29]. Even a few percent of biaxial tensile strain tends to reduce the bandgap (for example, a 2% strain can shift optical transition energies noticeably). In contrast, compressive strain could increase the bandgap slightly or induce phase changes in extreme cases. Furthermore, strain alters phonon frequencies and can change exciton dynamics (e.g. creating strain-localized excitons). The ability to withstand strain and the pronounced strain-tunability of its band structure underscore WS_2's attractiveness for strain-engineered devices and flexible nanoelectronics.

3.2 - Overview of 2D Material Growth Techniques

Two-dimensional materials like WS_2 can be produced by several methods, each with its advantages and limitations. The most common techniques are mechanical exfoliation, CVD, and MOCVD. Below we compare these methods and highlight why MOCVD is particularly promising for WS_2 synthesis.

Mechanical exfoliation, commonly known as the "Scotch tape" method, involves peeling thin layers from bulk WS_2 crystals. It was crucial in early 2D materials research because it yields pristine, high-quality monolayers with low defect density. However, exfoliation is random and not scalable – flake sizes are usually limited to tens of microns and they appear

at arbitrary locations and thicknesses [3]. Lack of uniformity across large areas makes mechanical exfoliation inadequate for applications requiring wafer-scale coverage [3]. It remains useful for fundamental studies and device prototypes where quality is paramount and only small areas are needed.

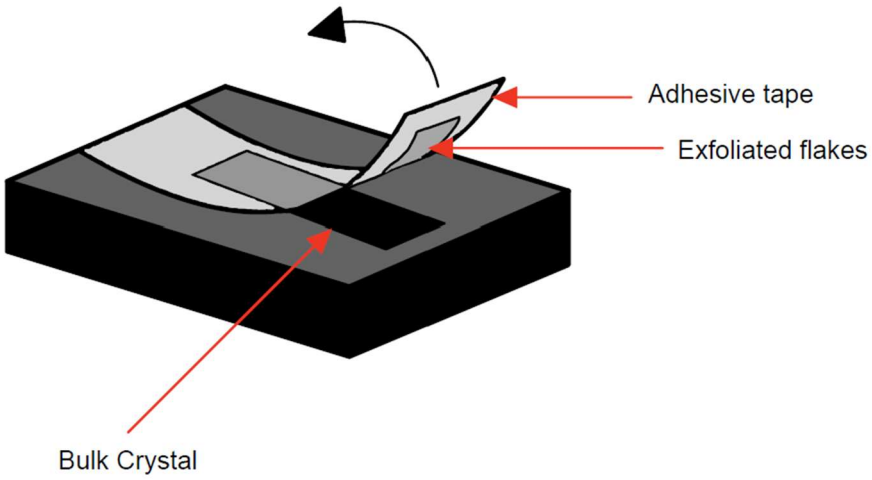

Figure 3.3: Illustration of the mechanical exfoliation process (Scotch tape method) used to isolate thin layers of 2D materials from a bulk crystal.

CVD has become a popular "bottom-up" synthesis route for large-area WS_2 and other TMD films [3]. In a typical CVD process, vapor-phase precursors (such as WO_3 or WCl_6 for tungsten and S or H_2S for sulfur) are reacted at high temperature in a furnace to deposit WS_2 on a substrate [3]. CVD can produce continuous monolayer films or networks of crystal domains over centimeter to wafer scales, far beyond what exfoliation can do. However, the quality of CVD-grown WS_2, while good, is often lower than exfoliated flakes – CVD films can

be polycrystalline or have more defects, and achieving uniform monolayer thickness without any multilayer islands can be challenging [3]. Growth parameters like substrate choice, temperature profile, and gas flow greatly influence the result [3]. Overall, CVD offers scalability but typically trades off some crystal perfection and uniformity when compared to mechanical exfoliation [3].

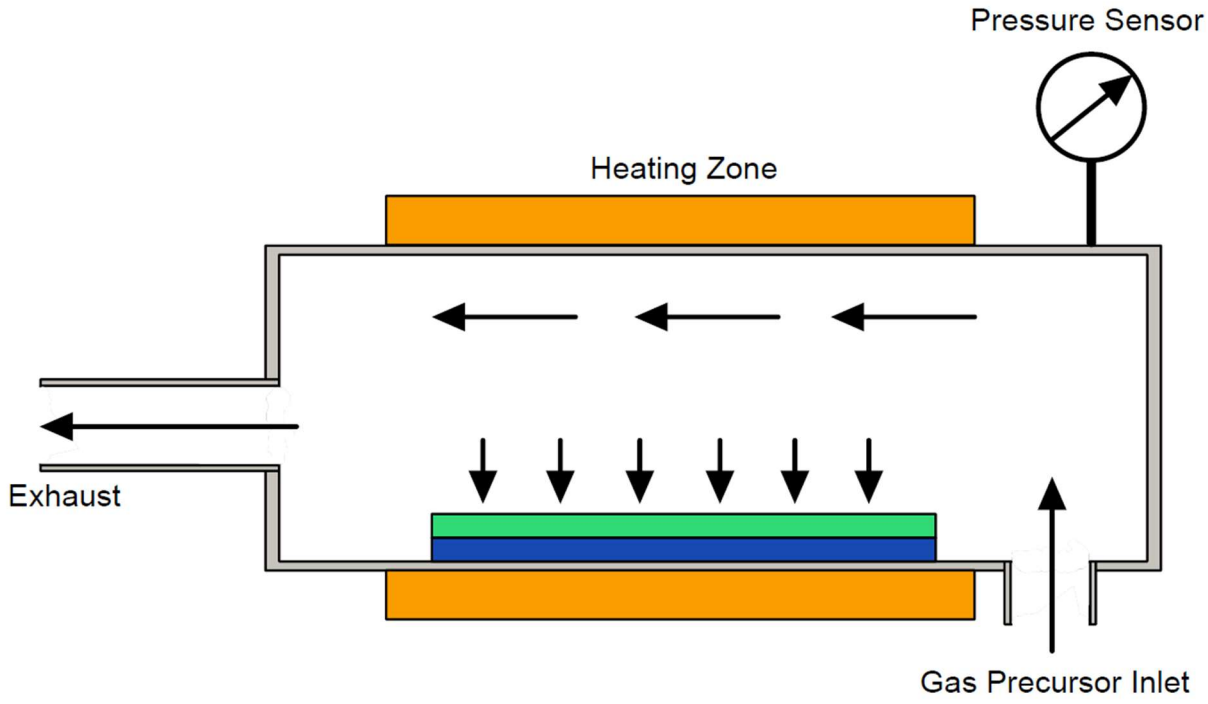

Figure 3.4: Schematic illustration of the Chemical Vapor Deposition (CVD) process for the synthesis of 2D materials.

MOCVD is a variant of CVD that uses metal-organic precursors (molecules containing the metal to be deposited) delivered in gas form. In the context of 2D WS_2, MOCVD has emerged more recently as a method to achieve wafer-scale growth with excellent uniformity [3]. During MOCVD growth, organometallic precursors (e.g. tungsten hexacarbonyl for W) and a reactive gas (e.g. Di-tert-butyl sulfide (DTBS) or organic sulfides for S) are introduced into a

reactor where they decompose on a hot substrate, leading to layer-by-layer WS_2 deposition [3]. The use of gas precursors affords precise control over the stoichiometry and partial pressures of each reactant, improving reproducibility and thickness control. MOCVD has demonstrated the ability to produce uniform monolayer WS_2 on entire wafers (in some reports up to 2–4 inch substrates) with electronic performance approaching that of exfoliated materials. For example, Kang *et al.* grew continuous WS_2 monolayers directly on SiO_2/Si over a 4-inch wafer via MOCVD, achieving electron mobilities of approximately 30 cm^2/V·s with less than 10% variation in mobility across the wafer surface, highlighting its exceptional uniformity [6]. The key advantage of MOCVD is its compatibility with semiconductor manufacturing – it offers large-scale, conformal coverage and can be adapted for heterostructures or doping by introducing different vapor precursors. Additionally, MOCVD often allows lower growth temperatures compared to thermal CVD because metal-organic precursors can decompose at more modest temperatures [30]. This can be beneficial for integrating WS_2 with substrates that have lower thermal budgets.

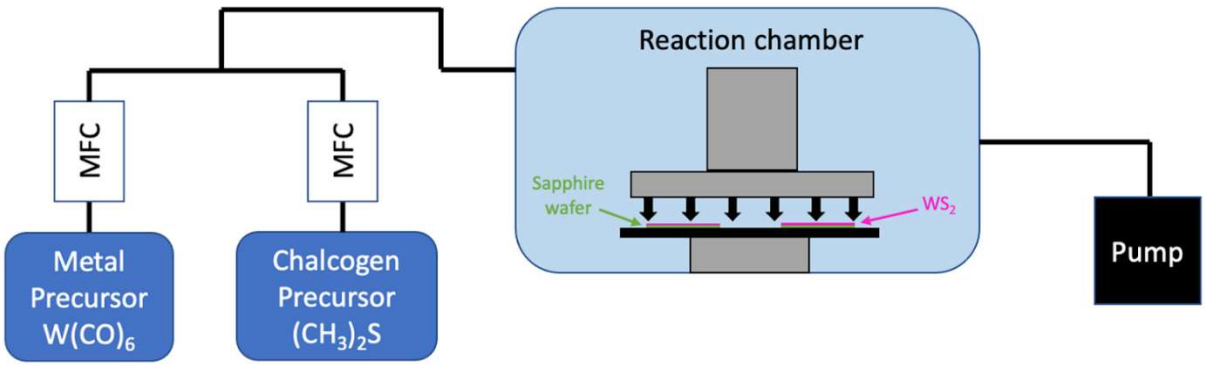

Figure 3.5: Schematic illustration of the Metal-Organic Chemical Vapor Deposition (MOCVD) process for the synthesis of 2D materials , highlighting precursor delivery via Mass Flow Controllers (MFCs).

MOCVD combines some of the quality benefits of bottom-up growth with the scalability of industrial processes. Unlike mechanical exfoliation, it can produce films on full wafers in a single run. Compared to conventional CVD, MOCVD provides more uniform and continuous monolayer coverage on large areas, precise control over precursor fluxes and ratios, which helps in tuning the nucleation density and stoichiometry [30], and the possibility of introducing dopants or alloying elements during growth by using appropriate precursors (for instance, adding a gas with a dopant element). MOCVD systems often use a cold-wall reactor design to limit unwanted deposition on chamber walls, improving material utilization and run-to-run consistency. Additionally, MOCVD can be adapted to grow on various substrate types (sapphire, SiO_2/Si, metals, etc.) by tailoring surface pre-treatments and precursors, which is valuable for integrating WS_2 into different device platforms.

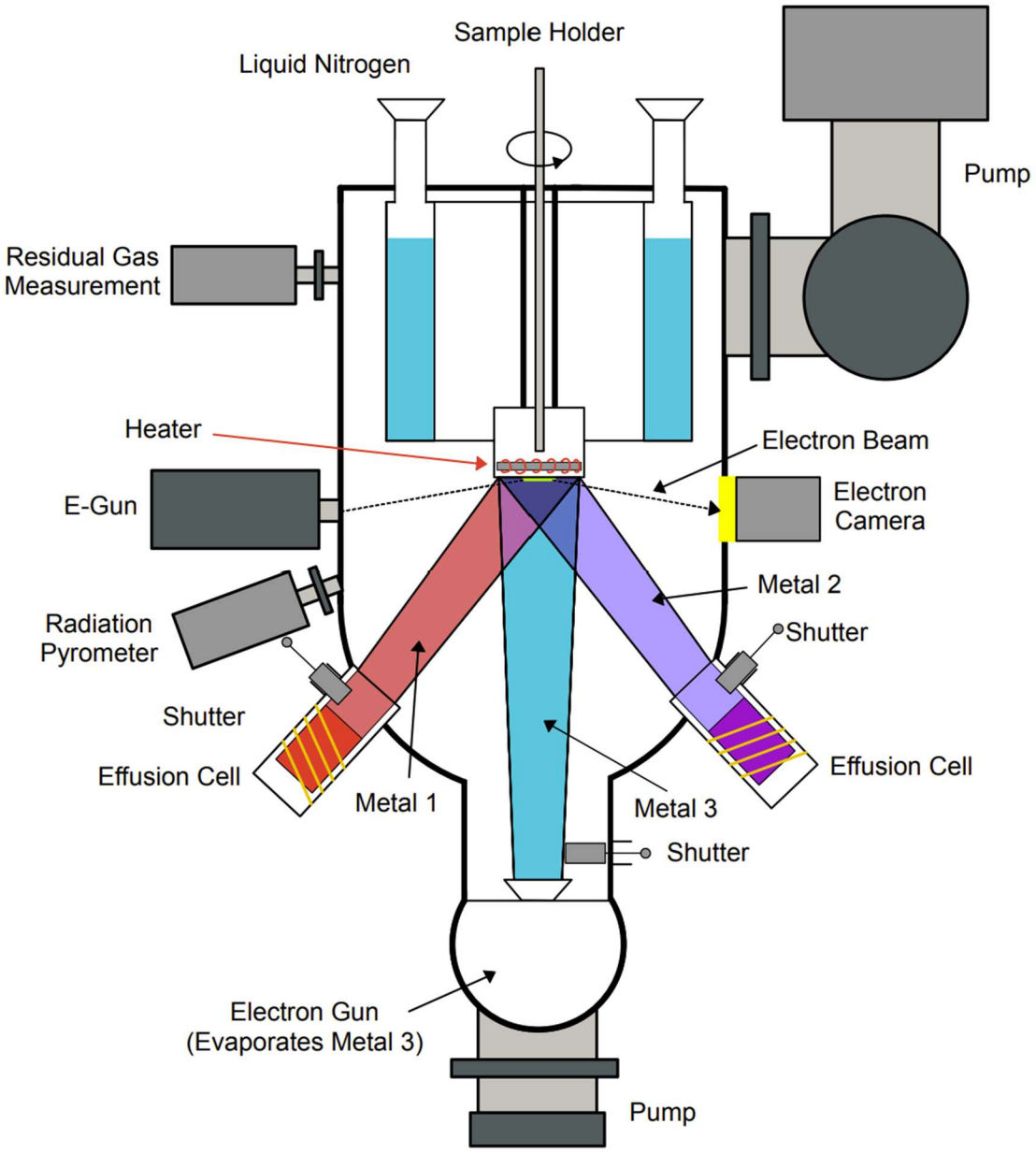

Figure 3.6: Schematic illustration of the Molecular Beam Epitaxy (MBE) process for the synthesis of 2D materials.

Molecular Beam Epitaxy (MBE) is another technique employed for the synthesis of high-quality WS_2 monolayers, offering precise control over thickness, composition, and

crystallinity. In MBE, elemental sources (such as tungsten and sulfur) are thermally evaporated in ultra-high vacuum (UHV) and deposited onto a heated substrate in a layer-by-layer fashion. Unlike CVD and MOCVD, which rely on chemical precursors, MBE uses physical vapor sources, allowing for cleaner growth with fewer impurities and greater atomic precision. This technique is particularly suited for fundamental studies and heterostructure engineering, as it provides atomic-layer control and abrupt interfaces. For instance, a recent study demonstrated the growth of epitaxial monolayer WS_2 on Ag(111) using MBE, showing high crystallinity and well-aligned domains due to strong interaction with the substrate [31].

Beyond CVD and MOCVD, emerging methods are being explored to overcome specific growth challenges. One such method is plasma-enhanced atomic layer deposition (PE-ALD), which uses alternate self-limiting surface reactions to build films one atomic layer at a time. While PE-ALD of WS_2 is still in early stages, it offers extremely uniform growth at lower temperatures, which could be beneficial for integrating WS_2 on temperature-sensitive substrates.

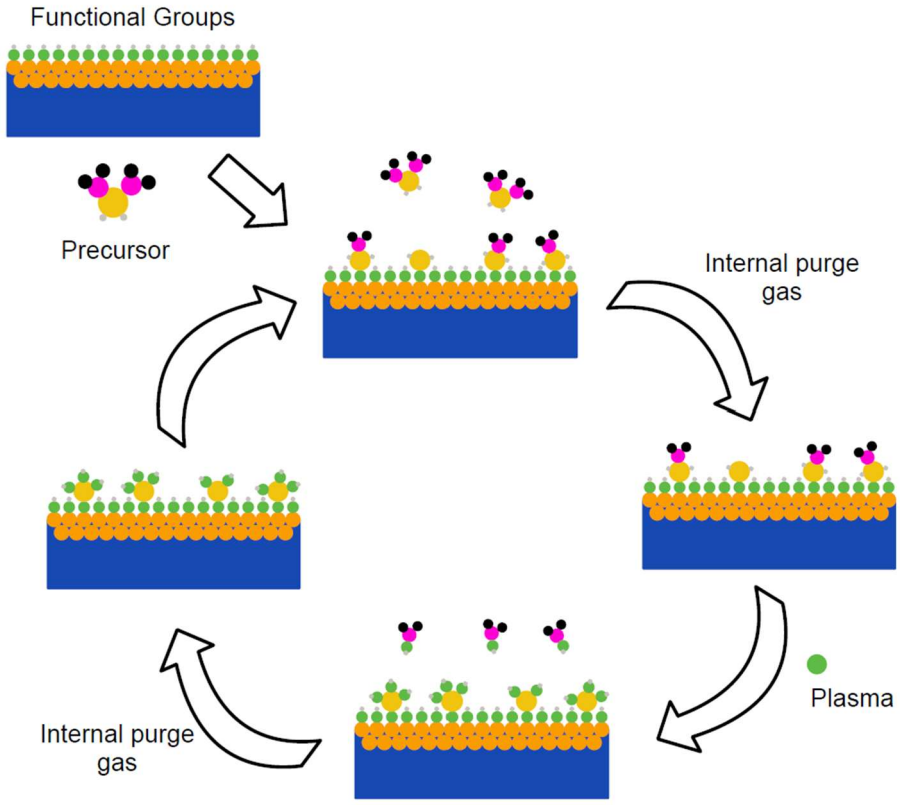

Figure 3.7: Cyclic schematic of the plasma-enhanced atomic layer deposition (PE-ALD) process.

Recently, sputtering has been developed to directly deposit WS_2 films: for example, sputtering of a WS_2 target onto heated substrates can yield monolayer or few-layer WS_2 over large areas [32]. Such physical vapor deposition (PVD) approaches confirm the feasibility of wafer-scale WS_2, but controlling layer number and phase requires further fine tuning. Chemical routes like sulfurization of solution-deposited films (e.g. spin-coated tungstic acid [32] or peroxotungstate compounds) have also been demonstrated, bridging solution processing and CVD. Overall, among all methods, mechanical exfoliation provides the

highest quality small flakes, whereas CVD/MOCVD methods are leading for scalable growth of WS_2 monolayers needed in practical applications.

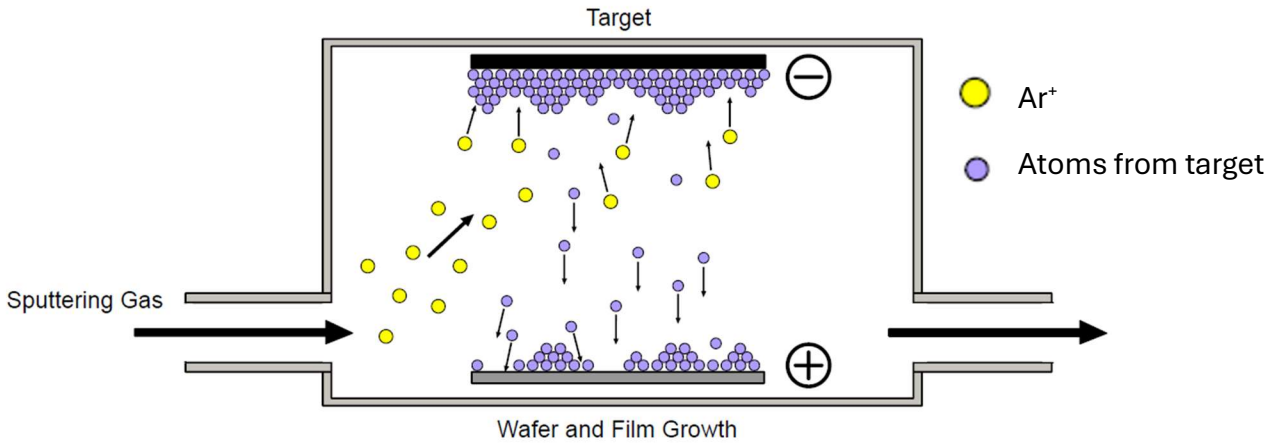

Figure 3.8: Schematic illustration of the sputtering process for the synthesis of 2D materials.

3.3 - Substrate Influence on WS_2 Growth

The substrate choice and its preparation profoundly impact WS_2 nucleation, domain orientation, and overall film quality in epitaxial growth. Sapphire (aluminum oxide, Al_2O_3) with a c-plane (0001) surface has emerged as one of the most common substrates for WS_2 and other TMD monolayers. The sapphire c-plane offers a hexagonal surface lattice that can template the hexagonal WS_2 structure, enabling epitaxial alignment. Indeed, many reports of large-area WS_2 films use c-plane sapphire as the growth platform [4]. However, a well-known challenge on perfect c-plane sapphire is the formation of mirror-twin domains: WS_2 crystals can nucleate in two equivalent in-plane orientations (rotated 60° from each other) due to the three-fold symmetry of the substrate [33]. When these oppositely oriented domains meet as the film coalesces, they form inversion domain boundaries (IDBs), which

are mirror-twin grain boundaries. Such boundaries are detrimental, as they exhibit metallic character that can create conduction pathways in the semiconducting WS_2 film [4]. They also disrupt the uniform crystal orientation needed for phenomena like spin–valley polarization that require a single crystallographic direction [4].

Figure 3.9: Representative of a 2-inch sapphire wafer used as a substrate in thin-film deposition processes.

Researchers have turned to substrate step engineering to suppress mirror–twin domains, deliberately introducing atomic step edges on the sapphire surface to break the symmetry. A slight miscut of the sapphire wafer off the c-plane (on the order of 0.1°–1°) or high-temperature annealing can produce a regular array of steps on the surface. These steps act as preferential sites for WS_2 nucleation. Critically, a step edge has a distinct "bottom" vs. "top" side in relation to the atomic terraces; this asymmetry can energetically favor one orientation of the nucleating WS_2 domain. Zhu *et al.* (2023) demonstrated that under certain

MOCVD conditions, WSe_2 (a sister compound to WS_2) nucleates predominantly at the bottom of the sapphire steps, yielding domains oriented at 60°, whereas adjusting the growth environment to be less selenium-rich caused nucleation at step tops and domains at 0° [33]. In both cases, the fraction of mirror twins was drastically reduced – films showed <15% area coverage by secondary orientation domains after coalescence, versus a much higher fraction on flat sapphire [33]. This result highlights how substrate steps coupled with surface chemistry can impart a preferred domain orientation in epitaxial TMD growth.

Building on this approach, Chubarov *et al.* (2021) achieved wafer-scale epitaxial growth of unidirectional WS_2 monolayers on 2-inch c-plane sapphire using MOCVD [4]. By optimizing the pre-growth annealing to produce well-defined atomic steps, they obtained coalesced WS_2 films in which >95% of the area was a single crystallographic orientation, essentially a single crystal separated only by small-angle (translational) grain boundaries [4]. The remaining defects were primarily translational domain boundaries (where two domains meet with a small lattice offset) rather than inversion domain boundaries [4]. The elimination of inversion boundaries was critical for improving electronic performance, as it removed unintended metallic conduction channels [4]. Similarly, Wang *et al.* (2022) demonstrated wafer-scale single-crystalline WS_2 on vicinal a-plane sapphire by a dual-coupling epitaxy strategy, wherein the lattice mismatch strain and step edge interactions were synergistically used to enforce one orientation [34]. These works underscore the importance of substrate orientation: even for the same material and substrate, a change in cut (c-plane vs. a-plane, or a small miscut angle) can mean the difference between a polycrystalline film and a nearly single-crystalline one.

In summary, sapphire substrates – particularly when intentionally miscut or stepped – provide an excellent template for aligned WS_2 monolayer growth. The step-edge nucleation sites lower energy barriers and select a single domain orientation [6], thereby mitigating the twin-domain problem that plagues 2D material epitaxy on high-symmetry surfaces [33]. Surface chemistry also plays a role: ensuring the substrate is appropriately terminated (for example, fully passivated by chalcogen atoms or other adsorbates) can determine whether nucleation occurs at the top vs. bottom of steps, influencing orientation [33]. Beyond sapphire, other substrates like hexagonal boron nitride (h-BN), graphene, and metal substrates (Au(111), etc.) have been explored, but each comes with its own challenges (e.g., transfer complexity or cost). Sapphire remains a flagship substrate for research-purposed and wafer-scale WS_2 growth due to its thermal stability and the high crystalline order it can impart. The advances reviewed here show that by engineering substrate surface steps and chemistry, one can obtain WS_2 monolayers that are predominantly aligned, greatly improving the prospects for electronics and optoelectronics that require single-crystalline thin films.

3.4 - Growth Optimization and Defect Control

Achieving high-quality WS_2 monolayers at scale requires optimizing many growth parameters to promote complete film coverage while minimizing defects. Key parameters include the growth temperature profile, precursor flow rates and ratios, chamber pressure, and growth interrupts or additives. Recent studies have shown that carefully tuning these parameters can improve domain size, coalescence, and defect densities in WS_2 films.

One crucial balance in WS_2 CVD/MOCVD is between nucleation density and lateral growth. If nucleation is too sparse, the film may not fully coalesce; if too dense, many small domains will form, increasing grain boundary density and potentially promoting bilayer growth before monolayers merge. A strategy developed by Tang *et al.* (2023) is the "migration-enhanced" two-stage MOCVD process, which explicitly addresses this balance [35]. In their approach, the growth is divided into two phases: (i) an initial low-temperature nucleation stage to create many nuclei, followed by (ii) a higher-temperature lateral growth stage with reduced precursor flux to enlarge the domains and fill the gaps [35]. Specifically for WS_2, Tang *et al.* used a nucleation step at ~700 °C to seed a high density of small WS_2 domains (~50 nm) covering ~24% of the surface [35]. They then ramped the temperature to ~820 °C and significantly lowered the tungsten precursor flow (to 25% of the initial), which extends the diffusion length of W adatoms and favors existing domains spreading out rather than new nuclei forming [35]. This two-step recipe yielded a fully coalesced monolayer WS_2 film (>99% area coverage) within 3 hours, with minimal bilayer areas (<20% second-layer coverage) [35]. Importantly, by throttling the W supply during the high-temperature phase, they suppressed secondary nucleation on top of the monolayer, which is the main cause of bilayer islands [35]. This result is a major improvement over single-stage growth, where premature bilayer nucleation often occurs once the first layer percolates [35]. The migration-enhanced process demonstrates how temperature ramping and precursor flow scheduling can be used to obtain a nearly defect-free monolayer across a wafer.

Another parameter that has garnered attention is the chamber pressure and carrier gas environment. MOCVD growth of WS_2 frequently employs hydrogen (H_2) as a carrier or

reductant gas. H_2 can help reduce oxide species and may assist in removing certain impurities. Tang *et al.* found that using pure H_2 at a reduced pressure of 20 hPa (around 0.02 bar) was crucial to avoiding carbon incorporation from the metal–organic precursors [35]. At higher pressures, incomplete precursor decomposition can leave carbon residue in the film, evidenced by the appearance of carbon-related D and G bands in Raman spectra of those samples. By lowering the pressure, volatile carbon byproducts were more effectively pumped away, and parasitic reactions in the gas phase were minimized [35]. This led to WS_2 films with significantly less carbon contamination. In general, carbon contamination is a known issue in MOCVD of TMDs, since precursors like $W(CO)_6$ or organometallic sulfides contain carbon. Approaches to mitigate carbon include using hydrogen and/or water vapor to react with carbon species. A novel variant called the "growth-etch" MOCVD (GE-MOCVD) method deliberately introduces a small amount of oxidant (e.g. water vapor, H_2O) intermittently during growth [36]. The water reacts at the surface, etching away carbonaceous fragments and even excess WS_2 nuclei, effectively *cleaning* the surface in situ [36]. Cohen *et al.* (2021) implemented this GE-MOCVD approach for WS_2 and WSe_2, and reported that it yields larger crystal domains and improved optical quality compared to a standard growth [36]. The water vapor pulse was believed to selectively etch unstable nuclei and passivate vacancy sites, resulting in WS_2 monolayers with stronger PL (indicating fewer non-radiative recombination centers) [36]. This approach shows promise for defect reduction, though care must be taken to not etch the primary layer. It represents an example of *in situ* defect mitigation during growth.

Aside from the process parameters, researchers have explored post-growth treatments to heal or passivate defects in WS_2. The predominant intrinsic point defects in CVD-grown WS_2 are often chalcogen (sulfur) vacancies, which can act as trap states. Chalcogen-rich growth conditions (e.g. a high S:W precursor ratio) are generally used to minimize S vacancies during growth [35]. For instance, Tang *et al.* maintained an H_2S (or organosulfide) flow such that the effective S:W ratio exceeded 6000, ensuring sulfur was not the limiting reactant [35]. This helps drive the reaction to fully saturate W with S and reduces the likelihood of W-rich, S-deficient regions. In terms of post-growth defect healing, chemical treatments have been demonstrated on WS_2 and WSe_2: one study showed that treating CVD WS_2 with organic thiol molecules could substitute sulfur into vacancy sites, effectively "healing" those defects [37]. The thiol-based treatment resulted in restored PL and improved electrical performance in WSe_2/WS_2 by filling S/Se vacancies [37]. While these post-growth fixes are outside the growth process, they highlight defect control's importance for functional devices.

Finally, the elimination of twin domains and grain boundaries – discussed in Section 5.6 with respect to the substrate choice – can also be considered as a form of defect optimization. By engineering the nucleation (through substrate steps or selective seeding), researchers aim to grow films that are as close to single-crystalline as possible, thereby removing line defects (grain boundaries) that scatter carriers and reduce mobility [33]. For example, using a sapphire substrate miscut towards the m-axis by 0.2° yielded WS_2 with predominantly a single orientation, effectively removing inversion boundaries [4]. The remaining grain

boundaries in such films are between like-oriented domains (translation boundaries), which are known to be less electrically disruptive than inversion boundaries [4].

Recent advancements demonstrate that combining optimized growth kinetics (two-stage processes, flow modulation) and surface/interfacial engineering (pressure, ambient, etchants) can significantly enhance WS_2 monolayer quality. Growth techniques like migration-enhanced MOCVD have achieved fully coalesced monolayers with minimal bilayers [35], and novel concepts like growth-etch cycling show that *in situ* cleaning can yield larger, cleaner domains. Coupling these process innovations with substrate engineering and post-growth passivation gives a multi-pronged strategy for defect control. The net result sought is a WS_2 monolayer that is continuous over the substrate, uniformly oriented, and free of common point defects or impurities – essentially approaching the perfection of a mechanical exfoliation sample, but at wafer scale.

Chapter 4 - Methodology

4.1 - Metal-Organic Chemical Vapor Deposition (MOCVD)

Figure 4.1: Photograph of the AIXTRON CCS 3×2" FT MOCVD system used for WS_2 growth. The reactor (inside nitrogen glovebox) is visible in the center, with the load-lock chamber on the right.

All WS_2 films in this research were grown in an AIXTRON CCS 3×2" FT MOCVD system (Figure 4.1). This reactor features a Close Coupled Showerhead® (CCS) design in a vertical, cold-wall configuration. The showerhead (gas inlet manifold) is water-cooled and positioned a small distance (on the order of 1–1.5 cm) above the substrate susceptor, ensuring uniform delivery of reactant gases across the wafer surface while minimizing gas-phase

prereactions. The showerhead contains separate internal plenums for different precursor types (designed initially to segregate metal-organics vs. hydride gases), which allows the metal precursor ($W(CO)_6$) and sulfur precursor (di-tert-butyl sulfide) to be introduced through independent pathways and mix only near the substrate. This separation helps prevent premature reactions or particle formation in the gas phase.

The reactor chamber itself is made of stainless steel with a quartz liner and is housed inside a nitrogen-purged glovebox (MBraun MB10) to maintain low oxygen and moisture during wafer loading/unloading. Wafers are loaded via a load-lock to avoid exposing the chamber to air. The susceptor accommodates up to 3 × 2 inch diameter substrates (or other configurations) and is heated from below by a three-zone resistive heater. The 3-zone heater, composed of tungsten alloy coils, enables independent control of each heating zone, allowing fine tuning of the temperature profile across the substrate. Such configurability ensures excellent thermal uniformity during growth, which is critical for achieving consistent film quality across the wafer. In our system, we calibrated the heater to achieve uniform substrate temperatures up to ~1200 °C, enabling the high-temperature steps required for sapphire annealing and WS_2 growth. Reactor temperature is monitored by thermocouples and optional pyrometric sensors, and the system can reach a maximum susceptor surface temperature of ~1400 °C if needed.

Gas flows and reactor pressure within the MOCVD growth system were precisely regulated using digital mass flow controllers (MFCs) and pressure control valves. High-purity carrier gases (H_2) and reactant gases were carefully metered by MFCs, while the reactor pressure was maintained using a motorized throttle valve positioned at the exhaust line. The CCS 3×2"

FT MOCVD system incorporates both absolute and differential pressure controllers, stabilizing gas pressures in both supply lines and the reactor chamber throughout the entire growth process. For our experiments, the reactor was operated at low pressure (50 mbar) during growth with N_2 as the inert gas, a regime found to promote larger domain sizes by reducing gas-phase supersaturation.

For the tungsten and sulfur precursors, tungsten hexacarbonyl ($W(CO)_6$) and di-tert-butyl sulfide (DTBS, $(t\text{-}Bu)_2S$ or $C_8H_{18}S$) were employed, respectively, forming an H_2S-free precursor combination commonly utilized in MOCVD TMD. $W(CO)_6$, a white crystalline solid with a high vapor pressure for a metal-organic precursor, sublimates at moderate temperatures (~1.6 mbar at 67 °C) and has a low melting point of around 150 °C. This allows effective precursor delivery via vapor draw or bubbling at manageable temperatures. In our experiments, $W(CO)_6$ was housed in a stainless steel bubbler maintained at 15 °C and at 1300 mbar to ensure a stable vapor supply. A controlled flow of carrier gas passed through the bubbler, and a dedicated MFC precisely regulated the tungsten precursor's vapor delivery. Additionally, a pressure controller maintained constant head pressure within the bubbler, ensuring reproducible precursor flow.

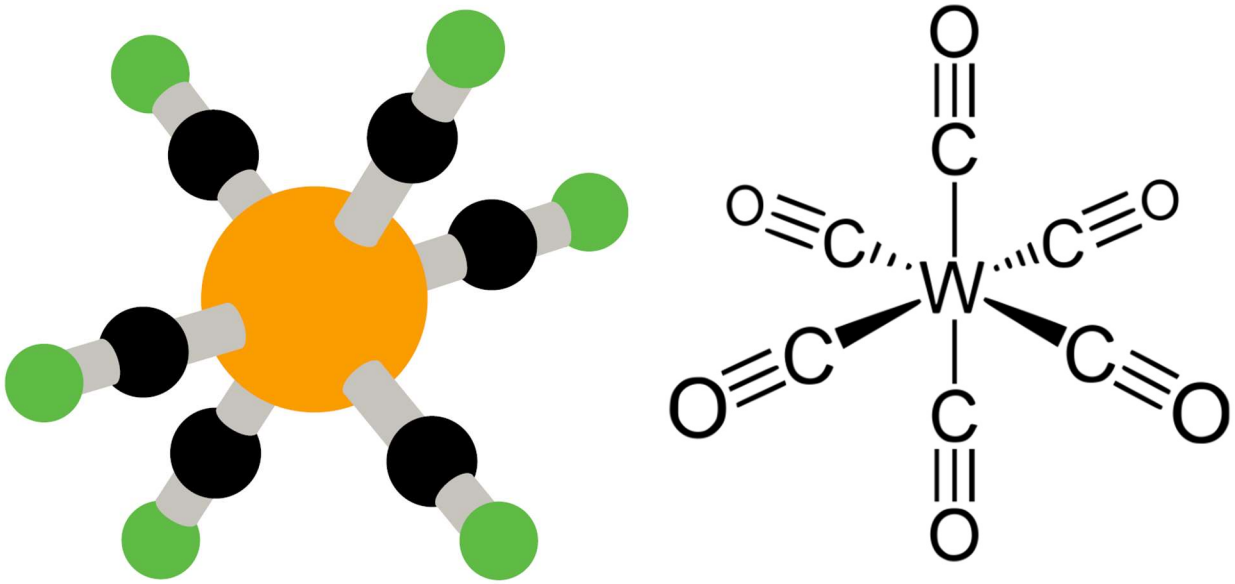

Figure 4.2: Molecular structure of tungsten hexacarbonyl ($W(CO)_6$), the organometallic precursor used for WS_2 growth.

Di-tert-butyl sulfide (DTBS) is a clear, colorless liquid (boiling point ~149 °C) with substantial vapor pressure at room temperature (~6.9 mbar at 25 °C). This means DTBS can be introduced via a bubbler at or near ambient temperature, typically maintained at temperatures around 10-55 °C. Because of its decent volatility, DTBS provides a steady sulfur flux without the need for heating. One advantage of DTBS (and $W(CO)_6$) is that they are less hazardous to handle than gaseous H_2S or WF_6 – using liquid/solid precursors avoids the direct use of toxic hydride or halide gases. This makes the process more compatible with the available lab safety infrastructure, albeit at the cost of some carbon incorporation as discussed below.

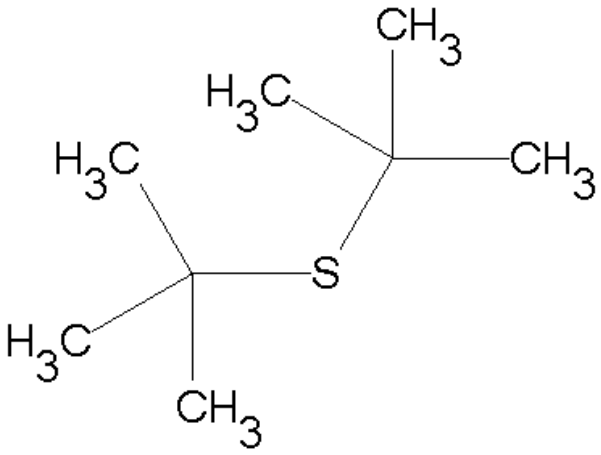

Figure 4.3: Molecular structure of Di-tert-butyl sulfide (DTBS), the chalcogenide precursor used for WS_2 growth.

Once delivered into the hot reactor zone, both precursors decompose to supply the necessary elements for WS_2 formation. Tungsten hexacarbonyl is known to thermally dissociate, releasing CO ligands and leaving behind reactive tungsten species. Complete decomposition of $W(CO)_6$ typically requires substrate temperatures in excess of ~300 °C, with higher temperatures (>600 °C) needed to ensure that tungsten atoms are liberated and can diffuse on the surface [38]. In our growth process (detailed in the next section), we introduce $W(CO)_6$ at substrate temperatures between ~550–850 °C, at which point the carbonyl readily breaks down. The by-product CO gas is swept out of the chamber by the carrier flow, though some CO can further react (e.g. CO + surface O → CO_2) if oxygen is present. Substrates were loaded onto a rotating susceptor positioned at 15 mm from the showerhead, optimizing uniform precursor distribution across the wafer surface. The sulfur precursor DTBS thermally cracks by cleaving the C–S bonds, releasing sulfur (likely in the

form of radical or atomic S, or gaseous byproducts like isobutylene and butene). Literature suggests that tert-butyl sulfides begin to decompose around 300 °C and largely dissociate by ~600–700 °C [38]. Consistent with this, we found that meaningful WS_2 growth only occurred when the substrate was above ~550 °C (little to no growth at 500 °C, indicating insufficient precursor decomposition). At typical growth temperatures (700–800 °C), DTBS provides an abundant flux of sulfur species.

The surface reaction to form WS_2 can be considered as:

$$W(CO)_6 + (C_4H_9)_2S \xrightarrow{\text{hot surface}} WS_2 + CO\uparrow + C_xH_y\uparrow$$

In essence, tungsten from $W(CO)_6$ reacts with sulfur from DTBS on the sapphire surface to form WS_2, while gaseous CO and hydrocarbon fragments are expelled. A high sulfur-to-metal ratio is deliberately used to drive the reaction fully toward WS_2 and avoid forming tungsten metal or sub-sulfides. The precursor flow ratios (W:S) used in comparable WS_2 MOCVD studies typically range from approximately 1:1000 to 1:5000. This large excess of sulfur ensures that each tungsten atom finds sulfur and is fully sulfidized into WS_2. It also helps suppress any premature decomposition of $W(CO)_6$ into tungsten metal or oxide; in a sulfur-rich environment, even if some tungsten atoms deposit before finding sulfur, they can be rapidly converted to WS_2. (Recent studies have noted that a thin tungsten-oxide layer can form on sapphire if tungsten is deposited in an oxygen-containing ambient [39]; in our case, we minimize this by avoiding air exposure and using excess sulfur, though an oxide nucleation layer might still play a role in domain alignment as discussed later.)

A known drawback of the $W(CO)_6$ + DTBS chemistry is the potential for carbon contamination in the films. Both precursors are carbon-containing ($W(CO)_6$ provides CO, and DTBS has tert-butyl groups), so incomplete decomposition or side-reactions can leave carbon byproducts on the growing film. Indeed, amorphous carbon (a-C) is often detected in as-grown MOCVD WS_2 films when using these precursors.

We used c-plane sapphire substrates (single-crystalline Al_2O_3 (0001)) as the growth platform for WS_2. Both on-axis (0° miscut) and slightly miscut wafers were investigated. The miscut substrates had an off-cut of approximately 0.15–0.2° toward either the sapphire a-axis or m-axis. These small intentional miscuts yield a surface with parallel atomic step-terrace structures, where the step orientation differs depending on the miscut direction. The rationale for using miscut sapphire is to provide aligned step edges that can guide WS_2 domain orientation, as discussed shortly.

Prior to growth experiments, substrates generally undergo rigorous cleaning procedures to ensure the removal of common surface contaminants, such as dust particles, organic residues, and metallic impurities. Typically, sapphire substrates are first degreased using sequential ultrasonic baths in solvents such as acetone, isopropanol (IPA), and deionized (DI) water, with each step lasting approximately 5 to 10 minutes. Additionally, chemical treatments like immersion in piranha solution (a mixture of sulfuric acid and hydrogen peroxide, typically in a 3:1 ratio) may be employed to effectively remove persistent organic films by oxidation, rendering the sapphire surface hydrophilic and contaminant-free. This immersion usually lasts around 10 to 15 minutes, followed by thorough rinsing with DI water and drying with nitrogen gas. Alternatively, oxygen plasma cleaning—usually performed at

approximately 300 W for around 5 minutes in an oxygen-rich atmosphere—is also effective in removing organic residues and enhancing surface cleanliness. Regardless of the specific method used, all cleaned substrates are handled carefully with gloves and tweezers to avoid recontamination. Immediately after cleaning, substrates are promptly loaded into the MOCVD system's load-lock chamber, ensuring minimal exposure to ambient conditions, which helps prevent re-adsorption of atmospheric moisture and carbon contaminants.

Once in the MOCVD reactor, the sapphire substrates underwent a high-temperature annealing step under an inert or reducing atmosphere. This anneal serves multiple purposes: (1) desorb any remaining surface impurities (water, CO_2, etc.), (2) smoothen the surface at the atomic level, and (3) if miscut, promote the formation of well-defined atomic steps on the surface. We performed two sets of annealing conditions in different runs, corresponding to 1050 °C and 1200 °C peak temperatures. In a typical procedure, after pumping down to the base pressure, the substrate was heated in flowing high-purity N_2 (500 sccm) to the target annealing temperature. For the 1050 °C anneal, we ramped at ~25 °C/min up to 1050 °C, and held for 30 minutes. For the 1200 °C anneal, we ramped at a similar rate up to 1200 °C and held for 10 minutes. During annealing we introduced a small flow of H_2, which can chemically reduce surface contaminants and possibly etch the sapphire slightly [40]. Indeed, hydrogen at high temperatures can interact with sapphire (removing some oxygen from the surface) and help produce an atomically flat, reconstructed surface [40]. After annealing, the sapphire surfaces appeared shiny and smooth, and in the case of miscut substrates, well-organized step arrays are formed. As noted in the literature, high-temperature annealing of miscut c-plane sapphire results in uniform terraces separated by

monoatomic steps, which provide lower-energy nucleation sites for subsequent epitaxial growth. Our AFM measurements (see Chapter 5) confirm the emergence of terraces ~100 nm to several μm wide separated by steps of one or a few atomic layers after the annealing process.

The slight miscut of 0.15–0.2° leads to a regular step morphology that can influence WS_2 island nucleation. Step edges often act as preferential nucleation sites because they can offer additional dangling bonds or surface energy variations. In our experiments, we observed that WS_2 tends to nucleate along the sapphire steps when they are present, rather than randomly on the terraces. Moreover, the presence of a unidirectional array of steps can break the in-plane symmetry and favor a single crystallographic orientation of WS_2 domains. For on-axis sapphire without steps, 2D nuclei can attach in two equivalent orientations rotated by 60° (because the sapphire (0001) surface is hexagonal, matching either the 0° or 60° alignment of WS_2 lattices).

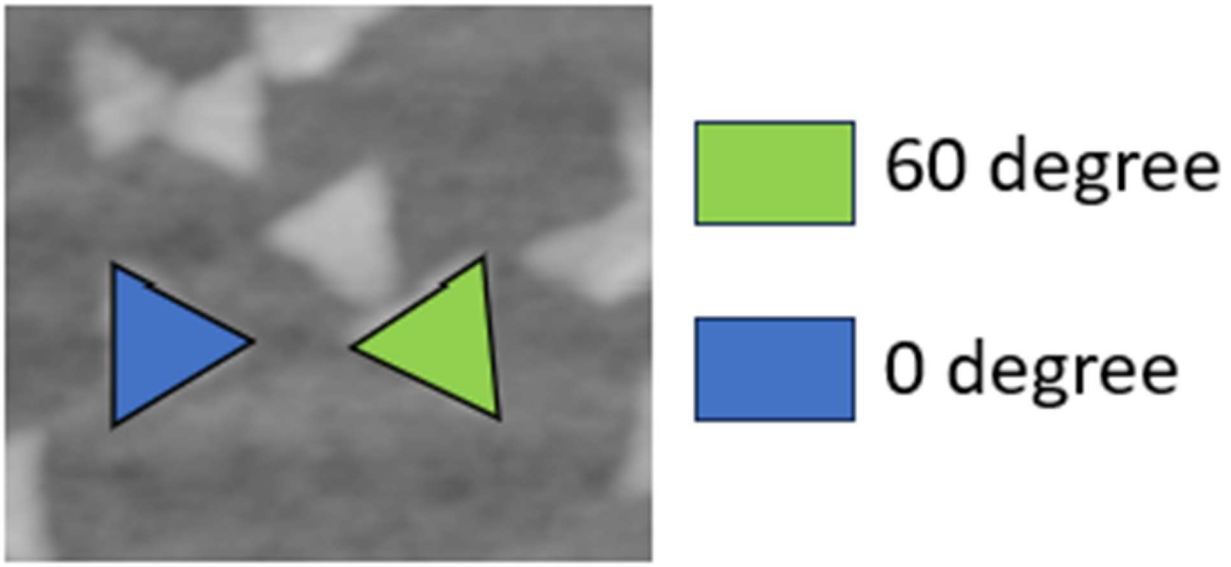

Figure 4.4: Difference in domain orientation between 60 degrees and 0 degrees.

This leads to the typical mirror-twin domains in CVD TMD films. However, on miscut substrates, the aligned steps select one orientation by energetically biasing nucleation at either the step edge or terrace in a consistent direction [33]. In line with recent reports, we found that the majority of WS_2 triangular domains on miscut sapphire aligned in the same orientation (either 0° or 60° relative to the lattice, depending on conditions), drastically reducing the occurrence of oppositely oriented twins [33]. In other words, the films grown on miscut substrates showed unidirectional domain alignment, which is highly desirable for obtaining single-crystalline continuous monolayers [4]. We systematically compared a substrate cut with 0.2° toward the m-axis versus one 0.2° toward the a-axis. Interestingly, the two miscut directions yielded different preferred WS_2 orientations (since the step geometry differs). Detailed results on domain orientation are presented in Chapter 5, but the key point

for methodology is that the miscut was an effective tool to control nucleation site and domain alignment.

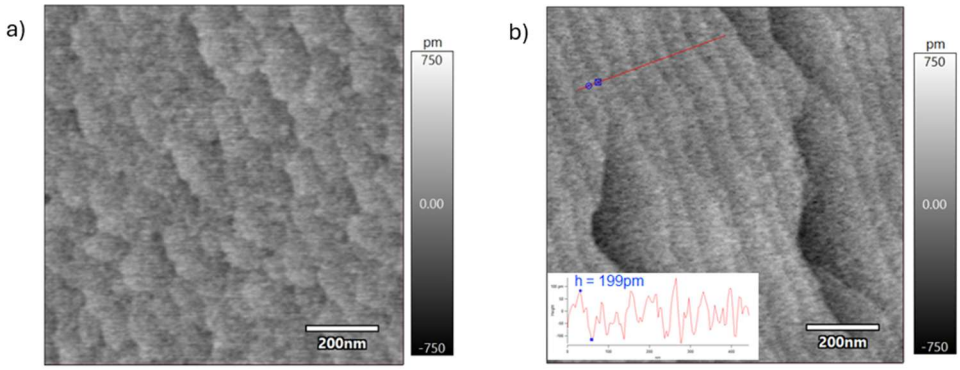

Figure 4.5: Comparison of sapphire substrate step-edge morphology after annealing at a) 1050 °C for 30 minutes and b) 1200 °C for 10 minutes.

Before growth, the annealed substrates were cooled down to the desired growth temperature under a protective atmosphere (typically N_2). The annealing process proved reproducible and crucial: consistently annealed sapphire surfaces led to more uniform WS_2 nucleation in subsequent steps. In summary, substrate preparation involved rigorous cleaning, high-T annealing (1050–1200 °C) to obtain atomically stepped surfaces, and careful temperature ramp-down to the growth regime, all of which set the stage for controlled WS_2 epitaxy.

After substrate annealing, the reactor temperature was adjusted to the WS_2 growth conditions. Our growth recipe employed a multi-step temperature profile consisting of a low-temperature nucleation step followed by a higher-temperature lateral growth step. Figure 4.6

illustrates schematically the timing and temperature sequence for a typical growth run (based on our process timing chart). Key process parameters are summarized below:

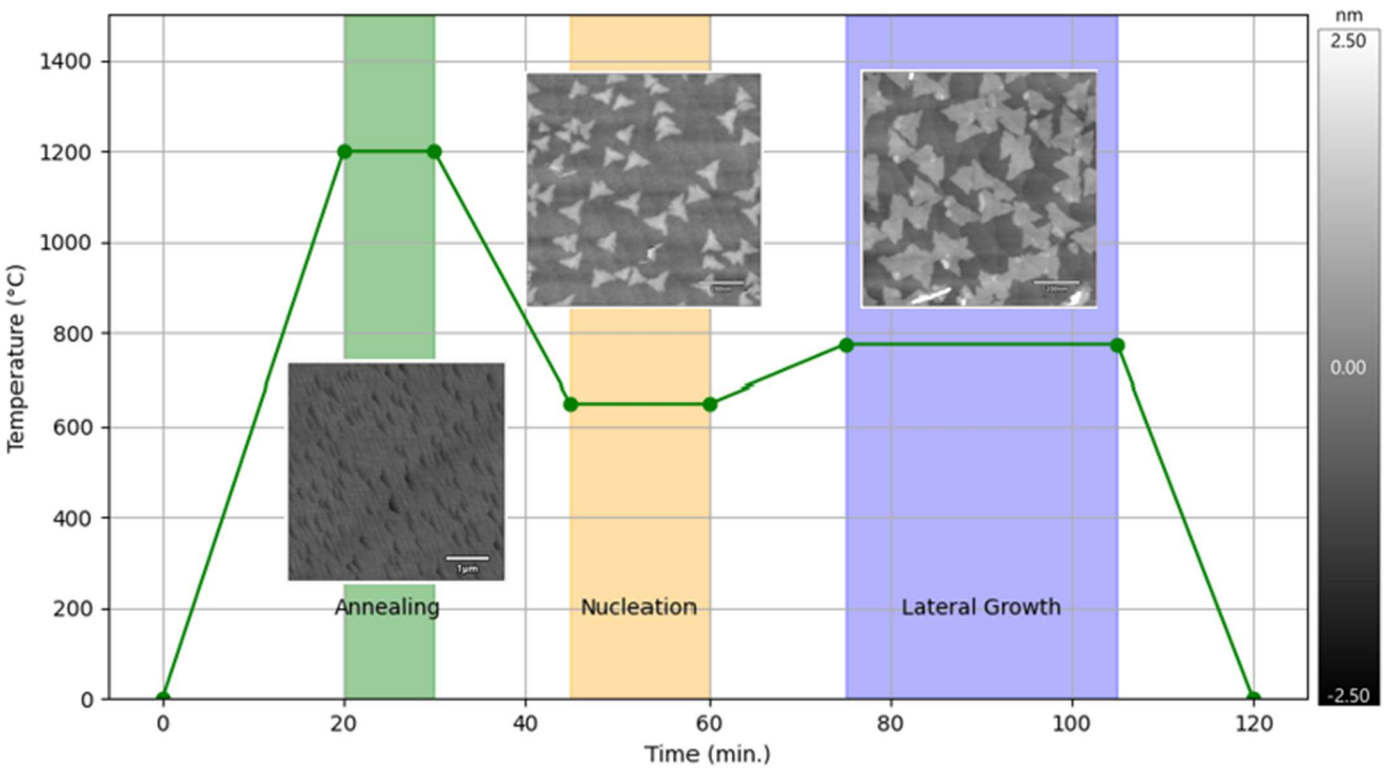

Figure 4.6: Temperature vs. time profiles for the annealing and nucleation growth processes.

- **Annealing:** Up to 1050-1200 °C for 10-30 min (as described above). After annealing, the temperature is lowered to the nucleation range. This cool-down is done under continuous gas flow (usually N_2 or N_2/H_2) to maintain a stable environment. We cool at a controlled rate (~10 °C/min) to avoid thermal shock to the sapphire and to allow gas switching. Once the temperature nears the nucleation setpoint, we stabilize for a few minutes before introducing the metal precursor and the chalcogenide precursor.

- **Nucleation step: Temperature 550–850 °C**, duration ~5–15 min. This is the initial growth stage where WS_2 nuclei (monolayer islands) form. We investigated the nucleation temperatures across a wide range:
    - At the low end (550–600 °C), nucleation is very dense – many small islands form quickly due to high supersaturation, but individual domains remain small.
    - At intermediate T (~650–750 °C), nucleation density decreases and islands grow larger.
    - At the high end (~800–850 °C), nucleation is extremely sparse (in some trials at 850 °C, almost no nuclei formed within a reasonable time, indicating we approached the activation energy limit for nucleation).

The effects of nucleation temperature and time on the film morphology were apparent: as nucleation temperature increased from 550 °C to 750 °C, the nucleation density dropped and the average domain size increased significantly. For example, nuclei density at 600 °C was on the order of ~ 62 per μm^2, whereas at 750 °C it fell to ~ 25 per μm^2, with domains growing correspondingly larger (around 95 nm in size). We also observed that longer nucleation times lead to higher total WS_2 coverage (since more nuclei have time to form); however, too long a nucleation step can overcrowd the surface with small domains that may later merge with misoriented neighbors. Thus, nucleation time was balanced to achieve a desired initial coverage (typically ~15–20% area coverage after nucleation).

- **Lateral Growth step:** During the lateral growth step, temperatures typically range from 675 to 775 °C with a duration of about 30 minutes, although this duration can be extended to achieve greater domain coalescence. This step specifically aims to laterally enlarge existing WS_2 monolayer domains until they merge into a continuous film or reach the targeted coverage. To promote surface diffusion and enhance lateral expansion at the edges of pre-formed domains—rather than initiating new nucleation events—the tungsten precursor ($W(CO)_6$) flow is usually decreased to about half its rate during the nucleation stage, while the DTBS (di-tert-butyl sulfide) flow is kept constant or increased slightly to maintain sulfur-rich conditions. Higher growth temperatures in this step significantly improve adatom mobility, allowing atoms to attach more efficiently at domain edges and enabling domains to grow larger before growth halts. For instance, at 675 °C, single-layer WS_2 domains up to approximately 55 μm were produced, whereas raising the temperature to 775 °C resulted in faster lateral growth and significantly larger domains, reaching about 120-125 μm in some experiments. However, temperatures exceeding roughly 800 °C risk causing WS_2 decomposition or evaporation, halting nucleation entirely and thus establishing an upper practical limit. Typically, a lateral growth at 675 °C for 30 minutes, following an initial nucleation step at 550 °C for 15 minutes, resulted in approximately 50% monolayer coverage on a 2" wafer, with domain sizes around 55 μm, as elaborated further in Chapter 5.

Throughout the growth, the reactor conditions (temperature, pressure, flow) were logged by the control software to ensure reproducibility. The multi-step process described – high-T

anneal, low-T nucleation, high-T lateral growth, controlled cooling – proved to be a robust sequence for growing large-area monolayer WS_2 on sapphire. The exact temperatures and times were optimized iteratively, as described next.

Developing the optimal growth recipe required numerous trial runs and systematic variation of parameters. In this section, we summarize the key strategies and adjustments that were explored to improve WS_2 film quality, along with the observations that guided our final methodology.

As discussed, one fundamental strategy was the two-step temperature sequence (nucleation at lower T, then growth at higher T). Early experiments that attempted growth at a constant temperature often resulted in either too many nuclei (when at low constant T) or almost no nucleation (at high constant T). By incorporating a temperature ramp, we could decouple the nucleation and growth phases – first create a controlled density of nuclei, then promote their expansion. This approach is analogous to "migration-enhanced" MOCVD processes reported in recent literature, which emphasize a low-T nucleation to maximize adatom diffusion lengths once the temperature is raised [35]. Through this method, we achieved larger domains and more uniform coverage than any single-temperature process. We optimized the nucleation temperature by observing the resulting island density and size under AFM and optical microscopy. The clear trend was: higher nucleation temperature → lower nucleation density, larger domains. For example, at 550 °C nucleation, islands were ~30-40 μm in size and very dense; at 750 °C nucleation, islands were ~95 μm. However, if nucleation density is too low, it can lead to incomplete coverage. Thus, we balanced the temperature to get a reasonably low density but not zero. The nucleation time was also

tuned: longer nucleation time increased overall WS_2 coverage linearly, but too long led to many bilayer nuclei (vertical growth) especially at lower temperatures. Our chosen 15 min was sufficient to seed ~15% area coverage, which after expansion could coalesce to >50%.

4.2 - Atomic Force Microscopy (AFM)

Figure 4.7: Photograph of the Asylum Research Cypher Atomic Force Microscope (Oxford Instruments) used for AFM imaging of WS_2 samples.

All AFM measurements were performed using an Asylum Research Cypher AFM (Oxford Instruments) in ambient air. Imaging was conducted in tapping mode (an intermittent non-contact imaging mode) to achieve high-resolution topographic maps of the WS_2 surface without damaging the sample. A stiff silicon cantilever (Olympus AC160TS or similar, spring constant $k \approx 42$ N/m, resonance frequency $f \approx 300$ kHz) was used as the AFM probe. This type

of probe is a standard choice for high-resolution AC mode imaging in air. Prior to scanning, the cantilever was tuned to its resonance and the drive amplitude adjusted to yield a free oscillation (far from the surface) of a few hundred millivolts. We then set the amplitude setpoint to ~70–80% of the free oscillation amplitude for engagement [18]. In practice, a free amplitude of ~250 mV and setpoint of ~200 mV were used, providing a gentle tapping interaction. This conservative setpoint ratio ensured stable feedback tracking with minimal normal force on the sample. During approach, the setpoint was fine-tuned so that the trace and retrace scan lines overlapped closely, indicating negligible hysteresis and optimal imaging force [18]. By using tapping (AC) mode, damaging lateral forces were largely eliminated, protecting the atomic-scale WS_2 layers and the tip from wear. Non-contact tapping is preferred over contact mode for 2D materials on hard substrates because it mitigates friction and sample deformation, critical for fragile monolayer WS_2 on sapphire.

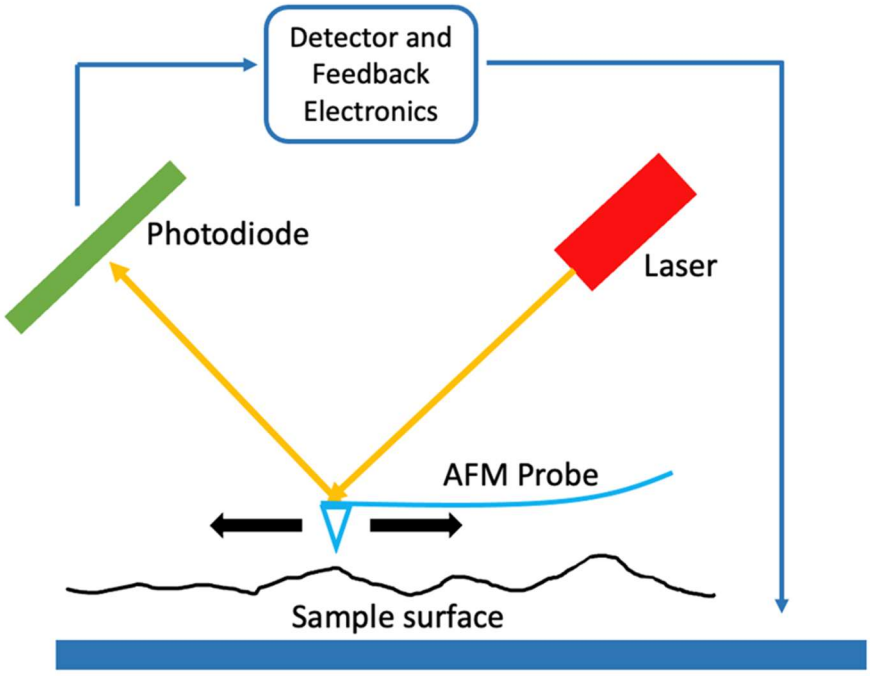

Figure 4.8: Schematic illustration of Atomic Force Microscopy (AFM) operating in tapping (AC) mode for surface characterization.

Imaging was typically carried out at multiple scan sizes, such as 1 μm × 1 μm and 5 μm × 5 μm areas, to capture both fine details and larger coverage. Each image was acquired at 512×512 pixel resolution (unless higher resolution was needed for small features). The scan rate was kept low (on the order of 0.5–1.0 lines/second) to allow the cantilever to respond accurately to surface topography. The Cypher AFM's closed-loop scanner minimizes creep and ensures linear calibration in all dimensions. All scans were done in height (constant amplitude) mode with the integral and proportional gains optimized to track the surface faithfully. These settings enabled high-resolution topographic imaging of monolayer WS_2 with sub-nanometer vertical sensitivity.

The WS_2 monolayer samples were grown on c-plane sapphire substrates via MOCVD and used as-received for AFM imaging (no transfer was necessary since growth was directly on sapphire). Before each AFM session, the sample was carefully prepared to ensure a clean surface. First, any loose particulates were removed by gently blowing the surface with dry nitrogen. No wet chemical cleaning was performed on the as-grown WS_2, to avoid unintentional removal or damage of the monolayer. The sample (a small cleaved or cut piece of the sapphire wafer, typically 1–2 cm in size) was then mounted on a magnetic steel sample puck using a minimal amount of adhesive. In our case, a tiny drop of silver conductive epoxy was placed between the backside of the sapphire and the metal puck, securing the sample. This mounting method not only firmly holds the sample in place, but also provides a conductive pathway to ground. Sapphire is an insulating substrate, so grounding the sample helped to dissipate any static charge and avoid image instabilities due to electrostatic forces.

All handling of the sample and cantilever followed standard clean procedures. We used clean nitrile gloves and curved tweezers for handling to avoid touching the surface directly [18]. The AFM cantilever was loaded into its holder using fine tweezers under an optical microscope to ensure proper laser alignment on the cantilever. After mounting, the sample and AFM head were allowed to equilibrate to the laboratory environment for ~5–10 minutes to minimize thermal drift during scanning. Throughout the preparation, precautions were taken to avoid contamination: the sample was kept in a covered petri dish when not being scanned, and the loading was done in a clean area to prevent dust deposition. These

measures ensured that the WS_2-on-sapphire surface remained as pristine as possible for AFM examination.

AFM images revealed the morphology of the sapphire substrate itself. The sapphire wafers, especially after high-temperature growth, exhibited atomically flat terraces separated by step edges. From line profile analysis on bare substrate areas, we observed step heights of approximately (0.2 ± 0.01) nm at the terrace edges. This corresponds closely to the height of a single atomic layer of Al_2O_3 along the c-axis [41]. In fact, the crystallographic step height for c-plane sapphire (0001) is ~0.216 nm (the thickness of one Al–O layer), so the AFM observation of ~0.2 nm steps confirms the atomic step-and-terrace structure of our substrates [41]. These terraces had lateral widths on the order of microns, separated by the single-layer steps, which is typical for well-polished and annealed sapphire. The presence of such atomic steps is important, as they can influence WS_2 domain orientation and coalescence during growth (step edges often act as preferential nucleation sites).

In addition to the substrate thickness, the WS_2 monolayer regions are observed as atomically flat islands protruding above the flat sapphire background. To quantify the thickness, line profiles were extracted across the WS_2/sapphire boundaries. The measured step height for monolayer WS_2 was consistently about 0.616 nm, as expected for a single layer. This ~0.616 nm topographic step is in good agreement with literature values for monolayer WS_2 [42]. (Reported AFM thicknesses for 1L-WS_2 typically range from ~0.6 - 0.7 nm [43], matching the ~0.616 nm interlayer spacing known from crystal structure plus any substrate interaction or adsorbate layer.) The clarity of the step in our height profiles confirms that the MOCVD growth achieved predominantly monolayer coverage. No additional discrete steps of 0.616

nm were seen on top of the monolayer islands, indicating an absence of bilayer or multilayer patches in the scanned regions (within the sensitivity of our measurement).

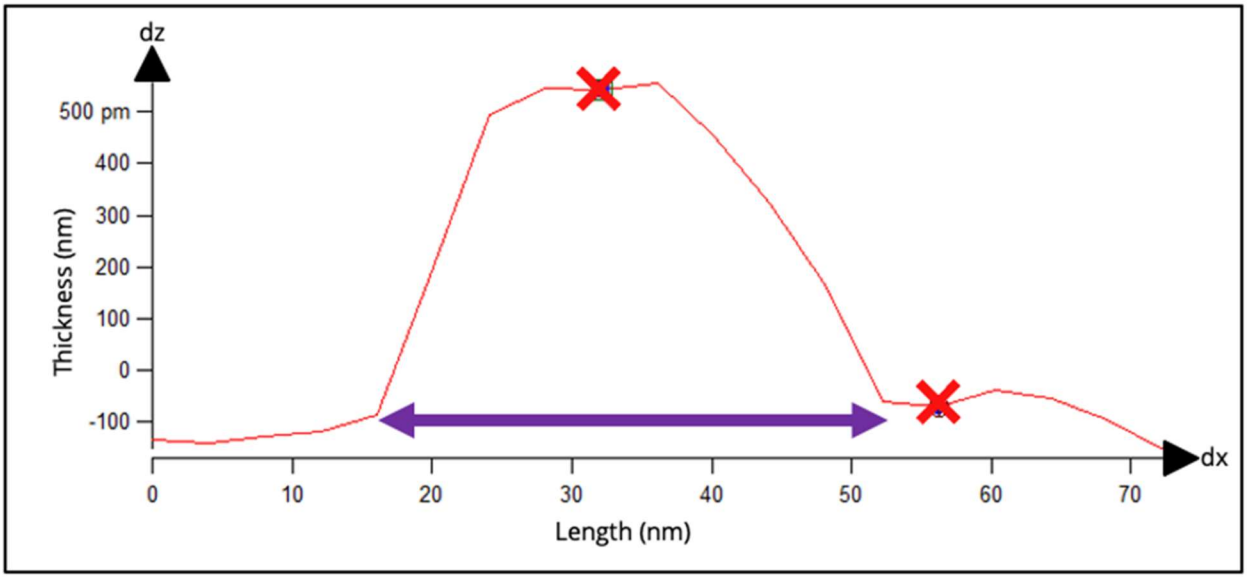

Figure 4.9: Line profile showing the thickness of a WS_2 monolayer domain extracted from AFM data, plotted as Thickness (nm) vs. Length (nm).

To ensure the accuracy of our height measurements (both the ~0.616 nm WS_2 and ~0.2 nm sapphire steps), the AFM's z-axis was calibrated prior to imaging, using a standard calibration grating (with known step heights) from Oxford Instrument. The known step height on the reference (on the order of tens of nanometers) allows one to adjust the AFM's sensitivity (invOLS) so that the measured height matches the standard. After this calibration, the AFM's vertical measurements are quantitative. Additionally, the internal sensor of the closed-loop scanner was zeroed on a bare substrate area before measuring the monolayer step heights, to eliminate any tilt or piezo drift. We also utilized the sapphire's own 0.2 nm steps as a secondary check: the consistency of those steps with the expected value

substantiate the accuracy of the sub-nm scale calibration. Overall, the combination of manufacturer calibration standards and intrinsic substrate references ensured that the AFM height values (e.g. 0.616 ± 0.03 nm for WS_2 monolayer) are accurate and reliable.

4.3 - AFM Image Analysis and Processing (ImageJ)

AFM topography data were analyzed to extract quantitative information about WS_2 coverage and morphology. We primarily used ImageJ (FIJI) for post-processing the height images exported from the AFM. To determine the area coverage of WS_2 on the substrate, a height threshold was applied to separate the monolayer regions from the bare sapphire background. In ImageJ, the height image (grayscale 16-bit) was adjusted so that pixels corresponding to WS_2 (higher elevation) could be distinguished from sapphire (lower). We set a threshold at roughly half the monolayer height (around 0.3–0.4 nm above the baseline) to create a binary mask. All pixels above this threshold were counted as WS_2-covered area, and those below as uncovered sapphire. This thresholding reliably highlighted the triangular WS_2 domains since the ~0.616 nm step gave strong contrast above any noise. ImageJ's *Analyze Particles* function was then used on the binary mask to calculate the total area of WS_2 regions. From this, the percent coverage of the surface by WS_2 was obtained. For instance, a 10 μm × 10 μm scan might show ~45% coverage by monolayer islands (depending on growth conditions). The threshold was chosen carefully to exclude noise or

minor roughness on the sapphire (which was atomically smooth) and was validated by overlaying the mask on the original image to ensure only true WS_2 regions were counted.

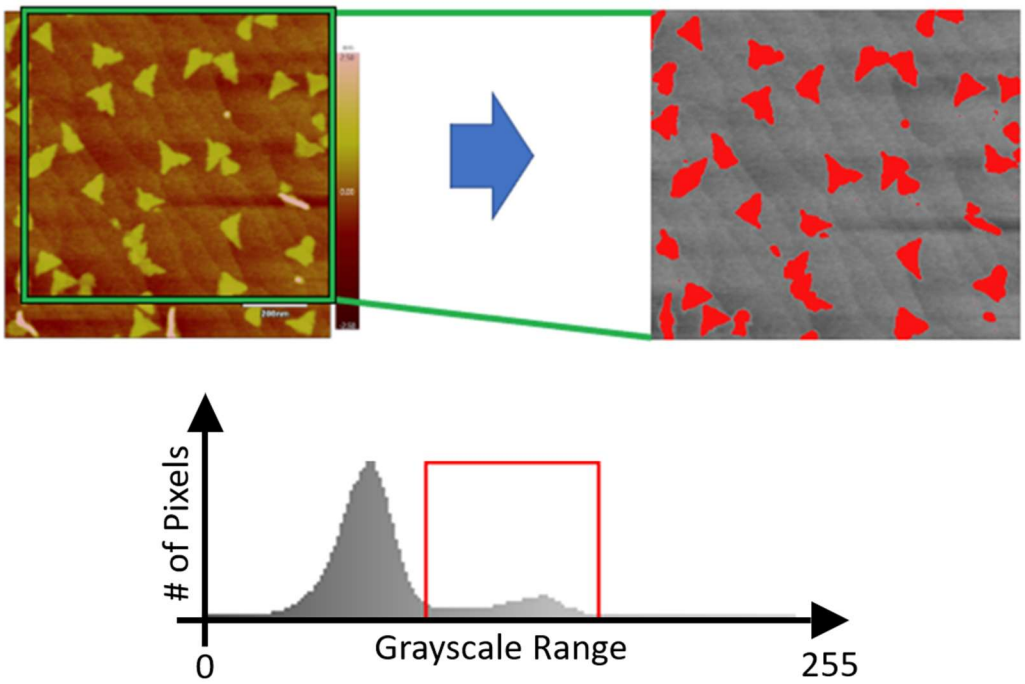

Figure 4.10: ImageJ thresholding process used to isolate and quantify WS_2 monolayer coverage based on color contrast in AFM images.

In addition to the overall coverage, the size of individual WS_2 domains was measured. The monolayer typically formed isolated triangular domains in early growth stages, and these were clearly visible in the AFM images. Using ImageJ, we either (a) performed particle analysis on the binary thresholded image (which yielded the area of each discrete island), or (b) manually outlined representative domains with the polygon selection tool to measure their area and linear dimensions. From the area, an equivalent circle diameter or triangle side-length was calculated for each domain to characterize its lateral size. We compiled statistics such as the average domain area and the size distribution. For example, we might find domain lateral sizes ranging from a few microns up to tens of microns, depending on the

growth time. The shape of the domains (mostly equilateral triangles, occasionally truncated or merged polygons) was noted qualitatively. Any instances of adjacent domains coalescing were also observed; in ImageJ we could visualize these as larger contiguous regions of interest (ROIs). This analysis provided insight into the grain size of the WS_2 monolayer, which is relevant for evaluating the material's continuity and the MOCVD growth kinetics.To validate the thickness and step height measurements, we used ImageJ's line profile tool on the AFM images. For a given AFM scan, multiple line sections were drawn across features of interest: e.g. across a WS_2 island edge crossing onto the substrate, and across substrate terrace steps. The software then outputs the height (z) as a function of lateral position for each line. These line profiles quantitatively confirmed the ~0.616 nm height of the WS_2 monolayer above the sapphire [42]. The profiles typically show a flat baseline on sapphire, a sharp rise of ~0.616 nm at the WS_2 boundary, and a flat top on the WS_2 domain – consistent with a single-layer. Similarly, profiles across sapphire step edges showed ~0.2 nm increments [41]. We often averaged multiple line profiles or took a histogram of pixel heights to improve precision in determining these values. The data from ImageJ (heights, distances) were cross-checked with the AFM controller's analysis software to ensure consistency. Line profiles were also useful to identify any double-layer regions: a step of ~1.23 nm would indicate a second WS_2 layer. In our scans, virtually all regions showed the single-layer height, confirming the monolayer nature of the film. All the extracted quantitative information (coverage, domain size, thickness) was recorded for comparison with other characterization techniques (e.g. PL) and with growth parameters. After processing, the AFM images were often flattened (plane-fit) and presented with appropriate color scales to clearly illustrate

the topography. ImageJ was an indispensable tool in this analysis, enabling both visual inspection and rigorous measurement of the AFM data.

Ensuring the precision and reproducibility of AFM measurements was a key consideration in our methodology. The vertical resolution of the Cypher AFM is on the order of angstroms, so the ~0.616 nm step of a monolayer WS_2 is well within the detectable range. By calibrating the Z scanner as described and using gentle tapping forces, we achieved height measurements with an uncertainty of only a few tenths of a nanometer. Repeated measurements of the WS_2 thickness on the same sample consistently gave values around 0.616 nm, confirming the precision of the technique. One potential source of error in measuring an ultrathin film is the presence of a thin adsorbate layer (e.g. water) on the substrate which can slightly alter the apparent height. However, sapphire is relatively low in adsorbed water compared to SiO_2, and the AFM was performed in ambient but low-humidity conditions, so any such effect was minimal. Moreover, since we measured the *difference* in height between WS_2 and adjacent bare substrate, any uniform offset (due to, say, a thin water layer on both) would cancel out. We estimate the systematic error in the absolute height to be within ±0.03 nm, which is sufficient for identifying monolayers.

To ensure reproducibility, we imaged multiple spots on each sample and also examined multiple samples grown under similar conditions. The monolayer height was reproducibly observed at ~0.616 nm in all cases. The lateral size and coverage measurements showed the expected trends with growth conditions (for example, longer growth yielded higher coverage), and these trends were consistently captured by AFM at different regions, indicating that the technique reliably reflects the true sample properties. Each AFM scan

was done twice (trace and retrace) and we confirmed that the features aligned perfectly without distortion, which evidences instrument stability. No significant drift was observed over the typical scan duration (a few minutes per frame), as facilitated by the closed-loop feedback and careful thermal equilibration. In some cases, after scanning a region, we would immediately scan the same area again to see if the act of scanning had caused any changes or damage (which also tested tip wear). We found that consecutive scans of the same area produced identical topographic images and height profiles, demonstrating that our tapping conditions were non-invasive (no tip-induced modifications to the WS_2).

We also took steps to avoid tip-related artifacts. A dull or contaminated AFM tip can lead to broadening of features and inaccurate height readings (due to convolution of tip shape). By using a high-quality tip and monitoring the image sharpness, we ensured the lateral resolution was sufficient to resolve the edges of WS_2 domains faithfully. The ~10 nm nominal tip radius imposes a lateral resolution limit but does not significantly affect the accuracy of step heights [44]. If any image showed signs of tip wear (e.g. blurring of fine details or double-tip effects), the tip was replaced and the calibration re-checked. In our experiments, a single tip could usually scan many (around 10) areas of WS_2 without degradation, due to the hardness of the tip and the gentle non-contact operation.

Finally, all measurements were performed under the same nominal settings to allow comparison across the dataset. This included using the same type of cantilever, similar setpoint ratios, and scan sizes. The consistency in methodology means that the measured differences in coverage or domain size between samples are attributable to the samples themselves and not experimental variation. Overall, the AFM provided a reliable and

reproducible means to measure the critical dimensions of the WS_2 monolayers, with each key measurement (thickness, coverage, etc.) repeatable across multiple scans and samples.

Chapter 5 - Experimental results

5.1 - Introduction

Growth of high-quality, monolayer WS_2 on sapphire is crucial for scalable 2D electronics. However, achieving large-area coalescence and unidirectional domain alignment in WS_2 monolayers via MOCVD remains challenging. Key obstacles include high nucleation densities leading to many small domains and the formation of inversion domain boundaries (mirror twins) when oppositely oriented domains merge [4]. These mirror twin boundaries act as metallic defects, degrading electronic and optical properties [4]. Recent advances in MOCVD growth have targeted these issues by carefully controlling substrate preparation and growth parameters. For example, pre-growth annealing of c-plane sapphire can create atomic step-terrace structures that guide epitaxy. Indeed, *in-situ* annealed sapphire steps have been shown to induce a preferred alignment of WS_2 domains, yielding coalesced films largely free of inversion boundaries [4]. Likewise, innovative MOCVD techniques – such as migration-enhanced growth and growth-etch cycling – have been developed to modulate nucleation and adatom diffusion. These approaches have enabled wafer-scale WS_2 monolayers with improved crystalline quality, including fully coalesced films grown in under an hour [35] and domains with enhanced optical properties due to reduced impurities. This chapter presents our experimental results on WS_2 monolayer growth via MOCVD on c-plane sapphire, focusing on how growth conditions influence film coverage, domain size, nucleation density, domain orientation, and step-edge-directed growth.

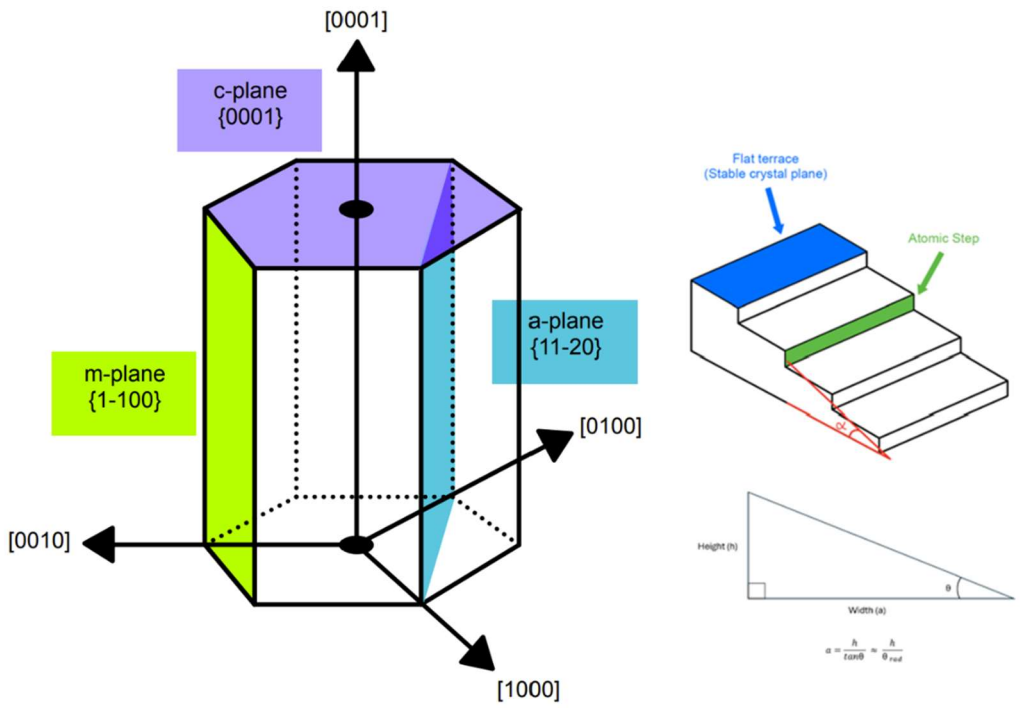

Figure 5.1: Hexagonal crystal structure of sapphire illustrating the m-, a-, and c-planes, alongside schematic representations of step-edge morphology showing step height, terrace width, and miscut angle.

We systematically varied the sapphire annealing temperature (1050 °C vs 1200 °C), nucleation temperature (550–850 °C), lateral growth temperature (650–775 °C), and substrate miscut (0°, 0.2° toward sapphire A-plane, 0.2° toward M-plane, and 0.15° towards M-plane as well). AFM was employed to characterize domain size distributions, monolayer coverage, domain orientations, and layer thickness (height). We elucidate the relationships between process parameters and WS_2 monolayer morphology by comparing these conditions. We also benchmark our findings against state-of-the-art WS_2 MOCVD reports – including migration-enhanced two-step growth, growth-etch MOCVD (with water-assisted

cycles), and step-edge epitaxy techniques – to highlight improvements and remaining challenges. The results show how optimizing nucleation and growth temperatures in tandem with substrate engineering (annealing and miscut) can dramatically influence the WS_2 monolayer coverage and crystal alignment. Key literature is integrated throughout to contextualize the observed trends and to draw parallels with similar strategies used for other TMDs (e.g. WSe_2 and $MoSe_2$).

5.2 - Impact of Growth Conditions on WS_2 Coverage

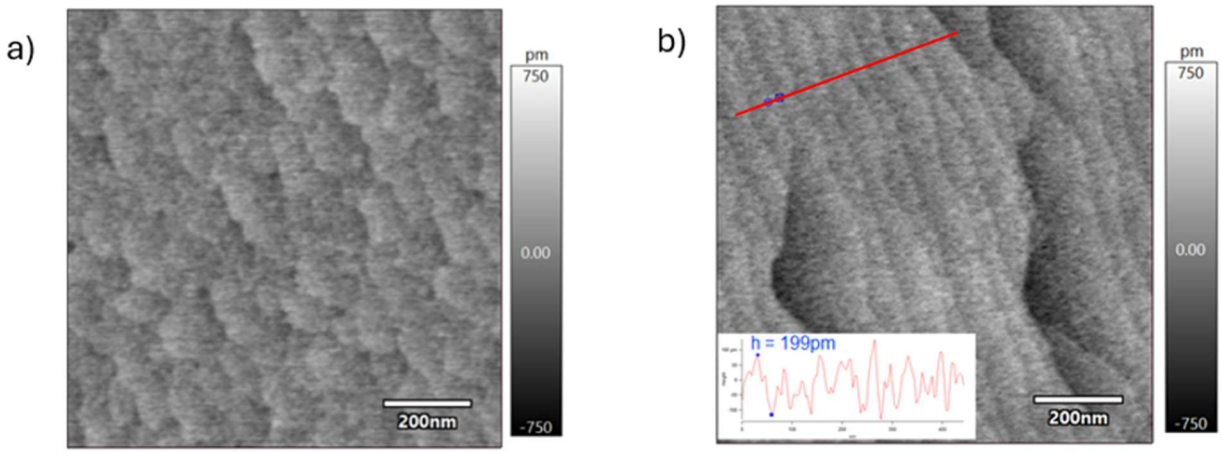

Figure 5.2: Step-edges morphology for annealing temp of a) 1050 °C for 30 min and b) 1200 °C for 10 min (steps towards m-plane).

Pre-growth annealing of the sapphire substrate proved to be a critical step for achieving higher WS_2 coverage. Annealing at 1200 °C for 10 min yielded well-defined atomic steps on the c-plane sapphire, whereas a lower annealing temperature of 1050 °C (even with longer durations up to 30 min) produced less developed step terraces. The improved surface regularity at 1200 °C directly translated to differences in the nucleation behavior and film

coverage. In our experiments with a fixed nucleation step (15 min) at 750 °C, substrates annealed at 1200 °C and 1050 °C both showed similar monolayer coverage (~15–21% for 1200 °C and ~15–19% for 1050 °C, under similar growth conditions). The higher-T anneal reduced random nucleation sites, funneling adatoms to step edges or other favorable sites, thus promoting lateral growth of fewer, larger domains. It can also be observed that WS_2 domains exhibit a more pronounced triangular shape at an annealing temperature of 1200 °C, in contrast to 1050 °C, where fewer triangular domains are present. This trend corroborates that sapphire steps act as preferential adsorption sites and reduce the overall nucleation density [4]. By minimizing uncontrolled nucleation, the 1200 °C anneal effectively increased the area each WS_2 domain could cover before impinging on a neighbor. In contrast, less-annealed surfaces (1050 °C) with fewer well-formed steps allowed more heterogeneous nucleation across the terraces, resulting in many small domains that only partially cover the substrate. These findings reinforce that a high-temperature anneal is beneficial for maximizing WS_2 coverage via epitaxial domain expansion on sapphire.

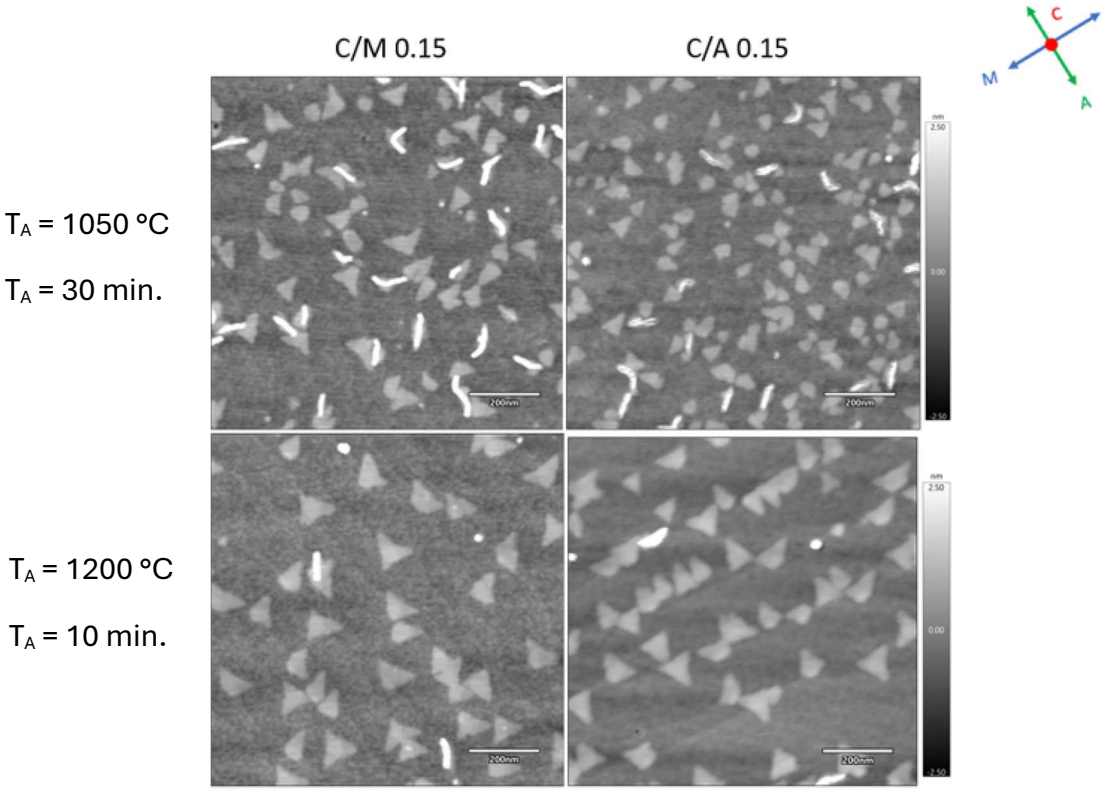

Figure 5.3: Comparison of WS_2 growth on sapphire substrates annealed at 1050 °C for 30 minutes and 1200 °C for 10 minutes, both at a nucleation temperature of 750 °C.

5.3 - Effect of Nucleation Time on WS_2 Monolayer Coverage

Extending the nucleation (growth) time in MOCVD has a clear quantitative impact on WS_2 monolayer coverage. In our experiments, increasing the nucleation time from 15 minutes to 75 minutes yielded roughly a linear rise in monolayer coverage from ~15% to ~75%. Qualitatively, the 15 min sample consists of small, well-separated triangular WS_2 monolayer islands, while the 50 min sample shows these domains growing larger and beginning to impinge on each other at ~50% areal coverage. By 75 min, lateral expansion of the monolayer

domains has created a nearly continuous film (~75% coverage), leaving only minor uncovered regions. This trend underscores that longer nucleation/growth duration directly increases monolayer coverage, as the existing domains have more time to expand and additional nuclei may form on remaining free surface. Similar time-dependent growth behavior is reported by Tang *et al.*, achieving ~24% monolayer coverage of WS_2 after a 15 min nucleation stage at 700 °C [35], and >99% coalesced monolayer film within a few hours by subsequently extending the overall growth duration (with optimized conditions) [35]. Houser *et al.* likewise observed that increasing MOCVD growth time from 5 min to 40 min transitions WS_2 films from a partial monolayer to a nearly full monolayer with the onset of bilayer formation [45]. These results collectively confirm that extended growth time strongly boosts monolayer coverage, although the rate of coverage increase may slow as it approaches completion due to coalescence effects and secondary layer nucleation.

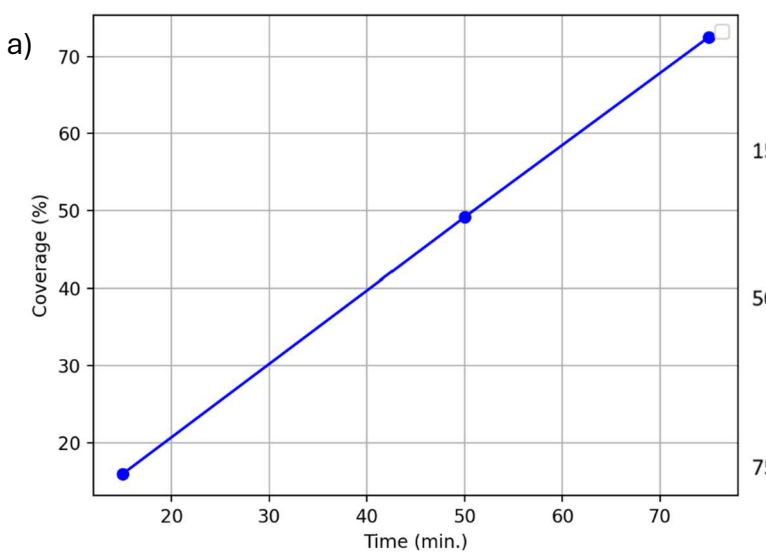

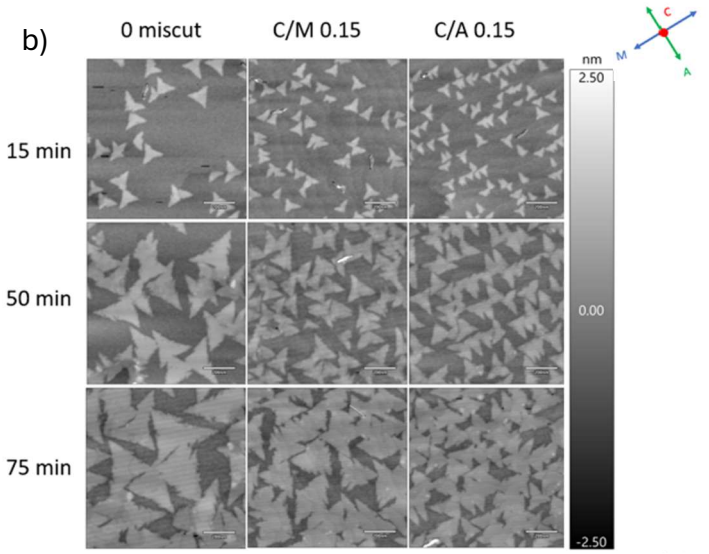

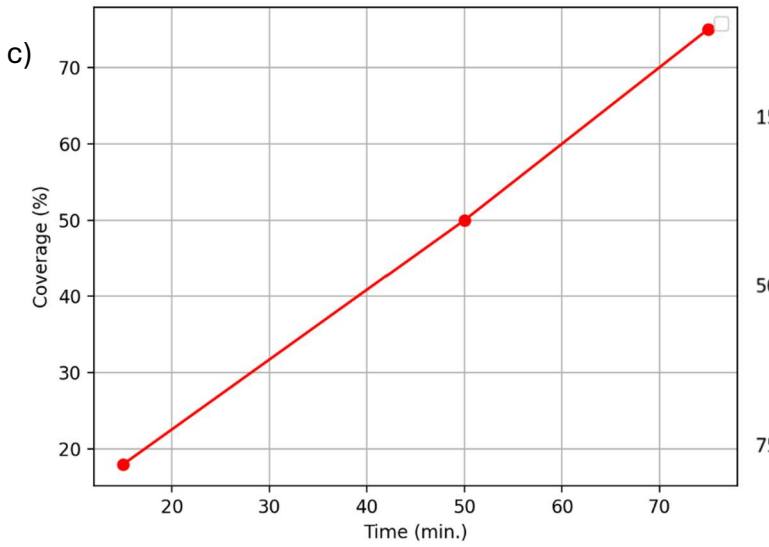

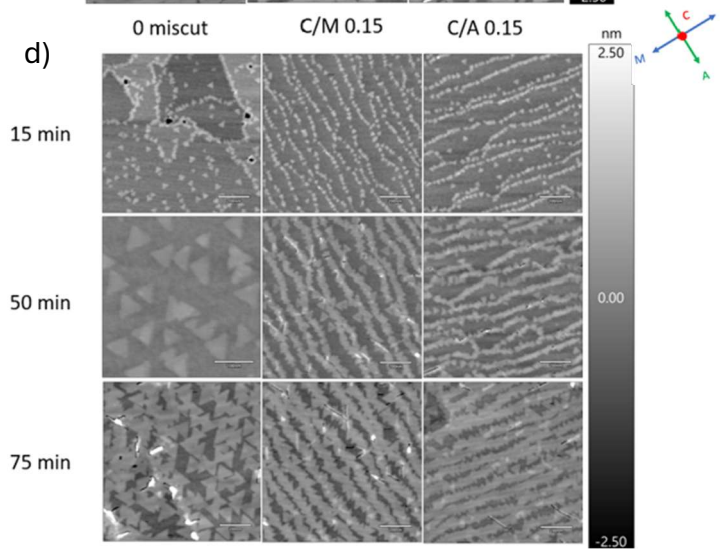

Growth #	Annealing Time (min.)	Annealing Temp. (°C)	Nucleation Time (min.)	Nucleation Temp. (°C)	ML Coverage (%)
2D0039	10	1200	15	700	~16%
2D0040	10	1200	50	700	~49%
2D0041	10	1200	75	700	~73%
2D0037	10	1200	15	550	~18%
2D0044	10	1200	50	550	~50%
2D0045	10	1200	75	550	~75%

Figure 5.4: Effect of Nucleation Time and Temperature on WS_2 Monolayer Coverage and Domain Morphology. **a)** Monolayer coverage as a function of nucleation time at 700 °C. **b)** 1um x 1um AFM images showing WS_2 domain growth at 700 °C for 15, 50, and 75 minutes, illustrating increased coverage with time. **c)** Monolayer coverage as a function of nucleation time at 550 °C. **d)** 1um x 1um AFM images of WS_2 domains at 550 °C for corresponding times, showing reduced coverage compared to 700 °C.

Beyond just the percentage of area covered, nucleation time also influences the density and size of WS_2 domains**.** A shorter 15 min growth primarily yields many small nuclei, whereas longer nucleation periods allow those nuclei to develop into larger domains. If new nucleation continues throughout the growth, one might expect a higher density of domains at longer times; however, our observations suggest that nucleation tends to saturate after an initial period, and subsequent time contributes mostly to lateral domain growth rather than the formation of new nuclei, in agreement with earlier observation in the literature. In other words, once a sufficient density of stable WS_2 nuclei has formed on the substrate, extending the growth time favors domain size increase over nucleation density. This behavior was intentionally exploited by Tang *et al*. through a two-step MOCVD process: an initial low-temperature nucleation step produced a high density of small WS_2 nuclei (~140 nuclei per μm^2, each ≤50 nm in size) covering ~24% of the area, and then a second, higher-temperature step promoted exclusively lateral growth of those nuclei, ultimately achieving a fully coalesced monolayer film [35]. The fact that our 75 min sample reached ~75% coverage (instead of simply three times more separate islands) indicates that most bare substrate

sites had nucleated by mid-growth, and thereafter the increase in coverage came from existing domains spreading laterally. This is advantageous for producing uniform films, since lateral expansion merges domains together, whereas continuous nucleation would create new islands and additional grain boundaries. Indeed, recent MOCVD studies emphasize that regulating the nucleation stage (in terms of time, temperature, and precursor flow) is critical for balancing domain density and size. By extending the nucleation/growth duration under appropriate conditions, one can obtain larger WS_2 grains and higher coverage, albeit with the caution that unchecked prolonged growth may start generating second-layer nuclei once the monolayer coverage nears completion [35].

5.4 - Nucleation vs. Lateral Growth Temperature

The growth of WS_2 monolayers in our MOCVD process was conducted in two stages – a low-temperature nucleation step (15 min) to seed the initial domains, followed by a higher-temperature lateral growth step to enlarge those domains. We investigated nucleation temperatures from 550 °C up to 750 °C (15 min each), combined with lateral growth temperatures ranging from 650 °C to 775 °C. The choice of these temperatures had a profound impact on final monolayer coverage. We observed a monotonic trend in coverage with nucleation temperature in the single-step scenario (no separate lateral growth stage, anneal 1200 °C, miscut 0.2° toward m-plane). From a low nucleation temperature (550 °C) to a high nucleation temperature (750 °C), the coverage looks to stay constant at 15-16%.

The coverage improved dramatically when a separate high-temperature growth stage was introduced after the nucleation. For example, nucleating at 650 °C (15 min) and then

ramping to 775 °C for a 30 min lateral growth enabled the WS_2 domains to cover about 50% of the substrate area, a substantial increase from the ~13–17% seen with 15 min at 650–700 °C alone. Similarly, at a 550 °C nucleation, adding a 30 min growth at 675 °C raised the coverage from ~16% (single-step) to ~50%, despite the extremely high nucleation density in that case.

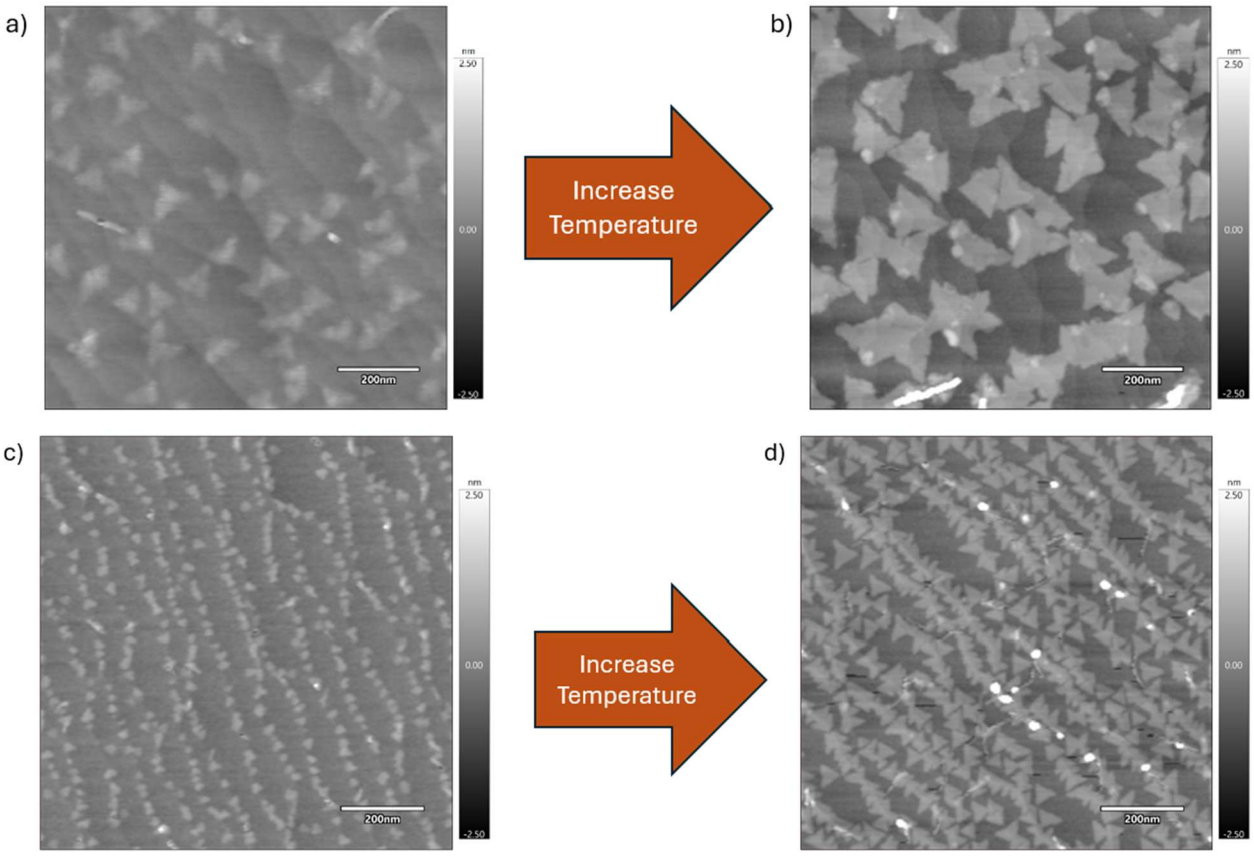

Figure 5.5: Effect of Lateral Growth Temperature on WS_2 Domain Size at Different Nucleation Temperatures. **a)** WS_2 domains nucleated at 650 °C for 15 minutes without lateral growth. **b)** WS_2 domains from a) subjected to lateral growth at 775 °C for 30 minutes. **c)** WS_2 domains nucleated at 550 °C for 15 minutes without lateral growth. **d)** WS_2 domains from c) subjected to lateral growth at 675 °C for 30 minutes.

The higher lateral growth temperature accelerates adatom surface diffusion and supply, allowing initial nuclei to expand outward more effectively before impinging on one another. Essentially, the two-step process takes advantage of low-T nucleation to create many starting points, then uses high-T growth to drive coalescence of those domains over a larger area. However, there is a trade-off: if the nucleation density is too high (e.g., at 550 °C), even though coverage improves with a lateral growth step, the many small domains quickly merge and can start forming multilayers or voids rather than a perfect monolayer film. On the other hand, if nucleation density is very low (e.g., 700-750 °C nucleation), one might not have enough nuclei to cover the surface even with prolonged growth.

Our findings align with the general understanding of 2D film coalescence. Chubarov *et al*. report that using a multistep MOCVD process (a lower-temperature nucleation phase followed by a higher-temperature growth phase) enables WS_2 domain coalescence into a continuous monolayer while minimizing the introduction of new nuclei in the second phase [4]. In their study, once the nuclei were established at 850 °C, increasing the temperature to 1000 °C greatly enhanced adatom mobility and lateral growth, allowing domains to stitch together into a wafer-scale film [4]. Notably, they achieved a coalesced monolayer in about 45 min of lateral growth time with an effective growth rate of ~1.6 monolayer/hour [4], vastly faster than the ~0.04–0.05 monolayer/hour rates observed in earlier one-step processes [4]. This underscores how favoring lateral expansion (through optimized conditions and extended growth) accelerates the attainment of high coverage. In our case, although we maintained constant temperature, the later time intervals similarly served as a lateral growth-dominated regime. The approximately linear increase of coverage

with time up to 75 min suggests that the growth rate per unit area remained fairly steady – each additional minute of growth converted roughly 1% of the substrate from bare to monolayer coverage. This is consistent with a process where the supply of adatoms continues to fuel outward domain propagation at a roughly constant rate. However, we anticipate that if growth were extended further towards full 100% coverage, the rate might begin to taper off. As the gaps between WS_2 domains shrink, adatoms have to travel farther (or wait longer) to find the last open spaces, and some may start contributing to second-layer growth on top of the monolayer instead of filling in the remaining voids [35]. Indeed, Tang *et al*. observed that as their WS_2 film reached close to coalescence, the probability of bilayer nucleation rose because adatoms landing on existing monolayer could not all reach an island edge before aggregating into a new layer [35]. This phenomenon sets a practical limit: purely lateral growth can drive coverage nearly to unity, but in the absence of perfect adatom capture at the edges, some atoms will eventually nucleate second layers once monolayer coverage is essentially complete.

5.5 - Domain Size and Nucleation Density

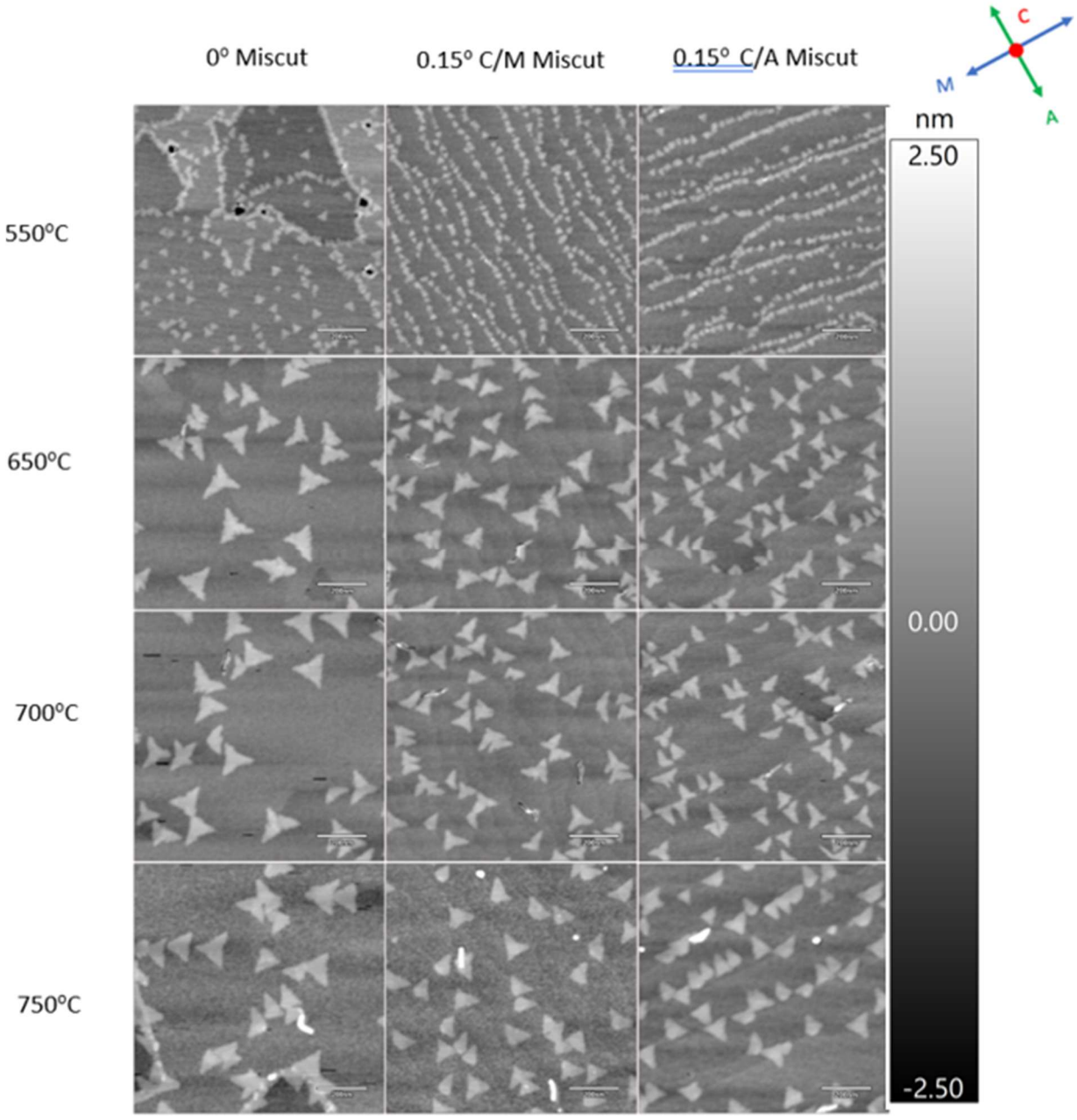

Figure 5.6: Comparison of WS_2 Domain Size and Nucleation Density as a Function of Nucleation Temperature and Substrate Miscut Direction.

A clear inverse correlation was observed between WS_2 domain size and nucleation density across the range of growth conditions. AFM images (Figure 5.6) reveal that at lower nucleation temperatures (e.g., 550–600 °C), the sapphire surface is populated by a very high density of tiny triangular WS_2 domains, whereas at higher nucleation temperatures (700–750 °C) far fewer domains nucleate, and each can grow substantially larger. We quantified domain size as the height of the triangular monolayer.

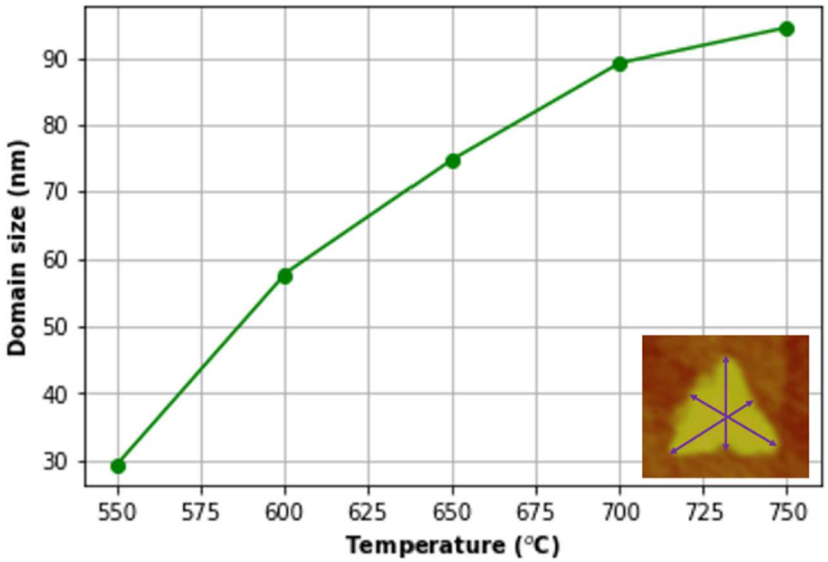

Growth #	Annealing Time (min.)	Annealing Temp. (°C)	Nucleation Time (min.)	Nucleation Temp. (°C)	Domain size (nm)
2D0014	10	1200	15	550	29.4
2D0013	10	1200	15	600	57.7
2D0012	10	1200	15	650	74.8
2D0011	10	1200	15	700	89.2
2D0015	10	1200	15	750	94.5

Figure 5.7: Effect of Nucleation Temperature on WS_2 Domain Size.

Both metrics showed the same trends. For instance, with a 15 min nucleation at 550 °C (anneal 1200 °C, miscut 0.2° M), the average triangle size was only ~30–40 nm, whereas at 750 °C nucleation it increased to ~90–100 nm (under otherwise similar conditions). These AFM-measured sizes indicate that roughly a 3–5× increase in linear domain dimension (and thus an order of magnitude larger area per domain) is achievable by raising the nucleation temperature from the low (550 °C) to high (750 °C) end of our range. This makes sense because higher temperatures reduce the density of critical nuclei – adatoms can diffuse longer and aggregate into fewer stable islands – allowing those fewer islands to gather more material and expand larger before impinging on a neighbor.

$$D_N = \left(\frac{Number\ of\ ML}{Area\ of\ image\ in\ um^2} \right)$$

The nucleation density, defined as the number of monolayer islands per unit area, showed complementary behavior. From image analysis of 1×1 μm^2 AFM scans, we measured nucleation densities ranging from about 270 domains/μm^2 at 550 °C nucleation down to ~25–35 domains/μm^2 at 750 °C (15 min nucleation, 1200 °C anneal). Figure 5.7 plots domain side-length (left axis) and nucleation density (right axis) versus nucleation temperature for a series of samples grown with identical annealing (1200 °C, 10 min) and no intentional miscut. The relationship is roughly inverse-exponential: small increases in nucleation temperature initially cause a steep drop in nucleation density and rise in domain size, then plateau at higher temperatures. For example, going from 550 to 600 °C, the density dropped from ~270 to ~62 domains/μm^2 while the average size doubled from ~30 to ~60 nm. Another

jump from 600 to 650 °C was accompanied by density drop further to ~42/μm^2 and the size increased to ~75 nm [5]. By 700 °C, density was ~30/μm^2 and side ~90 nm, and at 750 °C (with similar conditions) we recorded densities on the order of 25/μm^2 and domains ~95 nm.

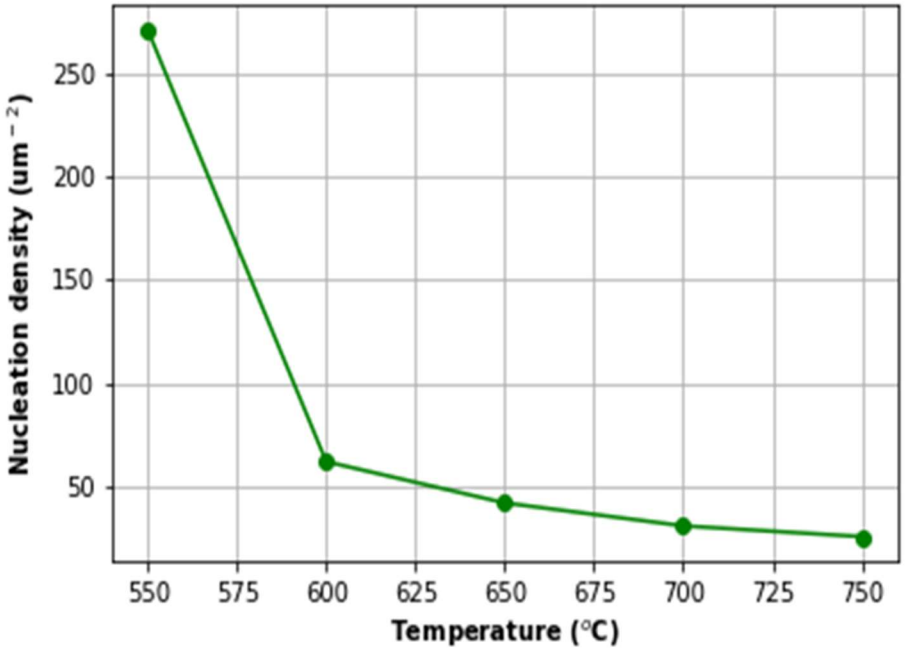

Growth #	Annealing Time (min.)	Annealing Temp. (°C)	Nucleation Time (min.)	Nucleation Temp. (°C)	Nucleation Density (um^{-1})
2D0014	10	1200	15	550	270
2D0013	10	1200	15	600	62
2D0012	10	1200	15	650	42
2D0011	10	1200	15	700	30
2D0015	10	1200	15	750	25

Figure 5.8: Effect of Nucleation Temperature on WS2 Nucleation Density.

It is useful to compare these domain sizes with literature reports for WS_2. Our largest single-crystal domains (~0.3 μm across for a nucleation temperature of 700 for 75 minutes) are relatively small in an absolute sense; CVD growth using oxide precursors at atmospheric pressure can routinely produce WS_2 domains tens of microns in size by deliberately suppressing the nucleation (e.g., using seeding promoters and very dilute precursor fluxes).

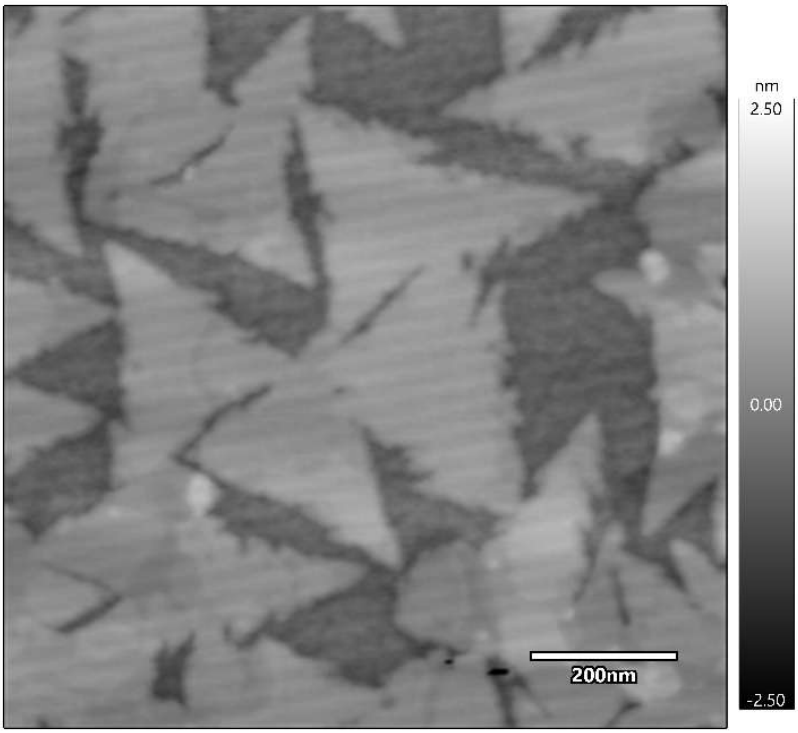

Figure 5.9: Largest WS_2 Domain Observed During Growth Experiments (~0.3 μm) using an annealing temperature of 1200 °C for 10 minutes and a nucleation temperature of 700 °C for 75 minutes.

In MOCVD with metal-carbonyl precursors, domain sizes have historically been much smaller (a few hundred nm) due to the high nucleation propensity of the precursors. For instance, early MOCVD experiments with $W(CO)_6$ noted that continuous monolayers

required extremely long growth times (~26 hours) and still yielded small grain sizes (10s to 100s of nm). Our results, achieving ~300 nm domains in just over an hour of total growth, indicate a significant improvement enabled by substrate conditioning and longer nucleation time. Moreover, by incorporating a growth-etch technique or pulsed precursor flow, others have managed to increase domain sizes in MOCVD further. In the GE-MOCVD approach, a small amount of an oxidizing agent (e.g., H_2O vapor) is introduced periodically during growth to selectively etch away smaller nuclei while larger domains survive and expand. This suppresses the high nucleation density that typically accompanies continuous precursor flow. Using GE-MOCVD, researchers have reported WS_2 domains on sapphire that are an order of magnitude larger than those from standard MOCVD, with dramatically improved crystal quality (e.g., sharper Raman peaks, higher PL). Although we did not employ water-assisted etching in our experiments, our two-step method inherently reduced effective nucleation density during the high-T growth phase—smaller nuclei from the 15 min low-T stage may either stop growing or sublimate at the higher temperature, effectively filtering out some nuclei. Indeed, we observed that the effective nucleation density after the high-temperature growth stage was often lower than after the initial nucleation stage. For example, one sample nucleated at 600 °C had an initial density of ~62/μm^2, but after a 30 min 775 °C growth, many of the smallest islands had not grown (or had dissolved), leaving ~47/μm^2 larger domains (with others presumably etched away or merged). This phenomenon is analogous to the GE-MOCVD concept (removal of excess nuclei), albeit achieved here simply by Ostwald ripening and high-T desorption rather than intentional water etching.

Another parameter to consider is the growth rate per nucleus, which we estimated by two metrics: (a) nucleation density evolution and (b) domain area increase. For instance, at 650 °C nucleation (15 min) followed by 30 min at 775 °C, the nucleation density stayed for both stages was ~42 to ~47 μm^{-2} (staying roughly constant, meaning no new nuclei appeared during the higher-T stage), while the average domain area grew from ~3.9×10^{3} nm^2 to ~1.06×10^{4} nm^2.

5.6 - Domain Orientation and Alignment

Surface steps on sapphire break the degeneracy between the two mirror-twin orientations (0° vs 60°), thereby reducing the formation of inversion domain boundaries (IDBs) that arise when oppositely oriented domains coalesce [4]. For example, Chubarov *et al*. demonstrated that nearly 95% of a coalesced WS_2 monolayer film on sapphire could be aligned in the same direction by utilizing substrate atomic steps to guide domain orientation [4] preferentially. In that work, the miscut substrate produced aligned steps which induced unidirectional epitaxy, yielding a film largely free of inversion domains and their associated mirror-twin boundaries [4]. This confirms that deliberate substrate miscut (and the resulting step array) is a powerful tool for promoting unidirectional domain alignment.

In our experiments, the 0.2° miscut toward the m-plane produced a modest ~60:40 orientation ratio favoring one domain orientation. This partial alignment indicates that the sapphire steps bias the nucleation of WS_2: one orientation (presumably the one energetically favored by the step-edge geometry) nucleates more easily on the step edges. In contrast, the other orientation is somewhat suppressed. The fact that our alignment is not as high as the

~95–99% reported in the literature suggests that further optimization is needed, for instance, a slightly larger miscut angle (to increase step density) or adjustments in growth conditions to enhance step-edge nucleation selectivity. Interestingly, the 0.2° a-plane miscut did not yield improved alignment in our case; the domain distribution remained ~50:50. This contrast between m- and a-plane miscuts could be due to differences in the atomic structure of the step edges: steps oriented toward different crystalline directions may present different bonding environments for adatoms. Recent studies on WSe_2 epitaxy have shown that surface chemistry and step orientation can determine whether domains prefer a 0° or 60° alignment relative to the substrate [4]. Thus, it is plausible that our a-plane steps favoured the opposite orientation (cancelling out any preference) or introduced competing nucleation sites. In contrast, the m-plane steps offered a clearer energetic preference for one domain orientation. Overall, controlling the substrate miscut direction emerges as a key lever for tuning domain orientation distribution, directly impacting the prevalence of inversion domains in the film.

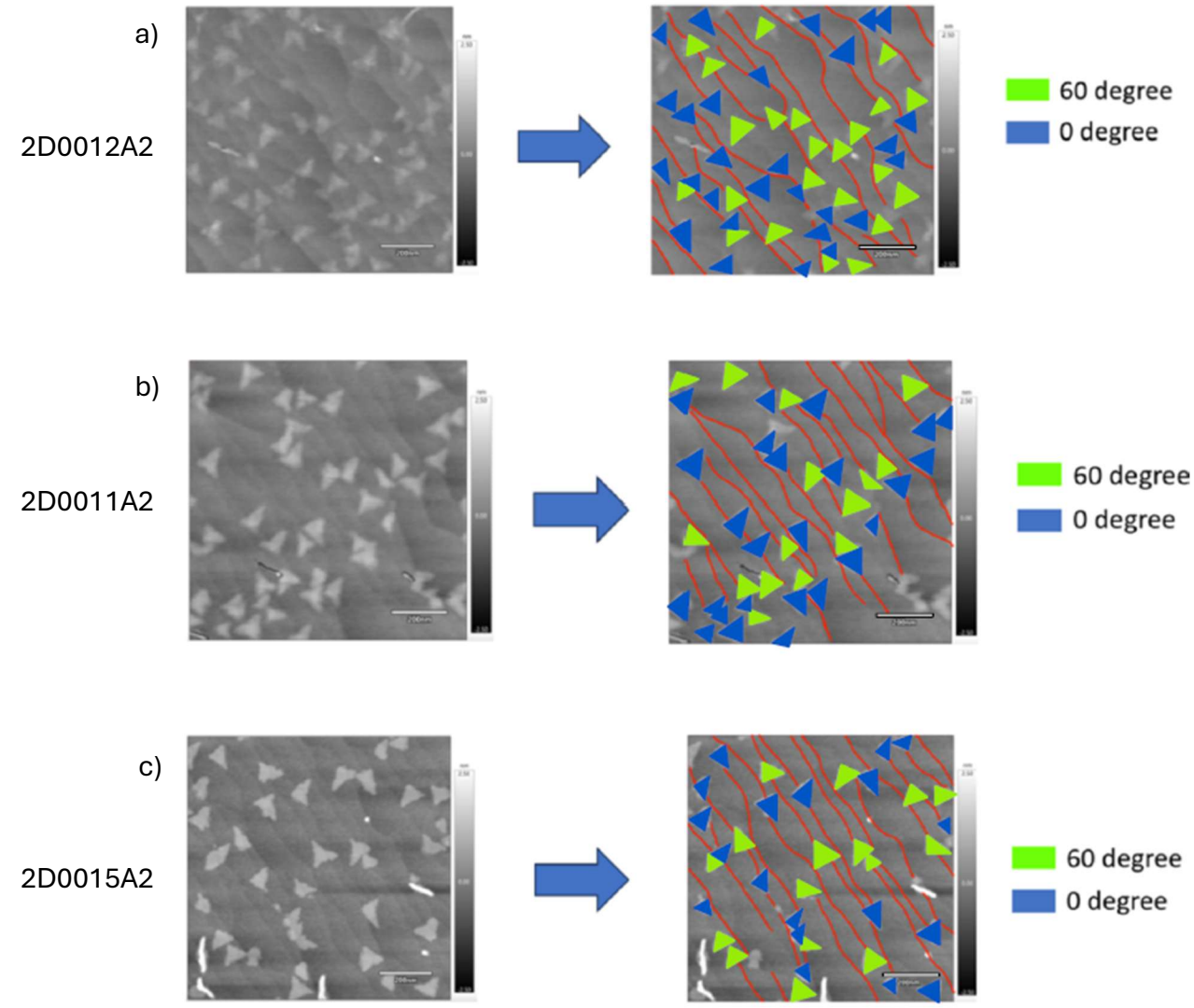

Growth #	Annealing Time (min.)	Annealing Temp. (°C)	Nucleation Time (min.)	Nucleation Temp. (°C)	Orientation (60°/0°)
2D0012A2	10	1200	15	650	28/22
2D0011A2	10	1200	15	700	24/15
2D0015A2	10	1200	15	750	22/15

Figure 5.10: Orientation Analysis of WS_2 Domains on Sapphire with 0.15° Miscut Towards the m-plane at Varying Nucleation Temperatures.

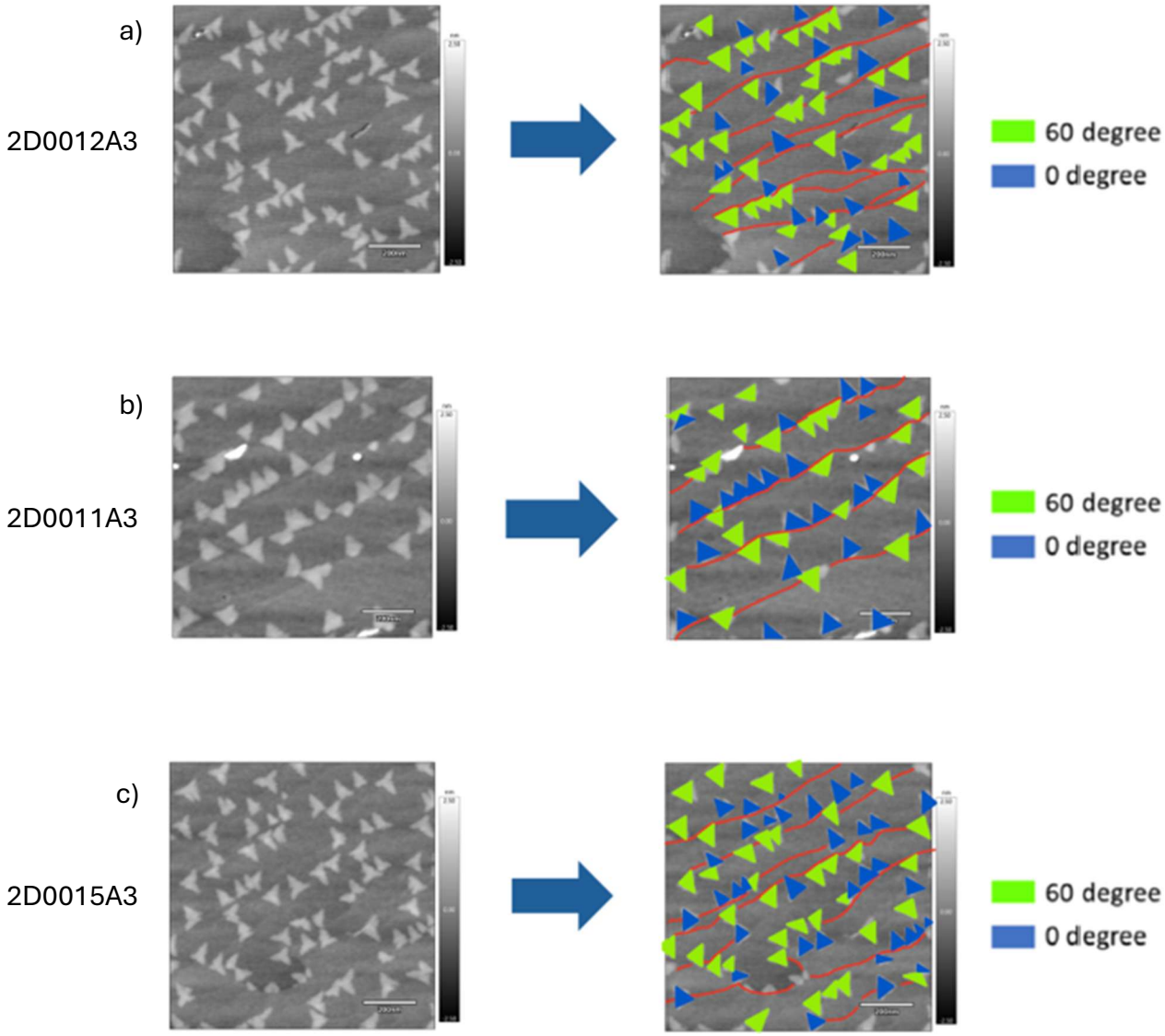

Growth #	Annealing Time (min.)	Annealing Temp. (°C)	Nucleation Time (min.)	Nucleation Temp. (°C)	Orientation (60°/0°)
2D0012A3	10	1200	15	650	24/23
2D0011A3	10	1200	15	700	24/22
2D0015A3	10	1200	15	750	37/35

Figure 5.11: Orientation Analysis of WS_2 Domains on Sapphire with 0.15° Miscut Towards the a-plane at Varying Nucleation Temperatures.

5.7 - Step-Edge Morphology and Monolayer Confirmation

Atomic force microscopy measurements were used to characterize both the WS_2 layer thickness and the substrate step morphology. The AFM topography confirms that the as-grown triangular domains are monolayer in thickness: height profiles across the domains show a step of approximately 0.6–0.7 nm from the sapphire surface up to the top of the WS_2 islands. This observed height agrees with the expected thickness of a single WS_2 layer (the van der Waals thickness of monolayer WS_2 is around 0.616 nm). We thus conclude that the domains discussed throughout this chapter are indeed monolayer WS_2, as intended, rather than multilayer stacks. In addition, no thicker layers (e.g. bilayers) were found in the regions profiled, indicating that the growth conditions effectively produced a single-layer film.

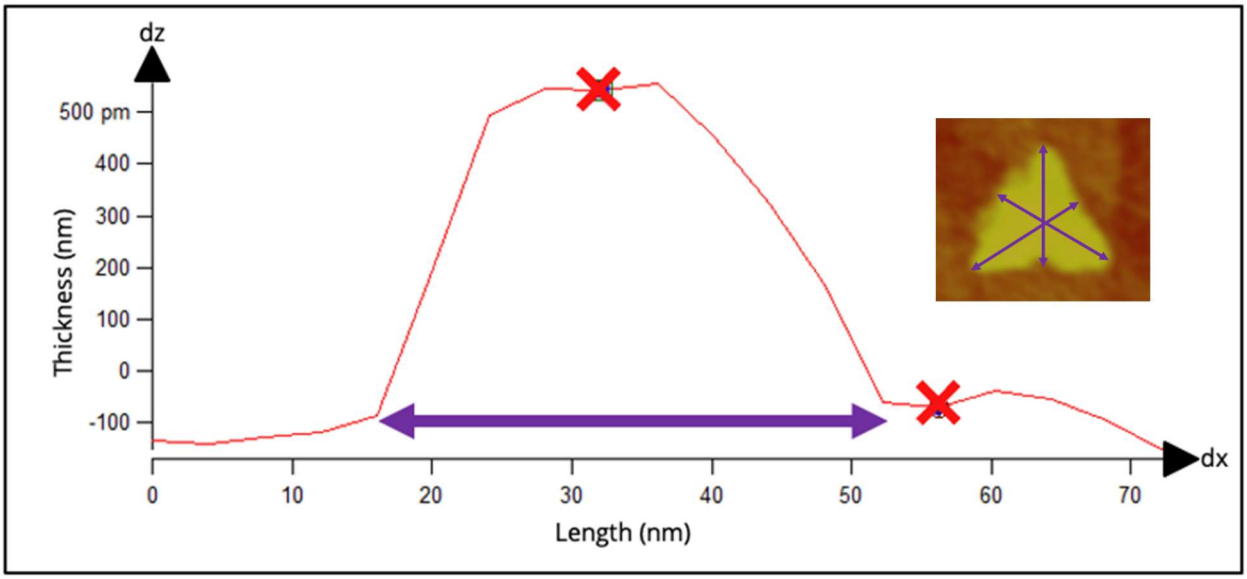

Figure 5.12: Line profile showing the thickness of a WS_2 monolayer domain extracted from AFM data, plotted as Thickness (nm) vs. Length (nm).

AFM analysis also provided insight into the step-edge morphology of the sapphire substrates after the high-temperature annealing. Bare sapphire regions exhibit atomically flat terraces separated by step height increments of ~0.2 nm, corresponding to a single atomic step on the c-plane sapphire surface, consistent with one-sixth of the c-axis lattice spacing for α-Al_2O_3. The terrace width on the 0.2° miscut substrates was on the order of tens of nanometers (roughly 60–80 nm measured between consecutive steps), in line with the expected spacing from geometric considerations. These dimensions (~0.2 nm step height and ~70 nm terrace length) match the miscut angle of 0.2°, confirming that the annealing process produced a well-defined array of atomic steps rather than irregular surface roughness. On the nominally on-axis substrate (0° miscut), the AFM still revealed some surface steps, but they were irregularly spaced and in some areas much farther apart (hundreds of nanometers or more), as is typical for a polished c-plane wafer with no intentional miscut.

The influence of this step morphology on WS_2 growth is evident when correlating with domain orientations and coverage. On the closely stepped surfaces (0.2° miscut), WS_2 domains tend to nucleate at step edges, which act as preferential sites due to their lower adsorption energy barrier. A dense array of parallel step edges guides the lateral expansion of the monolayers along specific directions, reinforcing the alignment effect.

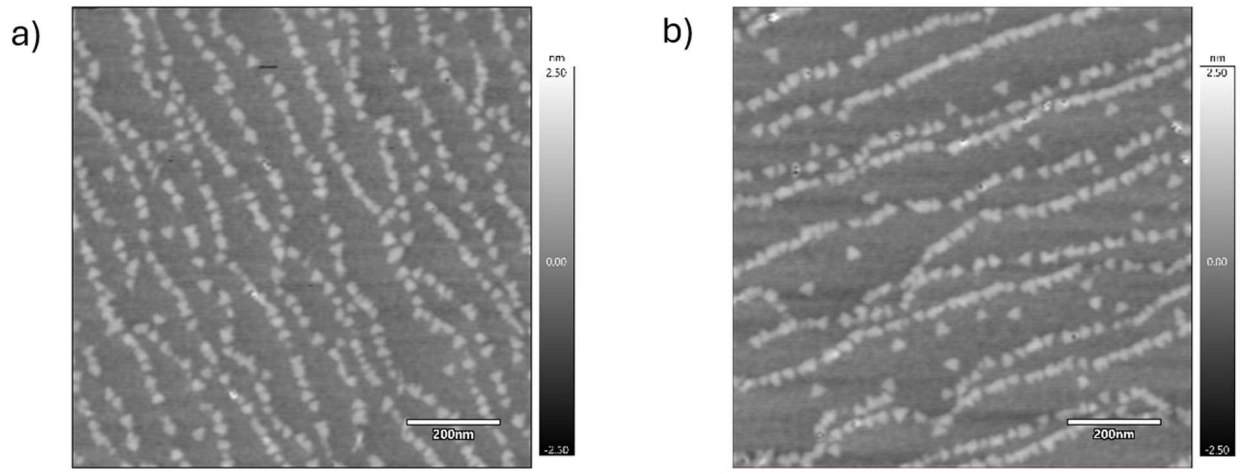

Figure 5.13: Controlled Growth of WS_2 Domains Aligned Along Step-Edges of Sapphire Substrates in a) m-plane and b) a-plane direction.

By contrast, expansive terraces (as on the 0° miscut substrate) present larger flat areas where nucleation can occur with less guidance, leading to more random domain orientations and placements. The step edges influence orientation and appear to impact the vertical layer uniformity of the growth. We observed that regions with well-defined, closely spaced steps yielded almost exclusively monolayer coverage. Once a monolayer patch covers a terrace, further lateral growth tends to continue outward along the substrate rather than stacking a second layer on top. This behavior suggests a layer-by-layer growth mode facilitated by the step edges: the WS_2 islands grow across a terrace until they encounter a step, at this point, new nucleation can occur at the next lower step terrace. Such an edge-mediated growth mechanism helps suppress the formation of bilayer or multilayer islands on top of the first layer.

Recent reports support the idea of using substrate steps to achieve layer-by-layer control. Chubarov *et al*. noted that regulating the monolayer growth rate (effectively controlling how quickly domains extend before new nuclei form) could significantly reduce the density of bilayer patches in epitaxial WS_2 films [4]. In our growth, the combination of a two-step process (separate nucleation and lateral growth stages) and the use of atomic terraces likely played a role in limiting bilayer growth. Only infrequent bilayer nuclei were observed, typically in regions away from step edges or with an extended growth time. In general, promoting nucleation at the substrate edges (either the substrate's steps or the edges of existing WS_2 domains) provides a route to confine new layer formation to the uncovered substrate areas. This approach is analogous to the step-flow growth mode in conventional epitaxy. We maintain a uniform monolayer thickness across the sample, by ensuring that adatoms attach at the perimeter of existing islands or at defined step sites. Achieving a uniform monolayer while minimizing multi-layer islands is crucial for device applications, as bilayer or thicker regions can act as electronic and optical heterogeneities.

5.8 - Summary of Key Findings

In Chapter 5, we investigated the growth of WS_2 monolayers by MOCVD, focusing on how nucleation time and growth dynamics affect the resulting film coverage and quality. The key findings can be summarized as follows.

First, extending the nucleation/growth duration markedly increases the WS_2 monolayer coverage roughly linearly (under our conditions, 15 min yielded ~15% coverage, 50 min ~50%, and 75 min ~75% coverage). Longer growth times allow the initial WS_2 nuclei to

expand laterally, converting more of the substrate surface into monolayer coverage. This demonstrates that growth time is critical for achieving near-full coverage films. Our results are consistent with recent reports that prolonged MOCVD growth (especially in multiple stages) can lead to fully coalesced monolayer WS_2 across wafer-scale areas [35]. However, we also note that simply extending time has limits: once the monolayer becomes almost continuous, additional deposition can trigger bilayer formation rather than increasing monolayer area [35].

Second, we found that lateral domain growth, rather than continuous nucleation of new domains, is primarily responsible for the increased coverage at longer times. After an initial nucleation phase that seeds the substrate with many small WS_2 islands, subsequent growth occurs predominantly at the edges of those islands. This lateral growth mode leads to much larger domain sizes at 75 min compared to 15 min, and the domains begin to merge. Crucially, higher coverage was achieved without a proportional increase in domain density, indicating that we suppressed additional nucleation in favor of enlarging existing domains. This insight aligns with the strategies reported in literature for improving film crystallinity: by limiting nucleation density and promoting lateral expansion, one obtains bigger single-crystalline domains and fewer grain boundaries [35].

Third, we investigated the mechanisms enabling the lateral growth. Sufficient adatom surface diffusion and fast edge incorporation are the enabling factors that drive the domain expansion. The growth conditions in our MOCVD process provided a regime where W and S adatoms could travel to find island edges and attach, rather than nucleating new islands indiscriminately. We discussed how the energetics favor adatoms joining existing lattices

(lower energy pathway) unless supersaturation is too high. By controlling growth temperature and precursor flux, one can tilt the balance toward edge growth – for example, higher temperature or lower W flux increases adatom mean free path and suppresses new nucleation [35]. These factors collectively ensured that, during extended growth, WS_2 domains spread laterally until coalescence began.

This chapter underscores that achieving high-coverage, high-quality WS_2 monolayers via MOCVD requires careful control of the nucleation and growth dynamics. A longer nucleation time (or total growth time) directly translates to greater monolayer coverage, but the manner in which that coverage is attained is crucial. Optimally, one should aim for an initial burst of nucleation to seed the surface with a moderate density of islands, then prolong the growth under conditions favoring lateral domain growth (e.g. adequate diffusion length, optimized precursor supply). Using this approach, we obtained up to 75% monolayer coverage in our experiments, with evidence that the domains were well on their way to coalescing into a continuous film. This is a significant step toward wafer-scale monolayer WS_2. The trends observed here mirror state-of-the-art developments reported by other researchers – for instance, multi-step MOCVD processes achieving full monolayer coverage and large grain sizes [35]. The fundamental growth mechanisms discussed (surface diffusion, edge kinetics, thermodynamic driving forces) provide a framework for further optimizing the MOCVD growth of WS_2 and other TMD monolayers. By harnessing these insights, one can minimize grain boundaries and avoid premature second-layer formation, thereby improving the electronic and optical quality of the WS_2 monolayer. Overall, the work in this chapter contributes to the understanding of how to grow uniform, large-area monolayer WS_2 by

MOCVD – a critical capability for integrating this 2D material into future devices and applications.

Chapter 6 - Discussion and Conclusion

6.1 - Influence of Substrate Annealing on Nucleation and Domain Orientation

Pre-growth annealing of the sapphire substrates proved to be a critical factor for controlled WS_2 nucleation. We found that annealing at a sufficiently high temperature (~1200 °C) produces well-defined atomic step terraces on the sapphire surface, whereas a lower-temperature anneal (e.g. 1050 °C, even if prolonged) yields a less developed step structure. The high-temperature anneal cleans and orders the substrate surface by removing contaminants and inducing step-bunching. These atomic step edges serve as energetically favorable nucleation sites for WS_2 adatoms. Consequently, substrates annealed at 1200 °C exhibit more uniform and *controlled* nucleation: adatoms are funneled to the step edges instead of random defect sites, leading to fewer random nucleation events across the terrace faces. In contrast, insufficient annealing leaves a disordered surface where nucleation can occur stochastically over the surface. The impact is evident in the nucleation density and initial domain size. With a fixed nucleation step (e.g. 15 min at 750 °C), a 1200 °C-annealed substrate showed a lower density of nuclei but larger average domain size compared to a 1050 °C-annealed substrate, even though the initial monolayer coverage was comparable (~15–21% in both cases). In other words, high-T annealing did not markedly change the fraction of area covered in the seeding stage, but it *did* change how that coverage was distributed: the nuclei were fewer in number and each could later grow larger laterally before impinging on neighbors. These observations align with reports that improved substrate preparation reduces uncontrolled nucleation and allows domains to grow bigger

by limiting competition for adatoms. In short, an adequately high annealing temperature (~1200 °C in our case) is essential to obtain an atomically ordered, clean sapphire surface that *sets the stage* for controlled WS_2 nucleation and growth.

An equally important aspect of substrate preparation was the intentional slight miscut of the sapphire wafers (~0.1°–0.2° off the c-plane) prior to annealing. This vicinal miscut leads to a regular array of aligned step edges after the high-temperature anneal, and it has a profound effect on the in-plane orientation of WS_2 domains. On nominally flat c-plane sapphire (with no miscut), triangular WS_2 monolayer domains nucleate with random in-plane orientations; due to the six-fold symmetry of the c-plane, domains typically appear in two preferred orientations rotated ~60° from each other, with no inherent bias towards either orientation. However, on a miscut substrate that has been annealed to produce aligned step-terraces, we observed that a majority of WS_2 domains adopt a unidirectional alignment along the step edges. Specifically, in growths on 0.15°–0.2° miscut sapphire, ~60% of the monolayer domains were oriented in the same direction (0° rotation), with the remainder rotated by 60°. This partial but significant alignment confirms that step-edge engineering can bias the epitaxial orientation of WS_2, favoring one crystallographic orientation over the other twin orientation. In practical terms, the combination of a high-temperature anneal and a slight substrate miscut yielded a film in which over half of the individual WS_2 grains were aligned in the same direction – a notable improvement toward epitaxial alignment on what is otherwise an amorphous or symmetric substrate surface. While not a complete elimination of twin domains, this result demonstrates a degree of orientational ordering that is rarely achieved on nominal sapphire and highlights the role of substrate steps in guiding domain orientation.

Consistently, we found that substrates that underwent rigorous preparation (thorough cleaning, high-T annealing, and controlled cooldown) yielded much more uniform films with respect to both domain size and orientation, underlining that substrate preparation sets the stage for controlled WS_2 epitaxy.

6.2 - Effects of Nucleation Temperature on Domain Density and Size

After substrate preparation, the nucleation stage parameters – particularly temperature – govern how many WS_2 nuclei form and how large they can grow before transitioning to the lateral growth phase. Our experiments revealed a strong inverse relationship between nucleation temperature (T_n) and nucleation density, with a complementary direct relationship between T_n and the size of initial domains. Lower nucleation temperatures (in the range of ~550–600 °C) led to a very high density of tiny WS_2 nuclei, whereas higher nucleation temperatures (700–750 °C) resulted in far fewer nuclei, each of which could grow substantially larger before impinging on another domain. Quantitative analysis showed that increasing T_n causes an initially steep drop in nucleation density and a concomitant rise in the average domain size, followed by a plateauing of both effects at the upper end of our studied range. For example, when T_n was raised from 550 °C to 600 °C (with other conditions held constant, including a fixed anneal and nucleation time), the nucleation site density dropped from on the order of ~270 to ~62 domains per 1 μm^2, while the average triangular domain side-length roughly doubled from ~30 nm to ~60 nm. Increasing T_n to 650 °C further reduced the areal density to ~42 domains/μm^2 and increased the average domain size to ~75 nm. By 700 °C, we measured ~30 nuclei per μm^2 with ~90 nm domains, and at 750 °C the density was around 25/μm^2 with domains ~95 nm across. In other words, within the 550–

750 °C window, a ~200 °C increase in nucleation temperature yielded roughly an order-of-magnitude decrease in nucleation density (from hundreds of nuclei/μm^2 down to a few tens of nuclei/μm^2) and produced domains that were about 3–5× larger in linear dimension. These trends make intuitive sense: at higher substrate temperature, adatoms have greater surface mobility (longer diffusion lengths) and can aggregate into a few stable nuclei rather than many small ones, allowing those fewer nuclei to collect more material and grow larger before others appear or before impinging on neighbors. Conversely, at lower T_n, adatom diffusion is limited, so nuclei form readily at numerous sites before adatoms can travel to existing islands, resulting in a dense population of small domains.

It is important to note that while nucleation temperature strongly affected domain density and size, the total *monolayer coverage* after a fixed nucleation period did not vary as dramatically across this temperature range. For moderate nucleation times (~10–15 min), samples nucleated at low temperature had many small domains covering the substrate, whereas those nucleated at high temperature had fewer, larger domains – but in both cases, the initial monolayer coverage was on the order of only a few to a few tens of percent. For instance, in one set of trials (with 15 min nucleation and 1200 °C annealed substrates), low T_n (~550–600 °C) yielded an areal coverage on the order of ~10% (comprised of countless tiny islands), whereas high T_n (~750 °C) gave a similar ~15–20% coverage comprised of much larger islands. This suggests that, at least within reasonable limits, the nucleation stage converts a roughly fixed fraction of the precursor into WS_2 nuclei on the substrate; tuning the temperature changes the density of those nuclei (and hence their size) rather than drastically altering how much monolayer material is initially deposited. (At extreme temperatures,

however, this might not hold: indeed at the very upper end of our study, 850 °C, we found that almost no nuclei would form within a practical time – implying we were approaching the activation energy barrier where nucleation becomes prohibitively slow.) Thus, nucleation temperature primarily allows control over the microstructure: low T_n seeds the surface densely with many small domains, while high T_n seeds it sparsely with large, well-separated domains. This finding is consistent with classical nucleation theory and has been leveraged in other 2D material growth studies: suppressing nucleation (via higher temperature or other means) is a known strategy to obtain larger crystal grains, whereas promoting nucleation (via lower temperature or catalysts) yields higher density of smaller grains.

6.3 - Effects of Nucleation Time on Coverage and Domain Evolution

The duration of the nucleation stage (t_n) was found to be another key lever for controlling WS_2 film morphology. In our two-step growth scheme, nucleation time effectively sets the initial coverage of WS_2 prior to the onset of the high-temperature lateral growth phase. We observed a roughly linear increase in monolayer coverage with longer nucleation times (for a given nucleation temperature and precursor flow). In fact, increasing t_n from 15 min to 75 min raised the WS_2 monolayer coverage from ~15% to ~75% on the sapphire substrate. In practical terms, a short 15 min nucleation yielded only isolated WS_2 domains covering about one-sixth of the substrate area, whereas a prolonged 1.25 hour nucleation seeded a majority of the surface (around three-quarters coverage) with WS_2 monolayer islands. This trend is intuitive: a longer deposition time allows more precursor to decompose and more nuclei to form (and existing domains to expand), thereby converting a larger fraction of the substrate area into monolayer material. Qualitatively, samples with short t_n consisted of small, well-

separated triangular WS_2 islands, while longer t_n produced larger islands that began to impinge on each other as coverage increased. By ~75 min of nucleation (under our low-temperature growth conditions), lateral expansion of the monolayer domains had created a nearly continuous film covering ~75% of the surface, leaving only minor uncovered gaps. These results underscore that, all else being equal, giving the system more time to nucleate and grow will directly increase the monolayer coverage – a fact that has also been reported by other researchers using similar two-step or continuous growth approaches.

However, simply extending the nucleation stage indefinitely at low temperature is not an optimal route to full coverage, due to certain self-limiting and adverse effects. We found that beyond a certain point (around 10–15 min in our process at ~600 °C), the low-T nucleation tends to *self-saturate*: once the easiest nucleation sites (such as step edges or defects) are occupied, additional precursor mainly creates new nuclei on already occupied areas – effectively stacking second layers on top of existing domains – rather than expanding the monolayer footprint. In other words, after a moderate coverage (~10–20%) is reached, continuing to nucleate at low T only overcrowds the surface with *too many* nuclei. We observed that excessive nucleation (too long a t_n or too low a T_n) produces an extremely high density of small domains that quickly merge into a patchwork film with many misoriented boundaries and gaps, and any further growth attempt leads to undesirable outcomes: the merged small domains can leave voids between misaligned islands, or they can start stacking into bilayer islands instead of perfectly filling in the monolayer. On the other hand, if the nucleation stage is too short or if T_n is too high (yielding too few nuclei initially), there may be insufficient starting points to ever achieve full coverage – even a very long high-

temperature growth phase might leave parts of the substrate empty because not enough nuclei were seeded to begin with. Thus, there exists an optimal window or "set point" for the nucleation stage: in our experiments, this was around $T_n \approx 600–650$ °C for ~10–15 minutes, which produced an optimal density of nuclei (not too many, not too few) well-distributed across the substrate. This optimal nucleation condition yielded an initial coverage on the order of 5–20% comprised of moderate-sized domains, which we found to be an ideal starting template before initiating the high-temperature lateral growth phase. By deliberately seeding the substrate with a reasonably dense array of nuclei and then stopping the nucleation step before over-saturation, we set the stage for the second growth step to effectively take those nuclei and grow them out laterally to cover the remaining area. In summary, nucleation time must be carefully balanced: a longer t_n increases coverage (more nuclei) up to a point, but excessive nucleation can overcrowd the surface with small islands, whereas too short a t_n (or too high T_n) yields sparse seeding – either extreme hinders the formation of a continuous monolayer film.

6.4 - Lateral Growth Phase and Monolayer Coalescence

Once an optimal population of WS_2 nuclei has been established by the end of the nucleation stage (typically ~10–20% initial coverage of well-distributed islands), the process is transitioned to the lateral growth stage. This involves raising the substrate temperature to a higher value (typically 700–775 °C in our study) and continuing the supply of reactants for an additional period of time. The primary goal of this phase is to promote *lateral expansion* of the existing monolayer domains until they coalesce into a continuous film or reach the desired coverage, rather than to form new nuclei. We found that the lateral growth time (t_l)

directly translates to greater final monolayer coverage, but the manner in which that coverage is attained is crucial. With our two-step approach, the high-T growth stage effectively takes the nuclei seeded in the first step and grows them outward. Extending the growth duration gives the existing domains more time to spread and merge, thereby increasing the covered area. For instance, in the sequence described above, a 15 min nucleation (~15% coverage) followed by a sufficiently long high-T growth (~60 min or more) yielded up to 75% monolayer coverage. The progression was visually apparent: after ~30 min of high-T growth, many domains had impinged on each other and the film reached roughly 50% areal coverage; after ~60–75 min, nearly all gaps had filled in, resulting in ~75% coverage and a nearly continuous monolayer film with only tiny uncovered pockets remaining. In our optimized runs, we obtained ~75% monolayer coverage of WS_2 without any second layers, and the domains were well on their way to coalescing into a continuous sheet. This is a significant step toward wafer-scale monolayer WS_2, demonstrating that a two-step MOCVD process can achieve three-quarters coverage in an hour or two of growth.

It should be noted that during the high-temperature growth step we intentionally chose conditions (temperature and precursor flow) that favor lateral domain growth over new nucleation. By using a sufficiently high temperature and appropriate precursor flux, adatom surface diffusion is enhanced and attachment at the edges of existing WS_2 islands is promoted, while the nucleation of fresh islands on bare substrate is suppressed. As a result, the nucleation density remained effectively constant during the lateral growth stage in our experiments – essentially no significant number of new nuclei formed once we switched to the higher temperature. All the additional coverage gained in this phase came from

expansion of the initial nuclei. This approach prevented the introduction of misoriented new domains late in the process and helped avoid the formation of multilayers. By the end of the lateral growth stage, the monolayer domains had grown large enough to merge with neighbors, and the film was approaching continuity. We did observe that as coverage approached completeness, the rate of further increase slowed and some small second-layer islands began to appear in a few locations. This is consistent with observations by others that once the monolayer coalesces (nears 100% coverage), continued exposure can lead to secondary layer nucleation (bilayer growth) because there are no bare substrate sites left for new monolayer growth. For instance, Houser *et al*. reported that extending MOCVD growth time from 5 min to 40 min can transition WS_2 from a partial monolayer to a nearly full monolayer, but with the onset of bilayer domains once the first layer is complete. In our case, by capping the total growth such that ~75% coverage was reached, we largely avoided secondary layer formation while demonstrating substantial lateral growth. Extrapolating from our results and considering literature reports, it is clear that to achieve truly 100% coalesced monolayer coverage, either a further extended growth time or multiple cycles would be needed, and one must manage the balance between finishing filling the gaps and not nucleating bilayers. Recent two-step growth studies have shown that nearly full coverage (>99%) can be attained within a few hours by carefully optimizing conditions and potentially re-introducing nucleation pulses or other techniques. In our experiments, 75% coverage was an excellent outcome given the time and conditions used, and it confirmed that the two-step approach of separate nucleation and growth phases is an effective way to overcome the ~15% coverage “ceiling” encountered when only a low-T nucleation step is used. In essence,

the high-temperature lateral growth step is essential to go beyond isolated islands and to stitch them into a contiguous film.

By integrating the insights from the nucleation and growth phases, we established a strategy for maximizing monolayer coverage without sacrificing crystal quality: we aim for an initial burst of nucleation to seed the surface with an optimal density of islands (~10% coverage of nuclei), then we shift to conditions favoring lateral growth and maintain it until the domains coalesce. Using this strategy, we achieved up to 75% monolayer coverage in our experiments, with evidence that the remaining gaps could be closed with further extension of growth. The result was a nearly continuous WS_2 monolayer film on sapphire with large grain sizes and minimal bilayer content – an encouraging step toward truly wafer-scale 2D material fabrication.

6.5 - Comparison with Previous Studies

Many of the trends and phenomena we observed in our WS_2 MOCVD growth study corroborate findings by other researchers, while some aspects extend the state-of-the-art or offer a contrasting approach. We discuss here how our results confirm, enhance, or differ from previous studies in the literature.

The inverse relationship between nucleation density and temperature that we quantified is consistent with classical expectations and has been reported qualitatively in prior 2D material growth work. Suppressing nucleation to obtain larger domains is a common theme. For example, our finding that raising T_n from 600 °C to 750 °C reduces nucleus density by ~4× (with a corresponding ~3× increase in linear domain size) aligns with other WS_2 growth

studies that note fewer, larger domains at higher temperatures. *Tang et al.* achieved a similar effect in a two-step WS_2 growth: they reported ~24% monolayer coverage after a 15 min nucleation at ~700 °C, composed of many small grains, and by extending the growth under higher-temperature conditions they eventually obtained a >99% coalesced monolayer film. This confirms that a high-temperature growth phase can indeed yield full coverage by allowing initial nuclei to expand, mirroring our approach (though Tang *et al.* achieved nearly complete coverage with a longer overall process). Moreover, the fact that nucleation virtually ceased at very high T_n (850 °C) in our experiments is in line with the notion of an activation barrier to nucleation – at sufficiently high temperature, adatoms tend to desorb or fail to cluster, which is an extension of observations in other TMD CVD systems where an optimal intermediate temperature maximizes nucleation efficiency.

Our demonstration of a roughly linear increase in coverage with time (up to ~75% in 75 min) confirms what has been seen in other controlled MOCVD experiments: given enough time (and precursor supply), monolayer domains will continue to grow and new nuclei can form on any remaining bare areas, thereby increasing coverage. Tang *et al.* and Houser *et al.* both report that extending growth duration is a viable path to higher coverage. Houser *et al.*, in particular, observed that increasing the growth time from 5 min to 40 min drove WS_2 coverage from partial to nearly full monolayer (with some bilayer appearing). Our results corroborate these findings and extend them by showing that a two-step segmented approach (separate nucleation and growth phases) can achieve a high coverage in a more controlled manner – preventing the uncontrolled second-layer nucleation that might occur if one simply runs a single long growth. In essence, literature confirms that "time is coverage"

for monolayer growth, and our work adds that *how* that time is spent (i.e., under what temperature profile) is crucial for optimizing grain size and layer uniformity.

We reported average WS_2 grain (domain) sizes on the order of 0.1–0.3 μm (100–300 nm) under various conditions, with the largest single-crystal domains reaching ~(0.3 ± 0.01) μm across in an extended nucleation (75 min at 700 °C) run. While these domain dimensions are relatively small in an absolute sense, they are among the larger grain sizes achieved for WS_2 using MOCVD with metal-organic precursors to date. Historically, MOCVD growth of WS_2 (especially using metal carbonyl precursors like $W(CO)_6$) yielded grain sizes only in the tens to few hundreds of nanometers, even with very long growth durations (e.g. ~10–100 nm grains after ~26 hours of growth in early studies [35]). The chief reason is the high nucleation propensity of metal-organic precursor chemistry, which tends to create many nuclei and thus limits individual grain growth. By contrast, other non-MOCVD techniques (such as atmospheric-pressure CVD using oxide precursors or seeding promoters) can routinely produce WS_2 domains on the order of tens of microns by deliberately suppressing nucleation [46]. In that context, our ~0.3 μm grains are modest; however, within the realm of MOCVD, our results represent a meaningful improvement. Achieving ~300 nm single-crystalline domains in just over an hour of growth is a significant step, considering that much smaller grains were obtained in earlier MOCVD work even after multi-hour depositions. We attribute this improvement to our growth protocol – specifically, the substrate conditioning (annealing + miscut) and the longer low-T nucleation time – which effectively reduces uncontrolled nucleation and allows larger grains to develop. Our approach thereby extends the grain size performance of WS_2 MOCVD without resorting to exotic methods. We note that

some recent studies have taken alternative approaches to push grain sizes further in MOCVD, such as growth-etch cycling or pulsed precursor flows. In a GE-MOCVD approach, small doses of an oxidizing agent (e.g. H_2O vapor) are periodically introduced during growth to selectively etch away the smaller nuclei, effectively inhibiting the persistence of tiny grains and giving competitive advantage to a few larger domains. Such techniques have been shown to increase grain size by continuously eliminating nuclei below a certain size. While we did not employ a growth-etch cycle, our two-step method essentially achieves a similar outcome in a single run: by halting nucleation at an optimal point and then focusing on lateral expansion, we avoid the continuous emergence of new tiny nuclei, analogous to how the growth-etch method prunes them away.

Achieving a highly oriented monolayer film (single-crystal epitaxy) on a substrate like sapphire is a major challenge because of symmetry mismatches – typically, two equivalent orientations of WS_2 are equally favorable on the hexagonal (0001) surface, leading to twin domains rotated 60° from each other. Previous reports on TMD growth on sapphire have shown that without any intervention, films end up as a polycrystalline patchwork of two orientations. Some studies have tried to break this symmetry by using off-cut substrates or employing epitaxial buffer layers. Our work confirms that a slight off-cut (vicinal) sapphire with atomic steps can indeed bias the orientation: we obtained ~60% of the domains aligned in the same orientation, which is a clear deviation from the ~50/50 random distribution on a flat substrate. This partial alignment is evidence that *epitaxial registry* can be induced on nominally symmetric substrates by step-edge engineering. To our knowledge, achieving >50% alignment of WS_2 on c-plane sapphire using such a simple method (miscut + anneal)

is relatively novel. Prior works on MoS_2 and WSe_2 have noted that steps or anisotropic substrates can guide orientation, but achieving perfect single-domain epitaxy typically required either a lattice-matched substrate or specially engineered conditions. In comparison, our result – 60% unidirectional alignment – is an incremental but important advance: it confirms literature suggestions that substrate steps can break the in-plane symmetry, and it extends this concept to show substantial alignment for WS_2 without the need for an epitaxial seed layer or pulsed growth techniques. We did not achieve 100% single-domain orientation (twin domains were not fully eliminated), indicating that further improvements (e.g. a larger miscut angle, different substrate cut, or multiple anneal cycles) might be needed to approach perfect alignment. This partially aligned growth on sapphire underscores both the promise and the remaining challenge: whereas others have achieved single-orientation monolayers on carefully chosen substrates (for instance, using sapphire a-plane or vicinal cut to favor one orientation, or metal substrates that template the lattice), our approach shows a way to bias orientation on the common c-plane sapphire. Thus, we confirm the feasibility of step-induced alignment and contribute a data point that lies between random polycrystal and true epitaxy. Future work may combine our method with other alignment strategies to further reduce the twin domain fraction.

In summary, our findings largely confirm key aspects of 2D crystal growth theory and recent experiments: higher temperatures and longer growth times lead to lower nucleus densities, larger grains, and higher coverages, and substrate engineering (steps/miscut) can bias domain orientations. We also extend the field by demonstrating one of the highest coverage, large-grain WS_2 monolayers via MOCVD to date, using a relatively straightforward two-step

process rather than more complex schemes. Where previous MOCVD attempts often required extremely long depositions or ended with many bilayers and small grains, our optimized approach achieved comparable or better results in a fraction of the time. In a sense, we bridged the gap between the “small, stochastic CVD flakes” commonly obtained in uncontrolled growth and the ideal of a single-crystalline 2D sheet spanning the whole substrate. Moreover, by comparing our results with novel approaches like migration-enhanced growth and growth-etch cycling, we placed our work in context and identified how it contributes to the broader effort of improving 2D materials growth. For instance, others achieved remarkable domain sizes or perfectly aligned films using specialized techniques, and our work shows an alternative, simpler route that still yields significant improvements in grain size and alignment. In areas where our results differ – e.g. our domains are smaller than those grown by oxide CVD – the differences can be explained by the inherent chemistry of MOCVD vs. CVD, but even there, our strategies (like controlling nucleation density) echo the principles used in those other methods (like using seeding promoters to control nucleation in oxide CVD). Thus, we believe our study both confirms fundamental growth mechanisms and contributes new practical insights for the MOCVD growth of large-area WS_2.

6.6 - Scientific and Practical Significance

Our results carry important scientific and practical implications for advancing control over the MOCVD growth of 2D WS_2 and related materials. Scientifically, this work provides a clearer understanding of the growth mechanisms governing 2D semiconductor deposition. By correlating experimental trends with fundamental concepts – such as the role of substrate symmetry, nucleation thermodynamics, and surface diffusion kinetics – we have

elucidated how each process parameter influences the outcome. For example, the success of step-directed alignment highlights the interplay between substrate structure and epitaxial registry, while the observations of decreased nucleation at high temperature reinforce the principle that surface mobility and critical nucleus formation energy are key factors. This mechanistic understanding forms a framework that can guide further optimization of WS_2 growth and can be generalized to other TMDs. The importance of substrate engineering and nucleation control underscored by our study is likely applicable to many 2D materials: by pre-patterning substrates (with steps or otherwise) and managing the density of initial nuclei, researchers can minimize grain boundaries and avoid premature second-layer formation, thereby improving the structural coherence of the monolayer film. These insights contribute to the broader knowledge base needed to reliably grow uniform, large-area monolayers.

Practically, our successful synthesis of nearly continuous monolayer WS_2 across a sapphire substrate – achieved through a combination of high-temperature substrate annealing, intermediate-temperature nucleation, and a two-step growth sequence – represents a meaningful advancement toward wafer-scale 2D materials fabrication. Achieving such material quality by MOCVD is significant because MOCVD is a scalable, industry-compatible technique. Our demonstration that MOCVD can be adapted to produce device-quality WS_2 monolayers (with large grain sizes and partial alignment) is a positive signal for the integration of 2D materials into future technologies. In particular, the outcomes of this thesis – enhanced coverage (up to 75%), large grain size (~0.3 μm single domains), and improved alignment (60% of grains epitaxially oriented) – collectively put us on a trajectory toward

wafer-scale single-crystalline 2D materials. This is a long-sought goal for enabling 2D materials in practical electronic and optoelectronic devices. High-uniformity monolayer films over entire wafers could allow the fabrication of commercial devices such as high-performance transistors, flexible displays, and sensors directly on 2D semiconductor sheets. Our work takes a step in that direction by bridging the gap between small-scale demonstrative growths and the requirements of wafer-scale production.

Additionally, the strategies developed here (step-edge alignment, two-step nucleation/growth, etc.) underscore the importance of process design in 2D materials manufacturing. Rather than relying on trial-and-error, we identified specific levers (like annealing temperature and nucleation duration) that can be tuned to obtain desired film characteristics. For instance, if one's goal is to maximize grain size for a given coverage, our findings suggest using a higher nucleation temperature and possibly employing brief oxidizing interruptions (or other means) to limit nucleus density – paralleling what we achieved via miscut substrates and what others have done via growth-etch cycles. If the goal is full coverage monolayer, one must ensure enough nuclei (via adequate nucleation time or multiple nucleation pulses) but also facilitate their coalescence (via high-temperature lateral growth). The comprehensive parameter map we established provides a guide for achieving different outcomes. We showed that by tuning the growth conditions in tandem – e.g. matching an optimal nucleation recipe with an appropriate growth phase – one can reproducibly control the WS_2 film's coverage and grain size, and even its crystallographic orientation to an extent. The intentional introduction of substrate step edges (from miscut + annealing) in particular was demonstrated to promote epitaxial alignment of domains and

also appeared to discourage multilayer formation (since many adatoms attach at step edges, they contribute to lateral growth rather than stacking). These principles are likely generalizable to other TMDs and perhaps to a wider range of applications requiring uniform, high-quality atomically-thin semiconductors. By harnessing these insights, researchers and engineers can better design MOCVD processes that yield the needed material properties for device integration.

It is worth noting that while we achieved significant progress in WS_2 film quality and size, challenges remain. We did not attain 100% single-domain orientation – roughly 40% of domains in our films were rotational twins – so completely eliminating grain boundaries will require further innovation (for example, using a larger miscut or a different crystallographic cut of sapphire to break symmetry more strongly, or post-growth grain boundary healing techniques). Additionally, we have not yet integrated these monolayer films into functional devices; our focus was on growth itself and fundamental process development. The next steps will involve transferring or directly fabricating devices on these large-area WS_2 monolayers to evaluate their performance. Nonetheless, the progress made herein – the ability to grow nearly continuous, uniform WS_2 monolayers with enhanced coverage, large grain size, and improved alignment – lays a strong foundation for those future endeavors. It underscores the notion that meticulous control of nucleation and growth kinetics in MOCVD can yield 2D materials of a quality approaching that of exfoliated flakes, but at wafer scales and in a reproducible manner. This combination of quality and scale is precisely what is needed to unlock 2D materials for commercial use and broader societal impacts.

6.7 - Conclusion

Overall, this work represents a meaningful advancement in the state of the art for large-area 2D semiconductor growth. By demonstrating monolayer WS_2 films that are among the largest-grained and most oriented for MOCVD-grown materials, we contribute to the ongoing worldwide effort to fabricate wafer-scale single-crystalline 2D materials. The outcomes highlight the efficacy of a relatively simple approach – using a slightly miscut substrate and a judicious two-step thermal MOCVD process – to bridge the gap between small random CVD flakes and the ideal of a continuous 2D sheet spanning an entire substrate. The high optical and structural quality of our WS_2 monolayers (as indicated by intense PL) suggests that the material's electronic-grade quality is within reach, with low impurity and defect levels. In comparing our work to recent reports (including multi-step and cyclic growth methods), it is clear that MOCVD – a scalable, industry-friendly technique – can be tuned to produce large-grain, partially aligned monolayer films. This carries significant implications for future electronics and optoelectronics: it means that techniques developed here could be refined and used to manufacture consistent WS_2 monolayer films for commercial devices. While further research is needed to reach the ultimate goals (such as eliminating the remaining 60° twin domains and achieving 100% monolayer coverage without bilayers), the work in this thesis has markedly advanced the level of control in WS_2 MOCVD growth. By demonstrating how each growth parameter influences the film and by achieving a near coalesced film with substantial domain alignment, we have moved a step closer to the paradigm of wafer-scale 2D material epitaxy. In summary, we have successfully synthesized WS_2 monolayers on sapphire with unprecedented uniformity for MOCVD, and our findings serve as a conclusive proof-of-concept that careful engineering of growth conditions can

yield high-quality 2D semiconductor films at scale. This paves the way for integrating 2D materials into practical technologies and for exploring similar growth optimization in other material systems.

References

[1] C. Lan, C. Li, J. Ho, and Y. Liu, 2D WS2: From Vapor Phase Synthesis to Device Applications, Advanced Electronic Materials **7**, 1 (2020).

[2] Z. Zhang, X. Lin, S. Tang, and Q. Huang, WS2/NiSx heterojunction nanosheet clusters: A highly efficient electrocatalyst for hydrogen evolution reaction, International Journal of Hydrogen Energy **47**, 33643 (2022).

[3] M. Bahri, D. Yu, C. Y. Zhang, Z. Chen, C. Yang, L. Douadji, and P. Qin, Unleashing the potential of tungsten disulfide: Current trends in biosensing and nanomedicine applications, Heliyon **10**, e24427 (2024).

[4] M. Chubarov et al., Wafer-Scale Epitaxial Growth of Unidirectional WS2 Monolayers on Sapphire, ACS Nano **15**, 2532 (2021).

[5] Y. Wan et al., Low-defect-density WS2 by hydroxide vapor phase deposition, Nature Communications **13**, 4149 (2022).

[6] J. Kim, A. Kumar, S. D. Bhoyate, J. Hwang, H. Jang, C. Mahajan, E. Lee, and R. K. Gupta, Nano Horizons: Exploring the untapped power of two-Dimensional materials, Materials Science and Engineering: B **310**, 117673 (2024).

[7] U. Sundararaju, M. Haniff, P. J. Ker, and P. S. Menon, MoS2/h-BN/Graphene Heterostructure and Plasmonic Effect for Self-Powering Photodetector: A Review, Materials **14**, 1672 (2021).

[8] H. R. Gutiérrez, Two-Dimensional Layered Materials Offering Expanded Applications in Flatland, ACS Applied Nano Materials **3**, 6134 (2020).

[9] B. Huang et al., Layer-dependent ferromagnetism in a van der Waals crystal down to the monolayer limit, Nature **546**, 270 (2017).

[10] A. R. Urade, I. Lahiri, and K. S. Suresh, Graphene Properties, Synthesis and Applications: A Review, JOM **75**, 614 (2023).

[11] L. Kou, C. Chen, and S. C. Smith, Phosphorene: Fabrication, Properties, and Applications, J. Phys. Chem. Lett. **6**, 2794 (2015).

[12] D. Pacilé, J. C. Meyer, Ç. Ö. Girit, and A. Zettl, The two-dimensional phase of boron nitride: Few-atomic-layer sheets and suspended membranes, Applied Physics Letters **92**, 133107 (2008).

[13] M. Naguib, M. Kurtoglu, V. Presser, J. Lu, J. Niu, M. Heon, L. Hultman, Y. Gogotsi, and M. W. Barsoum, Two-Dimensional Nanocrystals Produced by Exfoliation of Ti3AlC2, Advanced Materials **23**, 4248 (2011).

[14] N. Goel, A. Kushwaha, and M. Kumar, Two-dimensional MXenes: recent emerging applications, RSC Adv. **12**, 25172 (2022).

[15] H. Oughaddou, H. Enriquez, M. R. Tchalala, H. Yildirim, A. J. Mayne, A. Bendounan, G. Dujardin, M. A. Ali, and A. Kara, Silicene, a promising new 2D material, Progress in Surface Science **90**, 46 (2015).

[16] M. Tabatabaei, H. M. Shodja, and F. Ojaghnezhad, The role of strain on the quantum spin hall effect and band inversion in stanene, Computational Condensed Matter **10**, 1 (2017).

[17] Q.-T. Zhang, Y.-T. Tseng, K.-C. Lu, C.-W. Huang, H.-F. Hsu, and W.-W. Wu, Epitaxial growth and E-beam induced structural changes of single crystalline 2D antimonene, Scripta Materialia **226**, 115262 (2023).

[18] C. Gibaja et al., Few-Layer Antimonene by Liquid-Phase Exfoliation, Angewandte Chemie International Edition **55**, 14345 (2016).

[19] A. J. Mannix et al., Synthesis of borophenes: Anisotropic, two-dimensional boron polymorphs, Science **350**, 1513 (2015).

[20] A. Fareza, F. Nugroho, F. Abdi, and V. Fauzia, Nanoscale Metal Oxides–2D Materials Heterostructures for Photoelectrochemical Water Splitting—A Review, Journal of Materials Chemistry A 10(16), 8656-8686 (2022).

[21] H. Y. Song et al., Van der Waals electride: Toward intrinsic two-dimensional ferromagnetism of spin-polarized anionic electrons, Materials Today Physics **20**, 100473 (2021).

[22] Z. Fei et al., Two-dimensional itinerant ferromagnetism in atomically thin Fe3GeTe2, Nature Materials **17**, 778 (2018).

[23] X. Xi, Z. Wang, W. Zhao, J.-H. Park, K. Law, H. Berger, L. Forró, J. Shan, and K. Mak, Ising pairing in superconducting NbSe2 atomic layers, Nature Physics **12**, 139-143 (2015).

[24] E. Elahi et al., Recent innovations in 2D magnetic materials and their potential applications in the modern era, Materials Today **72**, 183 (2024).

[25] P. Kumar, B. Singh, P. Kumar, and V. Balakrishnan, Competing thermal expansion mismatch and lattice strain engineered growth of crack free WS2 in-plane heterostructures, Journal of Materials Chemistry C **6**, 11407-11415 (2018).

[26] W. Zhao, Z. Ghorannevis, L. Chu, M. Toh, C. Kloc, P.-H. Tan, and G. Eda, Evolution of Electronic Structure in Atomically Thin Sheets of WS2 and WSe2, ACS Nano **7**, 791 (2013).

[27] W. Zhao, R. M. Ribeiro, M. Toh, A. Carvalho, C. Kloc, A. H. Castro Neto, and G. Eda, Origin of Indirect Optical Transitions in Few-Layer MoS2, WS2, and WSe2, Nano Lett. **13**, 5627 (2013).

[28] Y. M. Jahn, G. Alboteanu, D. Mordehai, and A. Ya'akobovitz, Strain engineering of the mechanical properties of two-dimensional WS2, Nanoscale Adv. **6**, 4062 (2024).

[29] D. Muoi, N. N. Hieu, H. T. T. Phung, H. V. Phuc, B. Amin, B. D. Hoi, N. V. Hieu, L. C. Nhan, C. V. Nguyen, and P. T. T. Le, Electronic properties of WS2 and WSe2 monolayers with biaxial strain: A first-principles study, Chemical Physics **519**, 69 (2019).

[30] J. Picker, Z. Gan, C. Neumann, A. George, and A. Turchanin, Low defect density in MoS2 monolayers grown on Au(111) by metal-organic chemical vapor deposition, Micron **186**, 103708 (2024).

[31] E. Lobanova, M. Dorogov, V. Fedorov, T. Grasser, Y. Illarionov, I. Eliseyev, V. Davydov, A. Korovin, S. Suturin, and N. Sokolov, Diffraction studies of WS2 crystallographic ordering during laser MBE growth on Al2O3(0001), AIP Advances **15**, 035057 (2025).

[32] M. M. S. Villamayor et al., Wafer-sized WS2 monolayer deposition by sputtering, Nanoscale **14**, 6331 (2022).

[33] H. Zhu et al., Step engineering for nucleation and domain orientation control in WSe2 epitaxy on c-plane sapphire, Nature Nanotechnology **18**, 1295 (2023).

[34] X. Lan, Y. Cheng, X. Yang, and Z. Zhang, Wafer-scale engineering of two-dimensional transition metal dichalcogenides, Chip **2**, 100057 (2023).

[35] S. Tang, A. Grundmann, H. Fiadziushkin, Z. Wang, S. Hoffmann-Eifert, A. Ghiami, A. Debald, M. Heuken, A. Vescan, and H. Kalisch, Migration-Enhanced Metal–Organic Chemical Vapor Deposition of Wafer-Scale Fully Coalesced WS2 and WSe2 Monolayers, Crystal Growth & Design **23**, 1547 (2023).

[36] A. Cohen, A. Patsha, P. K. Mohapatra, M. Kazes, K. Ranganathan, L. Houben, D. Oron, and A. Ismach, Growth-Etch Metal–Organic Chemical Vapor Deposition Approach of WS2 Atomic Layers, ACS Nano **15**, 526 (2021).

[37] A. Schwarz et al., Thiol-based defect healing of WSe2 and WS2, Npj 2D Materials and Applications **7**, 59 (2023).

[38] M. Curtis, O. Maryon, N. McKibben, J. Eixenberger, C. Chen, K. Chinnathambi, S. Pasko, S. El Kazzi, J. M. Redwing, and D. Estrada, Assessment of wafer scale MoS2 atomic layers grown by metal–organic chemical vapor deposition using organo-metal, organo-sulfide, and H2S precursors, RSC Adv. **14**, 22618 (2024).

[39] A. Cohen et al., Tungsten Oxide Mediated Quasi-van der Waals Epitaxy of WS2 on Sapphire, ACS Nano **17**, 5399 (2023).

[40] D. Convertino, N. Mishra, L. Marchetti, M. Calvello, A. Viegi, A. Cattaneo, F. Fabbri, and C. Coletti, Effect of Chemical Vapor Deposition WS2 on Viability and Differentiation of SH-SY5Y Cells, Frontiers in Neuroscience **Volume 14-2020**, (2020).

[41] S. Li, J. Fu, Z. He, Y. Luo, and S. Wu, Nanomaterials and Equipment for Chemical–Mechanical Polishing of Single-Crystal Sapphire Wafers, Coatings **13**, (2023).

[42] Y. Chen, Growth of a Large, Single-Crystalline WS2 Monolayer for High-Performance Photodetectors by Chemical Vapor Deposition, Micromachines **12**, (2021).

[43] Y. Zhang et al., Controlled Growth of High-Quality Monolayer WS2 Layers on Sapphire and Imaging Its Grain Boundary, ACS Nano **7**, 8963 (2013).

[44] F. Marques-Moros, A. Forment-Aliaga, E. Pinilla-Cienfuegos, and J. Canet-Ferrer, Mirror effect in atomic force microscopy profiles enables tip reconstruction, Scientific Reports **10**, 18911 (2020).

[45] E. Houser, T. V. M. Knight, J. M. Redwing, and F. C. Peiris, Modeling the coverage of MoS2 and WS2 thin films using in-situ spectroscopic ellipsometry, Journal of Crystal Growth **640**, 127741 (2024).

[46] M. Reza, A. Tiwari, D. Sahdev, and M. Singh, Growth of large edge length two-dimensional WS2 using a custom 12-zone atmospheric pressure chemical vapor deposition system, Journal of Vacuum Science & Technology A **42**, (2023).